# A KNOWLEDGE BASED APPROACH IN GMTI FOR THE ESTIMATION OF THE CLUTTER COVARIANCE MATRIX IN SPACE TIME ADAPTIVE PROCESSING

A THESIS SUBMITTED TO
THE GRADUATE SCHOOL OF NATURAL AND APPLIED SCIENCES
OF
MIDDLE EAST TECHNICAL UNIVERSITY

BY

ERMAN ANADOL

IN PARTIAL FULFILLMENT OF THE REQUIREMENTS
FOR
THE DEGREE OF MASTER OF SCIENCE
IN
ELECTRICAL AND ELECTRONICS ENGINEERING

SEPTEMBER 2012

Approval of the thesis:

# A KNOWLEDGE BASED APPROACH IN GMTI FOR THE ESTIMATION OF THE CLUTTER COVARIANCE MATRIX IN SPACE TIME ADAPTIVE PROCESSING

submitted by **ERMAN ANADOL** in partial fulfillment of the requirements for the degree of
**Master of Science in Electrical and Electronics Engineering Department, Middle East Technical University** by,

Prof. Dr. Canan Özgen
Dean, Graduate School of **Natural and Applied Sciences** _____

Prof. Dr. İsmet Erkmen
Head of Department, **Electrical and Electronics Engineering** _____

Prof. Dr. Yalçın Tanık
Supervisor, **Electrical and Electronics Engineering, METU** _____

**Examining Committee Members:**

Prof. Dr. Sencer Koç
Electrical and Electronics Engineering, METU _____

Prof. Dr. Yalçın Tanık
Electrical and Electronics Engineering, METU _____

Assoc. Prof. Dr. A. Özgür Yılmaz
Electrical and Electronics Engineering, METU _____

Assoc. Prof. Dr. Çağatay Candan
Electrical and Electronics Engineering, METU _____

Dr. Ülkü Doyuran
Senior Lead Design Engineer, ASELSAN _____

**Date:** _____

**I hereby declare that all information in this document has been obtained and presented in accordance with academic rules and ethical conduct. I also declare that, as required by these rules and conduct, I have fully cited and referenced all material and results that are not original to this work.**

Name, Last Name:    ERMAN ANADOL

Signature          :

# ABSTRACT

A KNOWLEDGE BASED APPROACH IN GMTI FOR THE ESTIMATION OF
THE CLUTTER COVARIANCE MATRIX IN SPACE TIME ADAPTIVE
PROCESSING

Anadol, Erman

M.Sc., Department of Electrical and Electronics Engineering

Supervisor    : Prof. Dr. Yalçın Tanık

September 2012, 111 pages

Ground Moving Target Indication (GMTI) operation relies on clutter suppression techniques for the detection of slow moving ground targets in the presence of strong radar returns from the ground. Space Time Adaptive Processing (STAP) techniques provide a means to achieve this goal by adaptively forming the clutter suppression filter, whose parameters are obtained using an estimated covariance matrix of the clutter data. Therefore, the performance of the GMTI operation is directly affected by the performance of the estimation process mentioned above. Knowledge based techniques are applicable in applications such as the parametric estimation of the clutter covariance matrix and the estimation of the clutter covariance matrix in a non-homogeneous clutter environment. In this study, a knowledge based approach which makes use of both a priori and instantaneous data is proposed for the mentioned estimation process. The proposed approach makes use of Shuttle Radar Topography Mission (SRTM) data as well as instantaneous platform ownship data in order to determine distributed homogeneous regions present in the region of interest; and afterwards employs Doppler Beam Sharpening (DBS) maps along with the colored loading technique for the blending process of the a priori data and the instantaneous data

corresponding to the obtained homogeneous regions. A nonhomogeneity detector (NHD) is also implemented for the elimination of discrete clutter and target-like signals which may contaminate the STAP training data. Simulation results are presented for both the knowledge aided and the traditional cases. Finally, the performance of the STAP algorithm will be evaluated and compared for both cases. Results indicate that by using the developed processing approach, detection of previously undetectable targets become possible, and the overall number of false alarms is reduced.

Keywords: GMTI, knowledge aided processing, STAP, NHD, colored loading

# ÖZ

## GMTI UZAY ZAMAN ADAPTİF İŞLEMEDE KARGAŞA ÖZİLİNTİ MATRİSİNİN KESTİRİMİ İÇİN BİLGİ TABANLI BİR YAKLAŞIM

Anadol, Erman

Yüksek Lisans, Elektrik ve Elektronik Mühendisliği Bölümü

Tez Yöneticisi    : Prof. Dr. Yalçın Tanık

Eylül 2012, 111 sayfa

Hareketli Yer Hedefi Tespiti (GMTI) işlemi, yerden yansıyan güçlü radar yankılarının varlığında yavaş hareketli yer hedeflerinin tespit edilmesi için kargaşa bastırımı tekniklerine gerek duymaktadır. Uzay Zaman Uyarlamalı İşleme (STAP) yöntemlerinde, gereken kargaşa bastırımı filtresi uyarlamalı olarak oluşturulmakta, filtre katsayıları ise kargaşa özilinti matrisinin kestirimi kullanılarak elde edilmektedir. Bu nedenle GMTI işleminin başarımı, söz konusu kestirim işleminin başarımı tarafından doğrudan etkilenmektedir. Bilgi tabanlı yöntemler, kargaşa özilinti matrisinin parametrik olarak kestirilmesi ve homojen olmayan kargaşa ortamlarında kargaşa özilinti matrisinin kestirilmesi gibi uygulamalarda uygulanabilir olmaktadır. Bu çalışmada, söz konusu kestirim işlemi için önceden elde edilmiş ve anlık verilerden faydalanan bilgi tabanlı bir yaklaşım önerilmektedir. Önerilen yöntem, Shuttle Radar Topography Mission (SRTM) verisi ve anlık platform navigasyon verilerini birlikte kullanarak, ilgilenilen bölge içerisinde dağıtık olarak yer alan homojen bölgeleri bulmakta, bunun ardından da Doppler Beam Sharpening (DBS) haritalarını renkli yükleme tekniği ile birlikte işleyerek, elde edilmiş olan homojen bölgelere karşılık gelen ön bilgi ve anlık bilgiyi birleştirmektedir. STAP eğitim verisini kirletebilme ihtimali olan ayrık kargaşa

ve hedef benzeri sinyalleri elemek için bir homojen olmayan durum algılayıcı da gerçeklenmiştir. Bilgi tabanlı ve geleneksel yöntemler için benzetim sonuçları sunulmaktadır. Son olarak, her iki durum için STAP algoritma performansı elde edilerek karşılaştırılmaktadır. Elde edilen sonuçlar göstermektedir ki, geliştirilmiş olan yöntem kullanıldığında, daha önceden tespit edilmesi mümkün olmayan hedefler tespit edilebilmiş ve toplam yanlış alarm sayısı azaltılmıştır.

Anahtar Kelimeler: GMTI, bilgi tabanlı işleme , STAP, NHD, renkli yükleme

*To my family*

# ACKNOWLEDGMENTS

I have completed my thesis with the great assistance of various people, who helped me during my research and synthesis periods.

First, I would like to thank my supervisor Prof. Dr. Yalçın Tanık for his guidance, encouragement and objective views which helped me stay concentrated in every working hour I spent on my thesis.

I would like to express my deepest gratitude to my lovely family for their support and trust they have given to me.

Finally, I would like to indicate my appreciation to ASELSAN Inc. for her opportunities and supports during the completion of my thesis.

# TABLE OF CONTENTS

# LIST OF TABLES

TABLES

# LIST OF FIGURES

FIGURES

# LIST OF ABBREVIATIONS

| Abbreviation | Explanation |
| --- | --- |
| CA-CFAR | Cell Averaging CFAR |
| CFAR | Constant False Alarm Rate |
| CL | Colored Loading |
| CMT | Covariance Matrix Tapering |
| GMTI | Ground Moving Target Indication |
| DARPA | Defense Advanced Research Projects Agency |
| DBS | Doppler Beam Sharpening |
| DDL | Doppler Domain Localized |
| DEM | Digital Elevation Model |
| DFT | Discrete Fourier Transform |
| DFAD | Digital Feature Analysis Data |
| DoF | Degree of Freedom |
| DPCA | Displaced Phase Center Antenna |
| DTED | Digital Terrain Elevation Data |
| ECEF | Earth Centered Earth Fixed |
| ENU | East – North – Up |
| FFT | Fast Fourier Transform |
| IID | Independent and Identically Distributed |

| Abbreviation | Explanation |
|---|---|
| KA-STAP | Knowledge Aided STAP |
| KASSPER | Knowledge Aided Sensor Signal Processing and Expert Reasoning |
| KB-STAP | Knowledge Based STAP |
| MSL | Mean Sea Level |
| MSMI | Modified Sample Matrix Inversion |
| NGIA | National Geospatial-Intelligence Agency |
| NHD | Non Homogeneity Detector |
| NLCD | National Land Cover Data |
| SAR | Synthetic Aperture Radar |
| SINR | Signal to Interference plus Noise Ratio |
| SMI | Sample Matrix Inversion |
| SNR | Signal to Noise Ratio |
| SRTM | Shuttle Radar Topography Mission |
| STAP | Space Time Adaptive Processing |
| USGS | United States Geological Survey |
| WGS | World Geodetic System |

# LIST OF SYMBOLS

| Parameter | Explanation |
| --- | --- |
| $\mathbf{c_k}$ | Space-time observation of clutter for a single range bin $\mathbf{k}$ |
| $\mathbf{n_k}$ | Space-time observation of noise for a single range bin $\mathbf{k}$ |
| $\mathbf{s}$ | Target signal model |
| $E\{\}$ | Expectation operation |
| $(\ )^{\mathbf{T}}$ | Matrix transpose operation |
| $(\ )^{\mathbf{H}}$ | Hermitian transpose operation |
| $\odot$ | Hadamard element-wise multiplication operation |
| $\mathbf{R}$ | Interference covariance matrix |
| $SINR$ | Signal to Interference plus Noise Ratio |
| $K$ | Total number of range bins in the radar data cube |
| $L$ | Number of secondary range bins |
| $M$ | Total number of channels in the receiver array |
| $N$ | Total number of pulses in a coherent processing interval |
| $\mathbf{r_k}$ | Combined space-time observation for a single range bin $\mathbf{k}$ |
| $\mathbf{w}$ | Adaptive filter coefficients |

# CHAPTER 1

# INTRODUCTION

## 1.1   Literature Survey

Detection of slow moving ground targets for airborne radars is a challenging problem. Due to the motion of the platform and the squint angle of the antenna, target echoes become buried under the interference spread in the Doppler spectrum and may become impossible to detect using non-adaptive methods. To address this issue, several adaptive methods are proposed in the literature. One of these methods is the Space Time Adaptive Processing technique, which is mainly used for target detection under clutter and jamming conditions by means of interference suppression. However, traditional STAP methods generally perform the aforementioned interference suppression process by means of estimating the statistical properties of the surrounding interference environment, which only performs well under the assumption that non-homogeneities are not present in the training data. To account for the aforementioned heterogeneities during the estimation process, numerous knowledge aided methods are proposed in the literature.

In [1], the aim of Space Time Adaptive Processing (STAP) techniques is described as to obtain optimal results in detection scenarios where the target signal is weak and severe dynamic interference is present. It is stated that although STAP techniques were initially developed for the detection of exoclutter airborne targets with low RCS, they are currently used for Ground Moving Target Indication (GMTI) purposes on aerial reconnaissance platforms. The problem at hand is explained by stating that due to the motion of the radar platform, clutter returns are spread in the Doppler spectrum and mask the target returns, thereby making the detection process difficult. Non-adaptive

techniques such as the Displaced Phase Center Antenna (DPCA) technique are stated to be only performing well in the detection of large ground targets and resulting in several false alarms otherwise. It is claimed that electronic countermeasures such as jamming make the problem even worse. Adaptive processing in GMTI is stated to be an active research topic due to the need to detect targets buried under interference while maintaining the number of the false alarms low.

It is also stated in [1] that in traditional STAP algorithms, an interference covariance matrix is estimated using secondary range bins that are symmetrically placed around the primary cell under test, and the obtained estimate is used to provide interference suppression for the primary cell. This technique is stated to be relying on the assumption that the data in the secondary range bins is homogeneous and represent the interference in the primary range cell in a statistically accurate manner. It is asserted that in numerous real world scenarios such as airborne surveillance over urban or land-sea transition areas non-homogeneities exist, and result in substantial degradation of performance due to the violation of the underlying assumption of homogeneity. In order to distinguish homogeneous and non-homogeneous range cells, the use of a Non-Homogeneity Detector (NHD) is proposed. It is cited that by this manner, the performance degradation due to non-homogeneous training data is minimized.

The detection process of weak targets using a STAP implementation is described to be consisting of at least three steps, which are the NHD, a statistical process to be used on the homogeneous data and a hybrid process to be used on non-homogeneous data [1]. The non-homogeneities in the data are stated to be able to exist in a distributed or a localized manner in the environment. The distributed case is stated to be present when there are two or more kinds of terrain included in the illuminated area and is claimed to be counterable by means of generating a knowledge database of the illuminated terrain. A priori information such as map data or information from previous passes over the same terrain are given as examples which could be used in the afore-mentioned database. The second case is described as the discrete non-homogeneity case, and is stated to be present in environments that include urban areas, natural or man-made features or large targets in transmit sidelobes. The paper claims to address the issues regarding the second case.

The structure of the NHD is explained and two advantages of the aforementioned technique is listed [1], the first one being the reduction in false alarm count, and the second one being the ability to detect weak targets that were previously suppressed by the existence of another target in the secondary data; therefore the improvement in the detection performance. Further steps are given regarding the processing of homogeneous and non-homogeneous data and obtained results are given for real and injected data. Results show that the proposed technique results in a lower number of false alarms and improves detection performance by allowing the detection of previously undetected targets. The paper concludes in stating that the Knowledge Based STAP is an active research topic, and points to future work by stating the need for making decisions on which algorithm to use under changing conditions.

In [2], $\Sigma\Delta$–STAP is introduced as a GMTI technique for a forward looking radar. The optimal filter implementation for the case of homogeneous interference with a known covariance is given and it is stated that in real world scenarios the covariance matrix must be estimated using secondary data sets since it is not known beforehand. The need for reduced dimension STAP techniques is explained by stating that to estimate covariance matrices of higher dimensions larger secondary data sets need to be used, which in turn yields in worse estimates in the case of non-homogeneous environments.

Fully adaptive and partially adaptive cases of $\Sigma\Delta$–STAP is explained [2]. The adaptive weights for the fully adaptive case are shown to be calculated by means of a diagonally loaded sample covariance matrix. It is stated that for even moderate values of the number of processed pulses, the computational requirements of the fully adaptive approach is too cumbersome for real-time implementations. Afterwards, the partially adaptive case is introduced by describing the Pre-Doppler and the Post-Doppler approaches. Using a simulation tool called RLSTAP, Minimum Detectable Velocity (MDV) performance values are shown to be obtained for the fully adaptive and the partially adaptive techniques. It is concluded that partially adaptive methods provide good GMTI performance while maintaining low computational complexity.

In [3], a clutter suppression technique using STAP with sum and difference beams is presented. It is stated that the proposed approach can be implemented with ease

for airborne radar systems that already employ sum and difference beams for other purposes, which is stated to be a substantial practical advantage. The infrastructure for the proposed $\Sigma\Delta$–STAP technique is given, and processing steps such as non-homogeneity detection and sample selection are stated to be implementable as necessary.

By means of injecting a target signal on a real flight data obtained by the Multi Channel Airborne Radar Measurements (MCARM) system, performance values are obtained for the cases of $\Sigma\Delta$–STAP with Doppler domain localized (DDL) processing using the Modified Sample Matrix Inversion (MSMI) approach, Factored approach (FA) STAP using the Modified Sample Matrix Inversion (MSMI) approach, and the traditional pulse Doppler radar with cell-averaging constant false alarm rate (CA-CFAR) processing approach [3]. It is shown that the $\Sigma\Delta$–STAP with DDL processing using the MSMI approach can provide clutter suppression performances close to other approaches which employ many more channels. In conclusion, the advantages of the proposed approach and the limitations are presented.

In [4], a knowledge-aided method is proposed for use in covariance estimation during STAP processing of data which includes non-homogeneous clutter signals. The proposed technique is stated to be combining a priori data and observations in order to reduce detection performance loss due to errors in the estimation process of the clutter covariance. The proposed method is applied to both real and simulated data, and performance results are given.

It is stated that in traditional STAP methods, secondary data is used for training during the estimation process of the covariance matrix for the cell under test, which is an approximation to the optimal known covariance solution [4]. This implementation relies on the assumption that independent and identically distributed training data exists. In real life scenarios however, changes in clutter reflectivity, existence of target-like signals in training data and clutter discretes result in heterogeneous or non-IID data, and lead to errors in the covariance matrix estimation process. Consequently, the output SNR is degraded or the false alarm rate is increased.

The ratio of the SINR at the output of the adaptive filter to the optimal SINR is shown to have an expected value as below [4], [5].

$$E\left\{SINR|_{\hat{w}_k}/SINR|_{\hat{w}_{k/opt}}\right\} = (L + 2 - MN)/(L + 1) \qquad (1.1)$$

where $L$ denotes the number of samples used for the estimation of the covariance matrix, $M$ denotes the number of pulses in a coherent processing interval (CPI) and $N$ denotes the number of antenna elements. It can be seen that in order to obtain an SINR performance which is 3 dB worse than the optimal performance, at least $L = 2MN$ samples have to be used.

In [6], it is stated that the Defense Advanced Research Projects Agency (DARPA) has been leading the development of the first real-time knowledge aided (KA) radar architecture for the past years, aiming to address the issue of complex operational environments that include rapidly changing interference characteristics. DARPA's knowledge aided sensor signal processing and expert reasoning (KASSPER) program is stated to be designed for combining high resolution environmental knowledge with the adaptive space time beamforming process. The paper claims to provide an overview of the KASSPER program and give information about the advantages of the knowledge aided adaptive radar.

KA processing is stated to be separable into two separate approaches: the first one being named "Intelligent Training and Filter Selection" (ITFS), and the second one being "Bayesian Filtering and Data Prewhitening" [6]. The first case is described as the indirect use of a priori knowledge sources such as digital terrain and elevation data or SAR images for use in training data selection during the adaptive filter training process. Whereas for the second case it is stated that the aim is to improve the adaptation performance in heterogeneous clutter by making use of the prior knowledge directly in the filter. The second approach is cited to be also known as the blending or the colored loading techniques. Example results are given for both cases, showing improvements in target detection and clutter suppression performances.

In [7], a structure is developed to integrate external knowledge into the space-time beamformer of airborne radars. The proposed technique is stated to combine the a priori knowledge sources and the observed radar data, therefore lowering the sample support requirements for the space-time beamformer. The technique is applied to both full DoF and reduced DoF algorithms, and performance results are given for

simulated X-band radar data.

The reasoning behind DARPA's knowledge-aided sensor signal processing and expert reasoning (KASSPER) program is explained in [7] as the intention to develop radar signal processing techniques that make use of external knowledge sources about the operating environment that are known beforehand. Example knowledge sources are listed as digital terrain maps, land coverage data and the locations of structural features on the terrain. The goal of the paper is described as improving the convergence properties of adaptive filters used in clutter suppression in GMTI radar by making the training process more localized, therefore obtaining better detection performance in heterogeneous clutter environments.

It is also stated in [7] that knowledge sources can be incorporated either directly or indirectly when forming the beamformer output. The indirect use case focuses on the selection of training data based on terrain feature databases such as DTED maps or road network databases, whereas the direct use case aims to create nulls in the beamformer response at the locations of known interference sources. The direct use approach is stated to be followed, in which a site-specific clutter covariance model is used for determining constraints for the beamformer response.

Initially, the space-time model for the interference signal is introduced and by using the aforementioned model, the covariance matrix for clutter is obtained [7]. Afterwards, the Covariance Matrix Tapering (CMT) theory is invoked and it is shown that the clutter covariance matrix consists of a known and an unknown component. The aim of the following work is explained as suppressing the aforementioned components by making use of both deterministic and adaptive filtering.

After this step, full DoF STAP optimization problem is considered and constraints for the minimum variance space-time beamformer are introduced [7]. One of the constraints restricts the beamformer solution to be nearly orthogonal to the a priori covariance matrix by making use of the a priori knowledge. The solution given to the problem is shown to include a diagonal loading term and a colored loading term in addition to the sample covariance matrix. This is explained as the combination of the information in the sample covariance matrix and the a priori model. Afterwards, it is shown that the obtained solution can be converted to a two-stage filtering

6

solution, where the first stage performs the whitening operation on the data and the second stage calculates the adaptive beamformer weights using the whitened data. It is asserted that this implementation is shown to yield lower rank interference in the adaptive beamforming stage, which is required for lower sample support. It is also stated that using SAR images for determining and prefiltering clutter discretes and applying adaptive processing afterwards provides better false alarm performance.

Reduced DoF STAP is introduced for the cases where full DoF implementation is not applicable due to computational complexity and low sample support [7]. Transformation from the full DoF case to the reduced DoF case is given and the focus of work for the reduced DoF case is stated to be the technique known as multibin element-space post-Doppler STAP. Similar to the full DoF case, constraints are introduced to obtain the post Doppler weights. The obtained solution to the reduced DoF optimization problem is shown to have the same form as the full DoF case, including the colored and diagonal loading terms. The only difference is stated to be the inclusion of the reduced DoF versions of the data and steering vectors, together with the loading matrices.

The results obtained for the simulated KASSPER data set are presented and compared for the multi-bin post-Doppler implementation of the perfectly known covariance, sample matrix inverse and loaded covariance matrix cases [7]. The data set is stated to include heterogeneous clutter and array calibration errors. Results show that in the sample matrix inverse multi-bin Post Doppler case, due to the relatively large size of the training data, the clutter notch is wider compared to the loaded covariance matrix and optimal cases. Whereas in the diagonally and colored loaded cases, the clutter notch width is seen to be more adaptive, which is stated to provide better detection performance for targets with low radial velocities. Results for the loaded covariance matrix cases are compared for different number of samples in the training data and Pd and SINR loss values are shown.

In [8], the approach to the interference cancellation problem is explained as a two step process. It is stated that by initially cancelling the known interference component and applying adaptive processing afterwards, the solution to the problem will require fewer DoFs. It is claimed that the aforementioned approach provides local-

ization in training data and can perform in limited sample support cases, therefore providing better performance in heterogeneous clutter environments. Example applications are given as distributed clutter environments, discrete clutter environments and a combination of the two.

It is stated that the proposed approach can be applied in both the data domain and the reduced DoF domain as a pre-filter [8].

Knowledge-aided STAP weights are calculated and applied to both simulated (KASSPER) and real (TUXEDO) data, which include heterogeneous clutter, ground vehicles, ICM and calibration errors [8].

Obtained results are given for both traditional STAP and KA-STAP scenarios [8]. Results show that traditional STAP yields a wider clutter notch if the size of the training window is wider than that of the clutter features, which results in poorer MDV performance. Whereas KA-STAP provides closer to optimum performance by means of using low sample support together with colored or diagonal loading of the interference correlation matrix.

Discrete clutter colored loading technique is explained for Post-Doppler STAP [8]. In this technique, first a low resolution SAR map is generated and thresholded to detect discrete clutter. Then the space-time response for each clutter discrete is calculated. Afterwards, range dependent loading matrices are calculated for each Doppler bin in the post-Doppler space and are added to sample covariance matrices. Finally, the STAP processor is executed using the loaded covariance matrices at hand. Example values for the colored and diagonal loading levels are given with respect to the thermal noise level.

Composite colored loading technique is given for the case of simultaneously addressing distributed and discrete clutter [8]. In this technique, adding two separate loading matrices to the sample covariance matrix is proposed.

Detection summary is given for traditional STAP, STAP with distributed clutter colored loading and STAP with composite colored loading [8]. Results show that while the number of detections related to the actual target is close in all cases, traditional STAP yields in the maximum number of false alarms. On the contrary, composite

colored loading is seen to result in the least amount of false alarms.

In summary, it is asserted in [8] that colored loading techniques typically yield fewer false alarms when low sample support is required. Colored loading with the information obtained from SAR maps is stated to reduce the under-nulling strong of clutter discrete. Future work is described as focusing on detailed analysis and simulations for the determination of colored loading levels.

A KA STAP based adaptive GMTI algorithm for use in heterogeneous environments is proposed in [9]. It is cited that in non-homogeneous environments, STAP performance can be substantially degraded. To address this issue, colored loading and data pre-whitening techniques are given as examples to the KA STAP processing approaches. Example sources of a priori data are given as DTED maps, SAR images and hyperspectral imagery.

The underlying models for the received signal and covariance matrices are described and afterwards the proposed algorithm is explained. The proposed architecture for the detection process involves the linear combination of the sample based covariance matrix with the a priori one, and the algorithm flow is described in six steps [9]. The first step is defined as the calibration of the received data for array errors. Afterwards, the calibrated data is used to form K seperate SAR maps for the K receiving channels. In the next step, the a priori covariance matrices are formed. Next, the sample covariance matrices are estimated. Afterwards, the matrices at hand are linearly combined and the adaptive filter coefficients are obtained by means of the newly obtained covariance matrices. In the final step, CFAR processing is performed and target parameters are estimated.

Obtained results for the experimental data show that although for large sizes of sample support the KA method performs similarly to the traditional Sample Matrix Inversion (SMI) case, for smaller numbers the KA method provides improvements of about 10–15 dB [9]. The paper concludes in stating that the proposed KA method has fast convergence properties due to its low sample support requirements, and therefore claims that the proposed method will perform in a more robust manner in non-homogeneous clutter environments compared to the SMI case.

In [10], the concept of covariance matrix tapering is introduced and is stated to be the solution to a minimum variance optimum beamforming problem in which an additional stochastic process that is related to the original process by a Hadamard product exists. It is asserted that CMT's can be used to address problems such as insufficient sample support and non-stationary interference. The covariance matrix tapering techniques presented previously by Mailloux and Zatman are stated to be unified and explained. A two dimensional CMT which aims to yield more robust clutter cancellation in space time adaptive processing applications is also presented.

It is also stated in [10] that issues such as finite sample support, existence of non-stationary processes and array calibration errors, and computational complexity requirements can be the causes of the need for robust adaptive array beamforming. It is stated to be shown that estimation errors in the noise subspace eigenvalues can yield substantial degradation of the antenna array sidelobe levels as well as possible distortion of the mainlobe when a direct application of the sample matrix inverse is used. To address this problem, diagonal loading of the sample covariance matrix is proposed. It is stated that by using the aforementioned technique, low sidelobe levels can be achieved with as few as 1N–2N samples for N degrees of freedom. On the contrary, it is cited that an i.i.d. sample support of size several orders of magnitude greater than 2N is necessary to obtain the same low sidelobe levels in the case of the SMI beamformer implementation.

Obtained results are presented for an example scenario in which a jammer exists and optimal, SMI, diagonally loaded and Mailloux-Zatman CMT beamformer techniques are used [10]. It is seen that the SMI case yields in degraded sidelobe levels when 2N samples are used, whereas the diagonally loaded and the Mailloux-Zatman CMT cases present close to optimal results.

The presented 2D CMT for STAP is claimed to be advantageous in scenarios where large clutter discretes exist or there is a mismatch in the adaptive filter weights which cause undernulled clutter [10].

## 1.2  Previous Related Work in METU EEE Department

The work done in this thesis is a part of a research field which focuses on Ground Moving Target Indication and Space Time Adaptive Processing. The following research work has been done in the past related to the research area of this thesis and has been resourceful during the development of the work done in this thesis.

- The title of the first thesis is called "Simulation Based Comparison of Some GMTI Techniques" [11]. The work done in this thesis aims to compare the detection performances of several GMTI techniques such as DPCA, ATI and STAP by means of using simulated radar data.

- The second thesis is titled "Antenna Patterns for Detecting Slowly Moving Targets in Two Channel GMTI Processing" [12]. This thesis focuses on obtaining optimal antenna patterns for a two channel radar sensor in an attempt to optimize detection performance of endoclutter targets.

- The final thesis is called "Interference Suppression by Using Space Time Adaptive Processing for Adaptive Radar" [13]. This thesis establishes the space-time signal model and uses simulated data in order to compare the detection performances of the DPCA and the Optimal STAP techniques.

## 1.3  Thesis Motivation and Objective

Detection of ground targets in heterogeneous clutter environments is difficult to perform. While traditional adaptive processing approaches rely on the homogeneous interference assumption, real life test scenarios include the following situations:

- Clutter transition areas, such as coastal areas or woods – open fields,

- Target like signals (TSDs) contaminating the training data, such as other real targets or discrete clutter returns from manmade objects.

Such issues result in an increase in the number of false alarms due to undernulled or overnulled clutter, and cause suppressed target returns, yielding degraded detec-

tion performance. However, it is shown in the literature that it is possible to obtain better detection performance by means of applying additional processing steps which address these issues. The aim of this work is to make use of instantaneous and a priori knowledge sources in an attempt to improve STAP detection performance in previously mentioned situations. In order to achieve this goal, we propose a knowledge aided space-time processing approach which makes use of several additional processing blocks that precede the adaptive beamforming step.

Previous work done on this subject include separate studies on:

- Using a priori knowledge sources for the segmentation of homogeneous regions,

- Using Digital Terrain Elevation Data (DTED) and National Land Cover Data (NLCD) for selecting STAP training data,

- Using non homogeneity detectors in order to eliminate clutter discretes and target like signals which are contaminating the STAP training data.

The work done in this thesis aims to:

- Form a novel knowledge aided processing approach which combines the previously mentioned approaches while suggesting new types of information, which are readily available or obtainable, as sources of a priori knowledge,

- Present results obtained with the application of the proposed processing approach to real flight data obtained with the experimental SAR system.

The proposed processing approach is based on the reduced rank implementations of the space time adaptive processing, which was investigated in detail in previous research work done in METU EEE [11], [12], [13]. The work done in this thesis aims to perform the following operations in addition:

- Use the a priori knowledge in order to determine the homogeneous regions in the area of interest,

- Remove discrete non-homogeneities that may exist in the STAP training data,

- Perform a blending operation on the estimated and the a priori data,

- Reduce the size of the required sample support for STAP.

This approach is implemented and applied to the GMTI data acquired during flight trials with the experimental SAR system. Our results indicate the following improvements:

- Detection of previously undetected targets,

- Better detection performance for targets which are close together in range.

## 1.4 Thesis Outline

Chapter 1 briefly summarized the literature so far on STAP, reduced rank methods and knowledge aided approaches. Chapter 2 will introduce the space-time signal model, and present the full rank implementation and some of the reduced rank implementations of STAP. Chapter 3 will briefly introduce sources of knowledge which are commonly used in the literature for knowledge aided processing approaches and present the NHD and the colored loading methods. Chapter 4 will put forward a novel knowledge aided signal processing architecture which comprises of several blocks that make use of a priori and instantaneous data, and afterwards investigate the performances for the proposed approaches. Chapter 5 concludes the thesis.

# CHAPTER 2

# SPACE TIME SIGNAL PROCESSING CONCEPTS

For an airborne radar, clutter returns are coupled in azimuth angle and Doppler. Figure 2.1 depicts a geometrical representation of the clutter environment for an airborne radar. If a jammer also exists, the spectrum of the observed space-time data snapshots will be similar to the illustration depicted in Figure 2.2 [14].
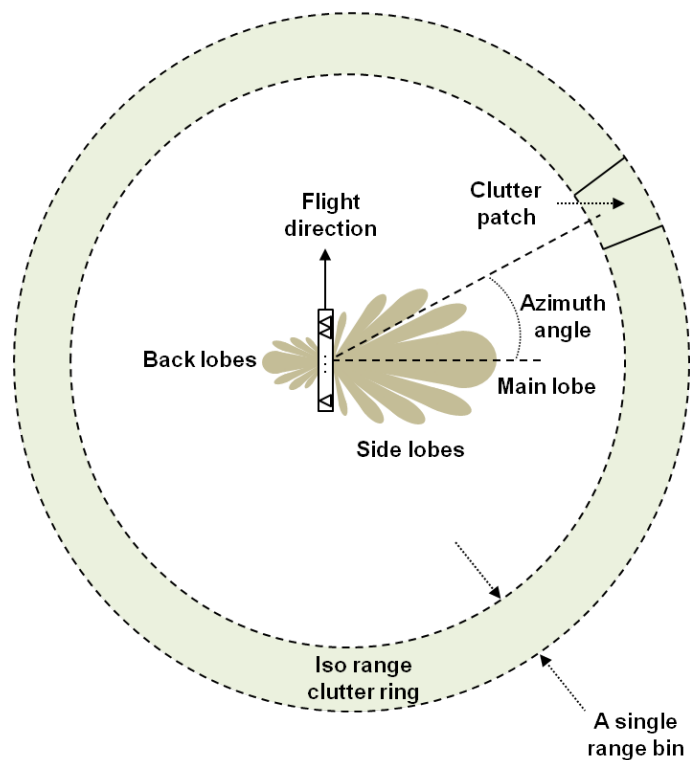


Figure 2.1: Geometrical representation of the interference environment for an airborne radar.
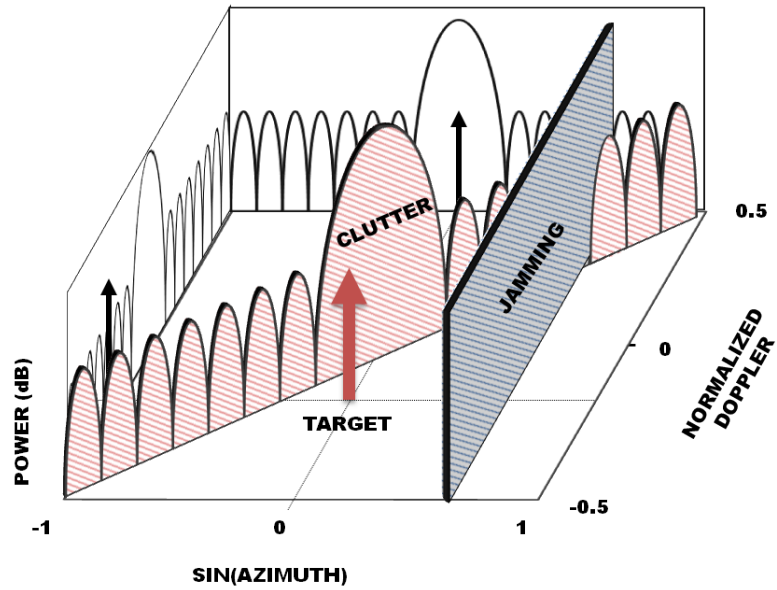
Figure 2.2: Spectral representation of the interference environment for an airborne radar.

It can be seen that although the target velocity is different than zero, target returns can still be buried under the clutter spread due to the motion of the platform. With the addition of the jammer signal, the detection problem becomes even more difficult. Space Time Adaptive Processing (STAP) aims to filter out the interference signals by means of adaptively constructing and applying a multidimensional finite impulse filter (FIR) to the received radar echoes. An example space time beamformer is depicted in Figure 2.3. In the following sections the space time signal model is introduced and full rank and reduced rank implementations of STAP are described.

15
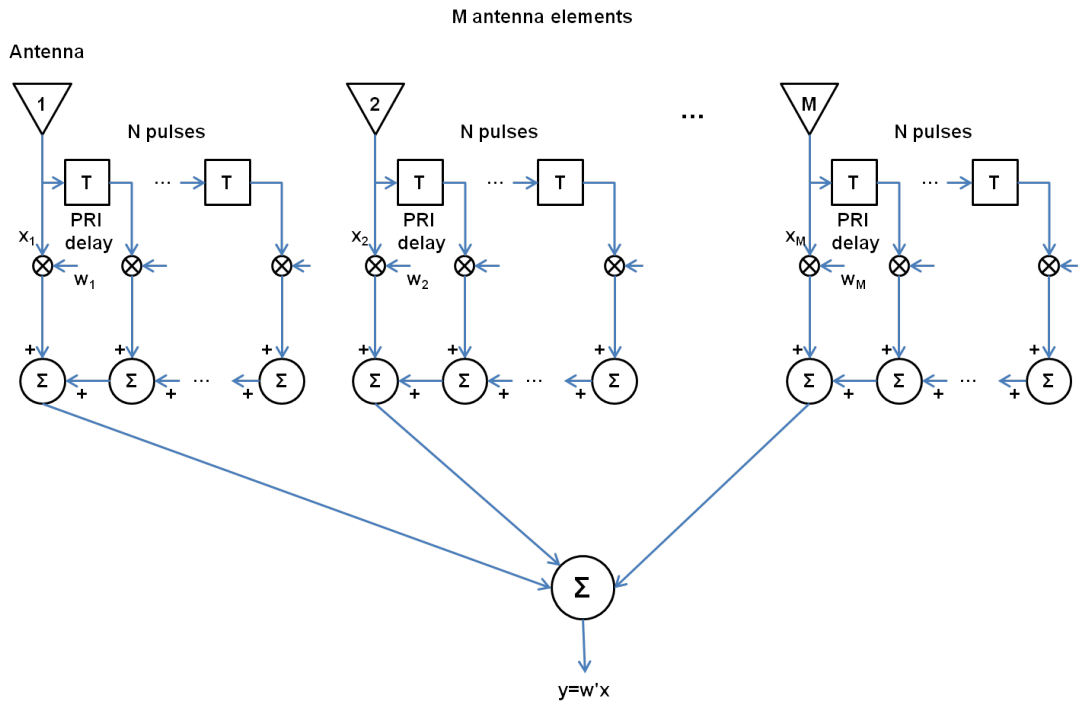
Figure 2.3: An example STAP beamformer. The delay lines represent the slow time samples (pulses). Samples which are obtained from different receiver channels and different time delays are combined by means of an adaptive filtering process, and a single output is obtained for every range bin.

## 2.1 Space Time Signal Model
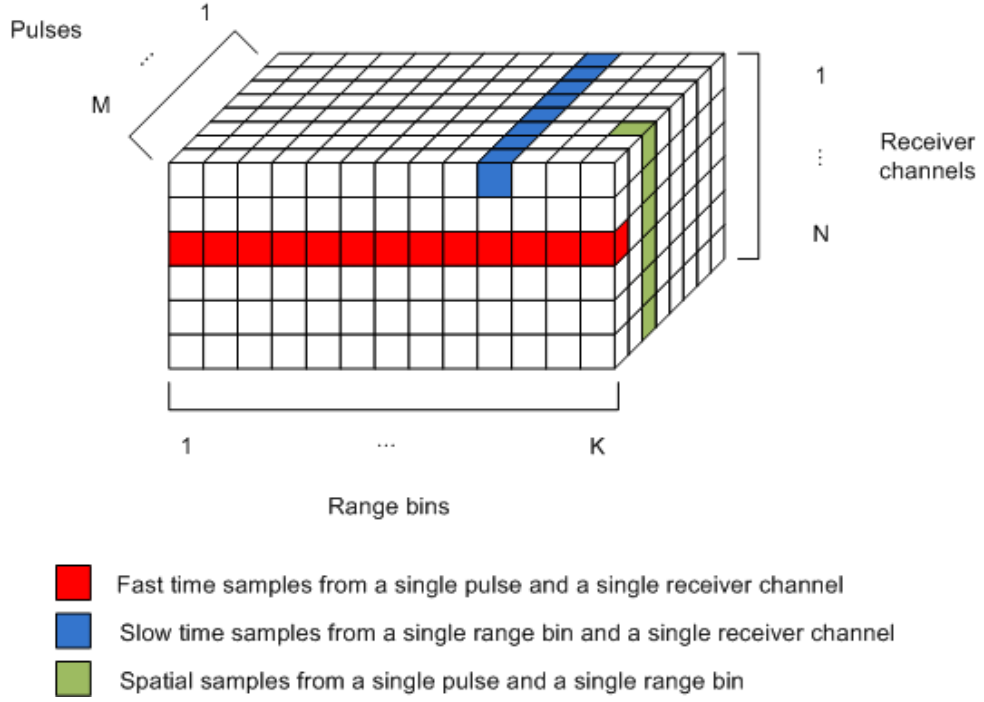


Figure 2.4: The space - time radar data cube.

In coherent radar signal processing, a Coherent Processing Interval (CPI) represents the time duration in which a number of slow time samples are phase coherently integrated. Figure 2.4 depicts the radar data cube of size $MxNxK$ for a system which uses an $M$ channel receiver array, $N$ pulses in one Coherent Processing Interval (CPI) and $K$ range bins. Let $\mathbf{r_k} \in C^{MN \times 1}$ denote the space-time observation vector for a single range bin $k$. Equation 2.1 states the binary detection hypotheses, where $H_0$ corresponds to the case in which no target is present and $H_1$ indicates that a target exists.

$$H_0 : \mathbf{r_k} = \mathbf{c_k} + \mathbf{n_k}$$
$$H_1 : \mathbf{r_k} = \alpha_T \mathbf{s} + \mathbf{c_k} + \mathbf{n_k}$$

(2.1)

$\mathbf{c_k} \in C^{MN \times 1}$ and $\mathbf{n_k} \in C^{MN \times 1}$ denote the space-time observations related to clutter and uncorrelated noise respectively. $\alpha_T \in C$ denotes the target amplitude and $\mathbf{s} \in C^{MN \times 1}$

17

represents the space-time observations associated with the target returns.

## 2.2 Optimum (Full Rank) STAP Implementation Approach

Assuming that $\mathbf{c_k}$ and $\mathbf{s}$ are uncorrelated, the optimum detector for the given problem is stated as the following in [12].

$$\left|\mathbf{s^H} R^{-1} \mathbf{r_k}\right|^2 \lessgtr \xi \tag{2.2}$$

where $R$ denotes the interference covariance matrix, which is obtained as

$$R = E\left\{(\mathbf{c_k} + \mathbf{n_k})(\mathbf{c_k} + \mathbf{n_k})^\mathbf{H}\right\} \tag{2.3}$$

This detector corresponds to the optimum filter coefficients $\mathbf{w}$ such that

$$\mathbf{w} = R^{-1}\mathbf{s} \tag{2.4}$$

Consequently,

$$\left|\mathbf{w^H r_k}\right|^2 \lessgtr \xi \tag{2.5}$$

As stated in [5], the full rank approach requires a total of at least $2MN$ i.i.d. samples for the covariance estimation process in order to yield an $SINR$ loss of 3 dB or better with respect to the optimal known covariance case. However, due to computational complexity issues and clutter heterogeneity, this requirement is rarely satisfied in real life test scenarios. Therefore, in an attempt to reduce the size of the required secondary data, various approaches are presented in the literature for reducing the number of Degrees of Freedom (DoF). Section 2.3 briefly introduces some of these concepts.

## 2.3 Reduced Rank STAP Implementation Approaches

Various reduced rank approaches which are found in the literature are described and compared in [12]. For purposes of completeness, they will be briefly introduced in the following subsections. Figure 2.5 illustrates various reduced rank methods and the relations between them [12].
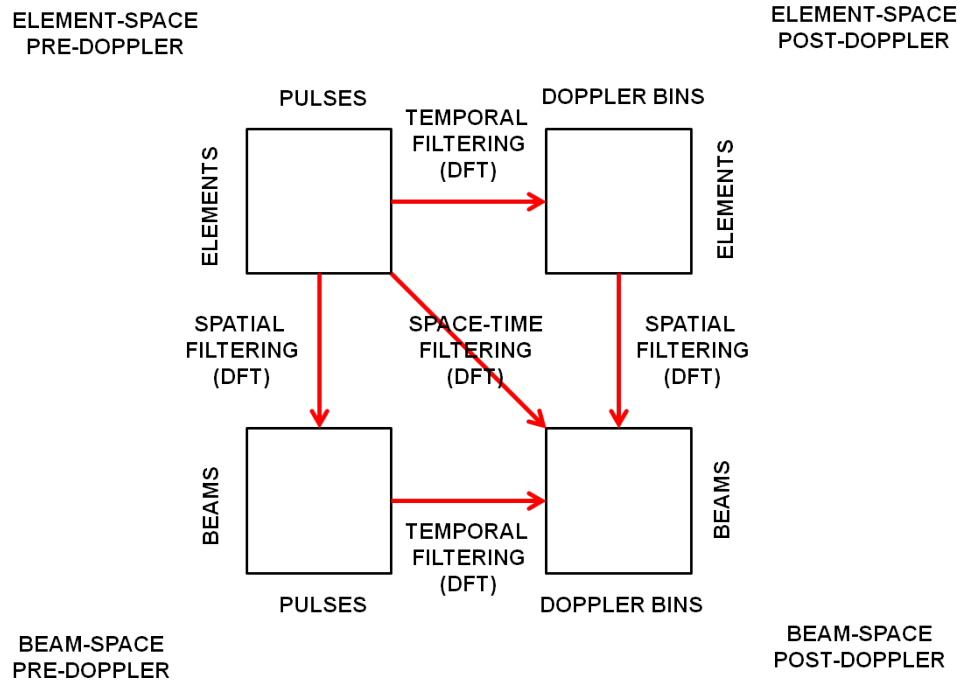


Figure 2.5: Comparison of the reduced rank STAP architectures.

## 2.3.1 Element Space Pre Doppler

Element space pre Doppler approaches aim to form sub-CPIs from the original CPI data matrix and calculate the space-time adaptive filter weights for these sub-CPIs. Afterwards, the filter weights are applied to the sub-CPI data matrices. Doppler filtering is performed in the final step to provide coherent integration gain and Doppler separation of targets. Since the adaptive filter weights of each sub-CPI perform a DPCA-like operation, this technique is also known as "Adaptive DPCA". In this technique, full spatial adaptivity is preserved and it is stated that jamming and clutter can

be suppressed at the same time. It is also asserted that this approach can be useful for changing environments such in the case of radar systems with rotating antennas [15].

### 2.3.2 Element Space Post Doppler

In the element space post Doppler approach, Doppler filtering is performed on the pulses obtained from each antenna element. The case in which only one Doppler bin is used is known as the factored Post Doppler approach, and requires that separate spatial adaptive processing is performed for each Doppler bin [15], [16]. The case in which more than one Doppler bin is used is known as the extended factored Post Doppler approach [16].

Figure 2.6 depicts the element space post Doppler rank reduction concept, where $T_{PRI}$ denotes the pulse repetition interval of the radar sensor.
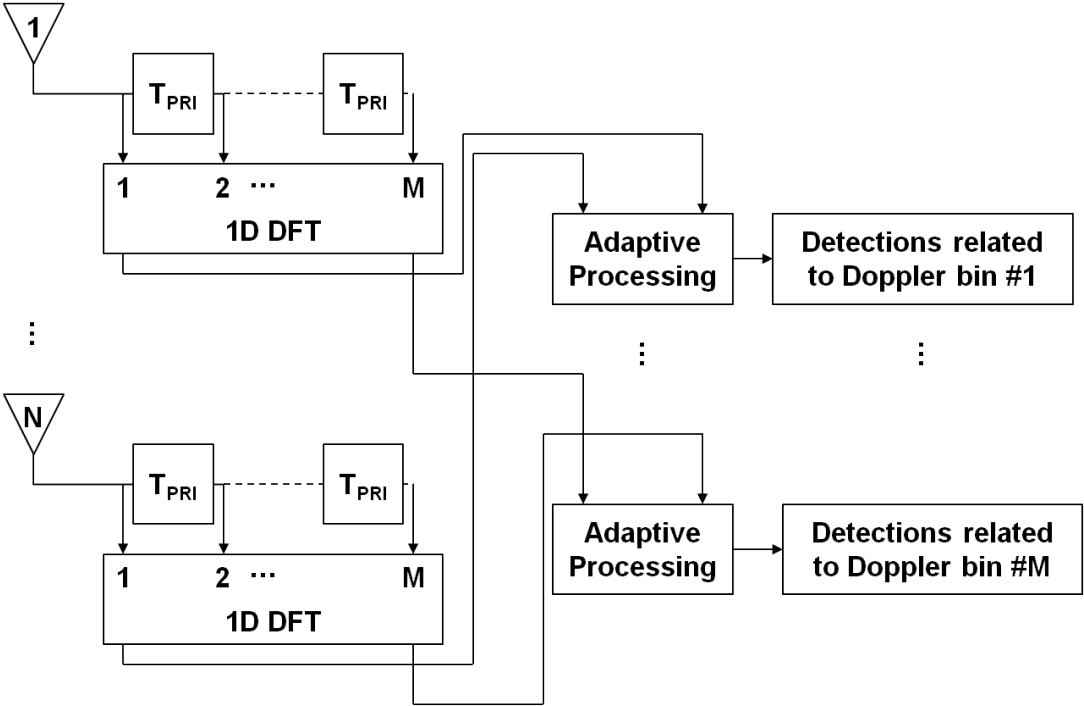


Figure 2.6: The element space post Doppler rank reduction concept.

Thus, the rank reduction matrix for the element space post Doppler case can be written as the following.

20

$$\mathbf{D_m} = \begin{bmatrix} \mathbf{I_{NxN}} \\ \mathbf{w_m^1 I_{NxN}} \\ \vdots \\ \mathbf{w_m^{M-1} I_{NxN}} \end{bmatrix} \tag{2.6}$$

where $\mathbf{D_m} \in C^{MNxN}$ denotes the rank reduction matrix corresponding to the $m^{th}$ Doppler bin, and $w_m$ is the complex Discrete Fourier Transform coefficient corresponding to the $m^{th}$ Doppler bin and the $i^{th}$ pulse, which is given as

$$w_m^i = exp(j2\pi f_m T_{PRI}) \tag{2.7}$$

Thus, the reduced rank versions of the space time observations and the covariance matrix are obtained as follows.

$$\mathbf{r_D} = \mathbf{D^H r} \tag{2.8}$$

and

$$\mathbf{R_D} = E\left\{\mathbf{r_D r_D^H}\right\} = E\left\{\mathbf{D^H r r^H D}\right\} = \mathbf{D^H} E\left\{\mathbf{r r^H}\right\} \mathbf{D} = \mathbf{D^H R D} \tag{2.9}$$

$$\mathbf{s_D} = \mathbf{D^H s} \tag{2.10}$$

where $\mathbf{r_D}$, $\mathbf{R_D}$ and $\mathbf{s_D}$ denote the reduced rank versions of the space time observations, the covariance matrix, and the target signal model respectively. $(\ )^\mathbf{H}$ denotes the Hermitian transpose operation.

### 2.3.3 Beam Space Pre Doppler

Beam space pre Doppler approaches aim to use the pulses received from each antenna element for beamforming for rank reduction purposes, which is stated to be a more practical approach than element space techniques for large array antennas [15]. After the beamforming process, sub-CPIs are formed from the desired beams. Similar to the element space pre Doppler case, Doppler filtering is performed in the final step. Displaced phase center antenna (DPCA) method is an example implementation of this approach.

Let $\mathbf{r} \in C^{NMx1}$ denote the space-time observations of a single range bin which are received from $N$ receiver channels for a total of $M$ pulses. $\mathbf{r}$ can be written as

$$\mathbf{r} = \begin{bmatrix} \mathbf{r}_1 \\ \mathbf{r}_2 \\ \vdots \\ \mathbf{r}_m \\ \vdots \\ \mathbf{r}_M \end{bmatrix} \tag{2.11}$$

where $\mathbf{r}_m$ denotes $N$ channel space-time observations corresponding to the $m^{th}$ pulse. Beam space pre Doppler approach combines the elements of $\mathbf{r}_m$ by applying beamformer weights in order to perform the rank reduction process. Figure 2.7 shows the beam space pre Doppler rank reduction concept.
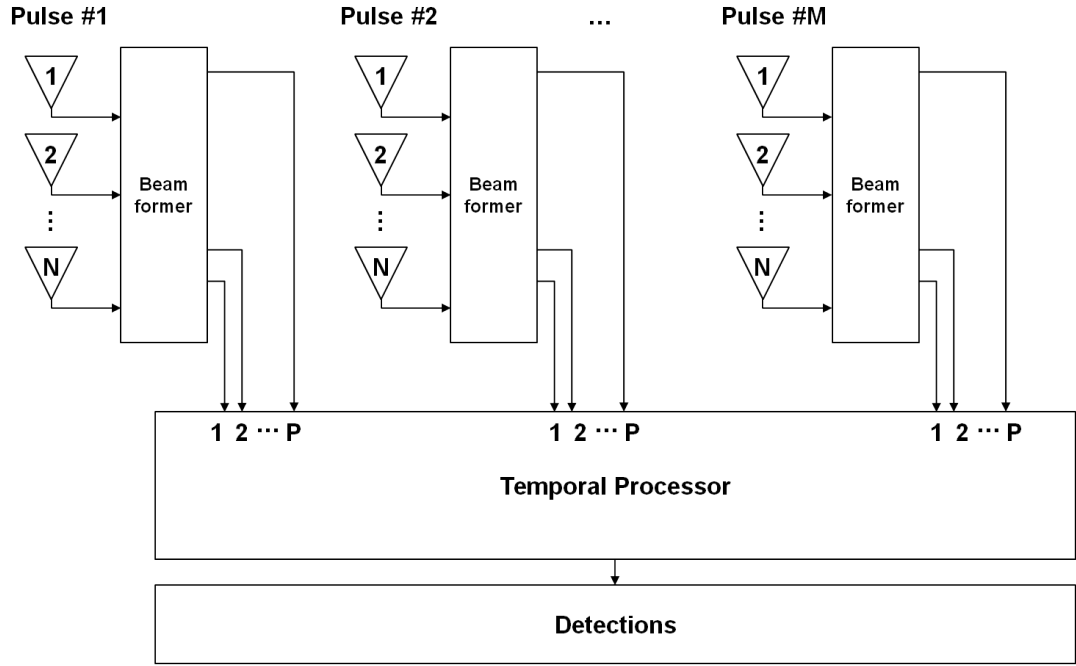
Figure 2.7: The beam space pre Doppler rank reduction concept.

where $P$ denotes the total number of beams at the output of the beamformer. Thus, the transformation matrix $\mathbf{H} \in C^{NMxPM}$ which is used for the rank reduction process can be written as

$$
\mathbf{H} = \begin{bmatrix}
\mathbf{w}_{11} & \mathbf{w}_{21} & \ldots & \mathbf{w}_{P1} & & \mathbf{0}_{Nx1} & \ldots & \ldots & \mathbf{0}_{Nx1} \\
\mathbf{0}_{Nx1} & \ldots & \ldots & \mathbf{0}_{Nx1} & & \vdots & & \vdots \\
\vdots & & \vdots & & \ldots & \mathbf{0}_{Nx1} & \ldots & \ldots & \mathbf{0}_{Nx1} \\
\mathbf{0}_{Nx1} & \ldots & \ldots & \mathbf{0}_{Nx1} & & \mathbf{w}_{1M} & \mathbf{w}_{2M} & \ldots & \mathbf{w}_{PM}
\end{bmatrix}
\tag{2.12}
$$

where $\mathbf{w_{ij}} \in C^{Nx1}$ denotes the beamformer coefficients. The beamformer creates a total of $P$ beams for every pulse received from the $N$ channel receiver array. Therefore, the rank reduction operation requires that $P < N$. The reduced rank versions of the space time observations and the covariance matrix are obtained as follows.

$$\mathbf{r_B} = \mathbf{H^H r} \tag{2.13}$$

and

$$\mathbf{R_B} = E\left\{\mathbf{r_B r_B^H}\right\} = E\left\{\mathbf{H^H rr^H H}\right\} = \mathbf{H^H} E\left\{\mathbf{rr^H}\right\} \mathbf{H} = \mathbf{H^H RH} \tag{2.14}$$

$$\mathbf{s_B} = \mathbf{H^H s} \tag{2.15}$$

where $\mathbf{r_B}$, $\mathbf{R_B}$ and $\mathbf{s_B}$ denote the reduced rank versions of the space time observations, the covariance matrix, and the target signal model respectively.

### 2.3.4   Beam Space Post Doppler

Beam space post Doppler approaches involve both the beamforming and the Doppler filtering processes prior to the adaptive filter weight calculation. This can be implemented by means of a 2D DFT process. It is stated that this approach can provide substantial suppression of clutter in a non-adaptive manner; however in order to suppress clutter and jamming simultaneously, use of more spatial degrees of freedom might be necessary [15].

Figure 2.8 depicts the beam space post Doppler rank reduction concept.
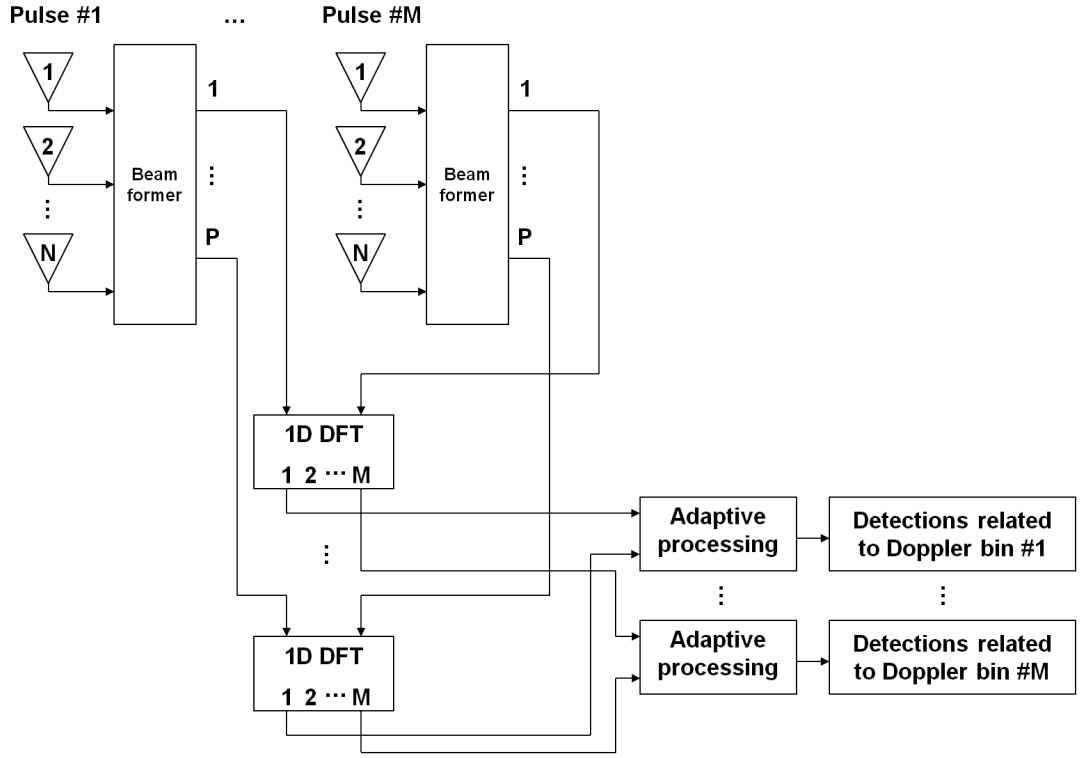
Figure 2.8: The beam space post Doppler rank reduction concept.

Since the beamforming and the Doppler processing steps are performed sequentially, the rank reduction matrix for the beam space Post Doppler case can be stated in terms of the matrices given in Equations 2.6 and 2.12.

$$\mathbf{H_D} = \mathbf{HD} \tag{2.16}$$

The reduced rank versions of the space time observations and the covariance matrix are obtained as follows.

$$\mathbf{r_{BD}} = \mathbf{H_D^H r} \tag{2.17}$$

and

$$\mathbf{R_{BD}} = E\left\{\mathbf{r_{BD}r_{BD}^H}\right\} = E\left\{\mathbf{H_D^H rr^H H_D}\right\} = \mathbf{H_D^H} E\left\{\mathbf{rr^H}\right\} \mathbf{H_D} = \mathbf{H_D^H R H_D} \tag{2.18}$$

25

$$\mathbf{s}_{BD} = \mathbf{H}_D^H \mathbf{s} \qquad (2.19)$$

where $\mathbf{r}_{BD}$, $\mathbf{R}_{BD}$ and $\mathbf{s}_{BD}$ denote the reduced rank versions of the space time observations, the covariance matrix, and the target signal model respectively.

### 2.3.5 Comparison of the Full Rank and the Reduced Rank Approaches

The full rank and the reduced rank processing approaches all offer different advantages, but at costs of various trade-off's. For purposes of comparison, Table 2.1 briefly summarizes the results presented in [12]. It can be inferred that the Element Space Post Doppler processing approach provides reasonable reduction in data and matrix sizes, and offers the means to analyze the effects of using different numbers of range bins in the estimation process. Since it is also the most widely preferred processing approach in knowledge aided STAP literature [7], [8], the Element Space Post Doppler processing approach is adopted in this thesis work.

Table 2.1: Comparison of the Full Rank and the Reduced Rank Approaches

| Processing Approach | Advantages | Disadvantages |
|---|---|---|
| Element Space Pre Doppler | DPCA like operation provides full spatial adaptivity | Greater number of secondary data is required compared to the other rank reduction methods due to the relatively greater number of degrees of freedom remaining after the rank reduction process |
| Beam Space Pre Doppler | Reduction in data and a more focused operation is possible by means of the reduced number of beams<br><br>Provides hardware simplicity with respect to a multi channel receiver system due to the analog RF beamformer | The number of DoFs are reduced without knowledge about the environment due to non adaptive beamforming |
| Element Space Post Doppler | Doppler processing yields a much smaller number of DoFs, which results in the reduction of data and matrix sizes<br><br>Enables the use of efficient matrix operations and provides reduction in computational complexity | Using fewer range bins yields degraded performance, whereas using many results in computational complexity |
| Beam Space Post Doppler | Beam forming along with Doppler processing provides further reduction in the number of DoFs, which results in the reduction of data size and simplification in processing steps | Severe performance degradation is possible due to the great decrease in the number of DoF's |

# CHAPTER 3

# KNOWLEDGE AIDED PROCESSING APPROACHES

Knowledge aided processing approaches aim to make use of the information at hand in order to improve the overall detection performance of a radar. The available information can be instantaneously acquired by the radar sensor or can be obtained from external knowledge databases. For the latter case, sources of a priori knowledge can be incorporated in space time signal processing in an indirect or direct manner [6]. The first method involves selection of training data based on prior information, whereas the second one focuses on using the obtained knowledge during the adaptive filtering process. In the following sections, examples of a priori knowledge sources are given and the aforementioned approaches are explained.

## 3.1 Sources of A Priori Knowledge

Numerous types of a priori knowledge sources are shown to be used in the KA-STAP literature [6], [17], [18]. Digital elevation maps such as Digital Terrain Elevation Data (DTED) and Shuttle Radar Topography Mission (SRTM) data or previously obtained radar imagery such as Synthetic Aperture Radar (SAR) or Doppler Beam Sharpening (DBS) maps can be given as examples for sources of such knowledge. These sources are briefly described in the following sections.

### 3.1.1 Digital Elevation Models

Digital Elevation Models (DEMs) are used for obtaining terrain elevation data in digital form and can be obtained via optical and radar interferometric methods. DEM data are available in various formats which differ in spatial sampling intervals and height accuracies. DTED and SRTM data are examples of DEM products.

#### 3.1.1.1 Digital Terrain Elevation Data

DTED is a DEM product offered by the United States National Imagery and Mapping Agency whose specifications are defined by the MIL-PRF-89020 standard. DTED products provide information about terrain height at equally spaced intervals of latitude and longitude. It is possible to obtain different levels of DTED products, ranging from DTED 0 to DTED 5, which offer different levels of horizontal and vertical accuracies.

Accuracy information for DTED levels of 1 and 2 are given in Table 3.1 [19].

Table 3.1: DTED Levels

| DTED Level | Absolute Horizontal Accuracy | Absolute Vertical Accuracy | Relative Vertical Accuracy | Spatial Resolution |
|---|---|---|---|---|
| DTED-1 | $\leq 50$ m | $\leq 30$ m | $\leq 20$ m | 3 arc sec |
| DTED-2 | $\leq 23$ m | $\leq 18$ m | $\leq 12$ m (slope $\leq 20\%$) <br> $\leq 15$ m (slope $> 20\%$) | 1 arc sec |

where the absolute horizontal accuracy is defined as the 90% circular error with respect to the World Geodetic System (WGS); and the absolute and relative vertical accuracies are defined as the 90% linear errors with respect to the Mean Sea Level (MSL).

### 3.1.1.2 Shuttle Radar Topography Mission Data

SRTM is the product of an international research effort which aimed to obtain Digital Elevation Models for 80% of the Earth's land mass, from 56°S to 60°N [20]. It was completed in February 2000 in 11 days via the X and C band radar systems located aboard the space shuttle Endeavour. SRTM data sets were initially produced by the United States National Aeronautics and Space Administration (NASA), however they are currently offered by the United States Geological Survey (USGS). SRTM data complies to the Interferometric Terrain Height Data (ITHD) 2 specs, which is stated to have sampling intervals of 30 m x 30 m, 16 m absolute x 10 m relative vertical height accuracies and an absolute horizontal accuracy of 20 m [21].

Figure 3.1 depicts the SRTM data which covers all of Turkey. A zoomed view which focuses on the Black Sea coast can be seen in Figure 3.2. Finally, Figure 3.3 presents the georegistered SRTM data which is associated with the region of interest in the aforementioned area. Details of the georegistration process will be presented in Section 4.1.3.
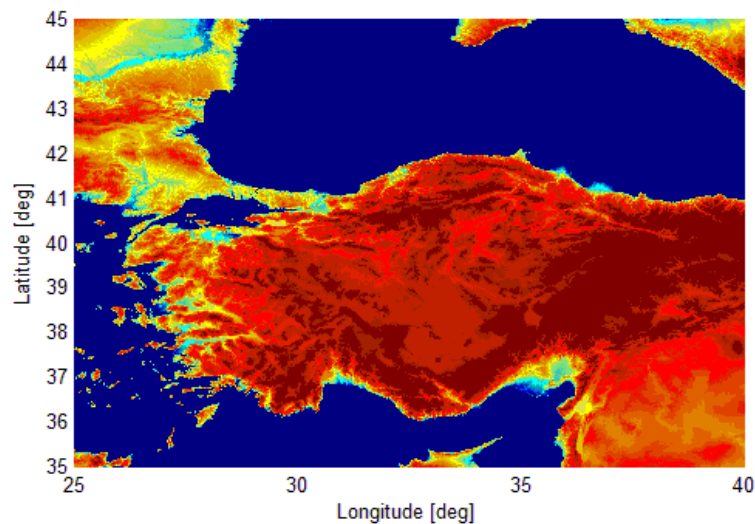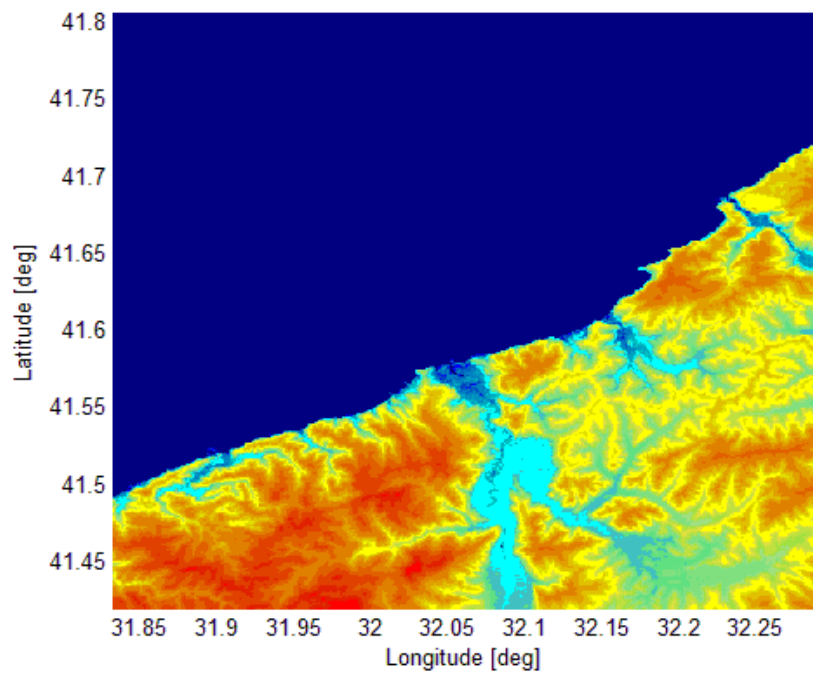


Figure 3.1: SRTM map of Turkey.

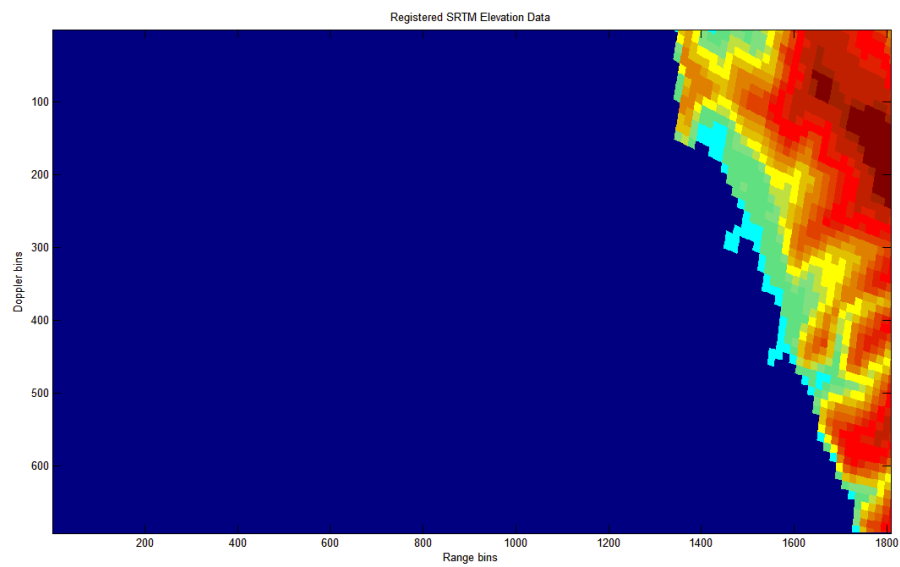Figure 3.2: SRTM map of northern Turkey.



Figure 3.3: Zoomed view of the SRTM map of northern Turkey.

### 3.1.2   Digital Feature Databases

Digital feature database products are a collection of topographic data offered by the United States National Geospatial Intelligence Agency which aims to complement the DTED products by providing information about surface features in the region of interest such as vegetation, land cover, buildings, roadways and infrastructure. One example is the Digital Feature Analysis Data (DFAD) which is a collection of digital cartographic data offered by the United States National Geospatial Intelligence Agency and contains information about surface features such as vegetation, buildings and infrastructure. The DFAD products have a spatial resolution of 1 arc second. Another example is the National Land Cover Data (NLCD), which is a collection of land cover classification data offered by the United States Geological Survey (USGS) and covers most of the United States. The NLCD data products consist of 9 major classifications such as barren land, water, urban areas etc. and include 21 minor classifications such as high intensity residential urban areas, low intensity urban areas. The NLCD data products have a spatial resolution of 30 m.

The land cover classifications of NLCD is given in Table 3.2.

Table 3.2: NLCD Land Cover Classifications

| Code | Major Classifications | Minor Classifications |
|------|----------------------|------------------------|
| 11 | Water | Open Water |
| 12 | Water | Perennial Ice/Snow |
| 21 | Developed | Low Intensity Residential |
| 22 | Developed | High Intensity Residential |
| 23 | Developed | Commercial/Industrial/Transportation |
| 31 | Barren | Bare Rock/Sand/Clay |
| 32 | Barren | Quarries/Strip Mines/Gravel Pits |
| 33 | Barren | Transitional |
| 41 | Forested Upland | Deciduous Forest |
| 42 | Forested Upland | Evergreen Forest |
| 43 | Forested Upland | Mixed Forest |
| 51 | Shrubland | Shrubland |
| 61 | Non-natural Woody | Orchards/Vineyards/Other |
| 71 | Herbaceous Upland | Grasslands/Herbaceous |
| 81 | Herbaceous Planted/Cultivated | Pasture/Hay |
| 82 | Herbaceous Planted/Cultivated | Row Crops |
| 83 | Herbaceous Planted/Cultivated | Small Grains |
| 84 | Herbaceous Planted/Cultivated | Fallow |
| 85 | Herbaceous Planted/Cultivated | Urban/Recreational Grasses |
| 91 | Wetlands | Woody Wetlands |
| 92 | Wetlands | Emergent Herbaceous Wetlands |

### 3.1.3 Imagery Data

Overhead imagery data can be implemented as a knowledge source in Space Time Adaptive Processing. Depending on the type of imagery used, information about the terrain type or about the radar reflectivity of terrain can be obtained. Sources of imagery data include SAR images, DBS maps and optical imagery; where optical images provide information about the type of terrain, SAR and DBS imagery provide information about the radar reflectivity of the region of interest.

Optical aerial imagery, SAR images or DBS maps can be used in order to obtain in-

formation about the terrain in the region of interest

### 3.1.3.1 Synthetic Aperture Radar Maps

Synthetic Aperture Radars provide an alternate means of obtaining aerial reconnaissance data by offering images of the region of interest from a bird's eye point of view, similar to electro-optical sensors. However, unlike traditional electro-optical sensors, SAR sensors provide their own illumination; which is beneficial for day and night operation and robustness to atmospheric effects such as clouds and fog.

A major advantage of SAR imagery over other radar imagery is that, SAR maps provide constant range and cross-range resolution regardless of the operational range of the radar, whereas traditional real beam radar imagery yields coarser cross-range resolution as the operational range of the radar increases. Figure 3.4 depicts a sample X-band SAR image which was obtained from a region near Gölbek, Ankara by an experimental SAR sensor.



Figure 3.4: A sample X-band SAR image.

SAR images are obtained by illumination of the region of interest by the radar sensor and therefore provide information about the radar reflectivity of the terrain in the illuminated area. This information can be used during the STAP training process in order to determine regions of similar reflectivity characteristics.

### 3.1.3.2 Doppler Beam Sharpening Maps

DBS maps are similar to SAR images as both of the techniques aim to obtain a better azimuth resolution than the azimuth resolution obtained by real beam radar imaging. Similar to SAR image formation algorithms, DBS techniques aim to achieve this by means of benefiting from the forward motion of the platform and making use of Doppler processing. However, DBS techniques differ from SAR algorithms in that they do not rely on azimuth matched filters but depend on geometrical transformations on the axes of data.

DBS map formation process relies on the following assumptions:

- Range bins are coarse

- Dwell time is short

- Range walk is negligible

- Doppler walk is negligible

In GMTI mode operation, observation times are shorter due to high values of pulse repetition frequency and range bins are larger compared to SAR imaging modes. This allows the range and Doppler walks to be negligible for the aforementioned observation durations, and makes way for DBS imaging using GMTI mode data.

The data collection geometry for the DBS formation process is depicted in Figure 3.5. Several parameters related to the data collection geometry are self explanatory in the figure. In addition, points A and B represent the geographical locations of the beginning and the end of the line which defines the center of the operational swath. The process of forming a DBS map from the received GMTI mode radar data is given in Appendix B.
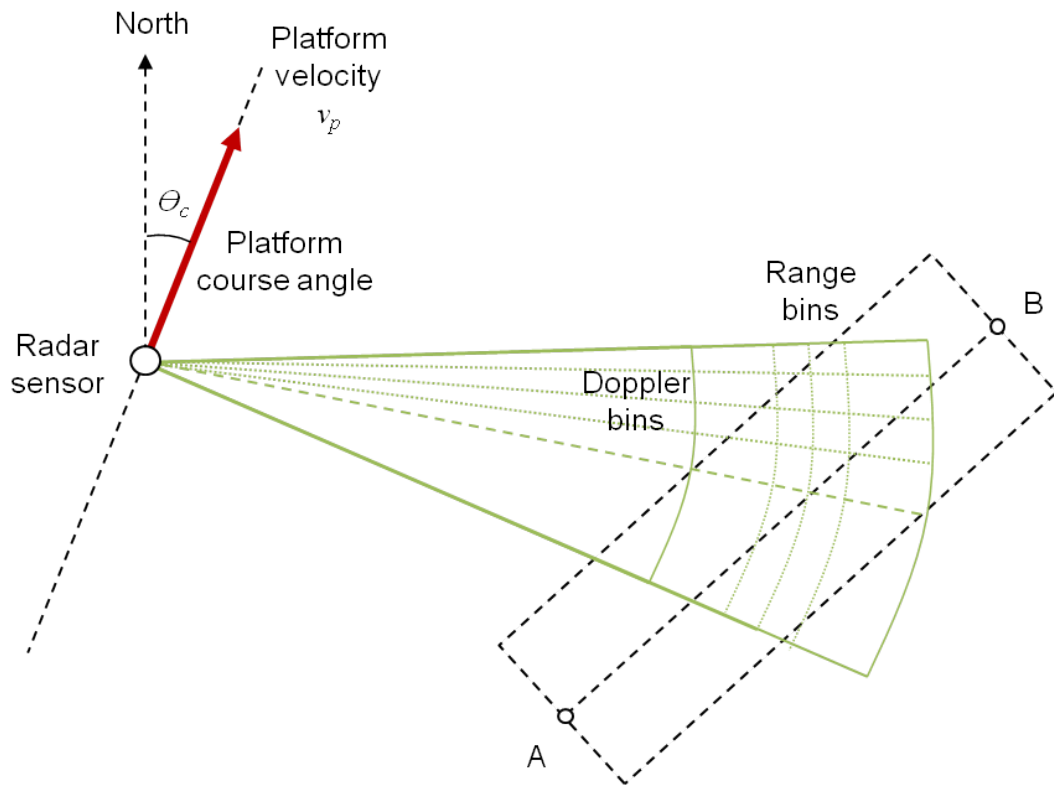
Figure 3.5: DBS Map Formation Geometry.

Figure 3.6 shows the DBS map corresponding to a coastal area near the northern shore of Turkey where docks and other terrain features are visible. Figure 3.7 displays the same data after it is overlaid onto the corresponding SRTM elevation data of the region of interest to give a three dimensional view of the end product of the georegistration process.
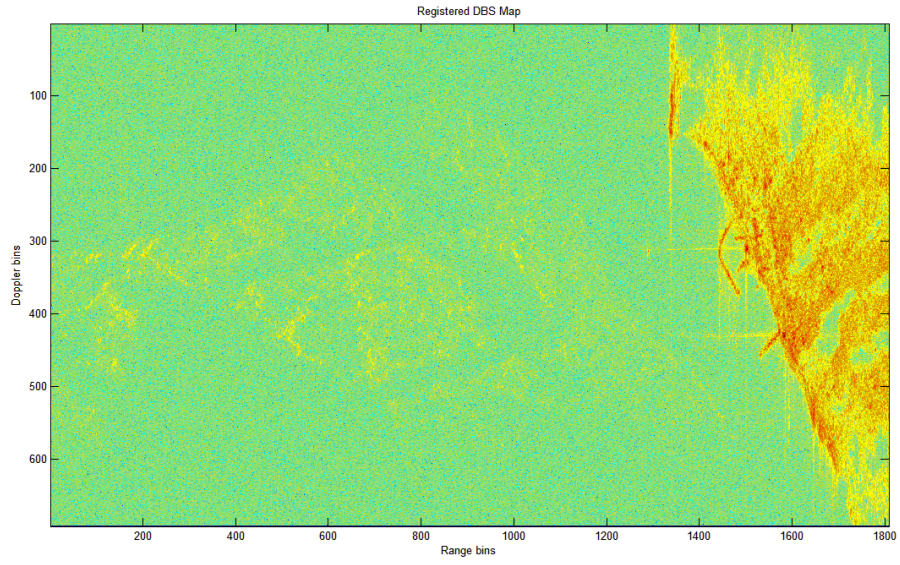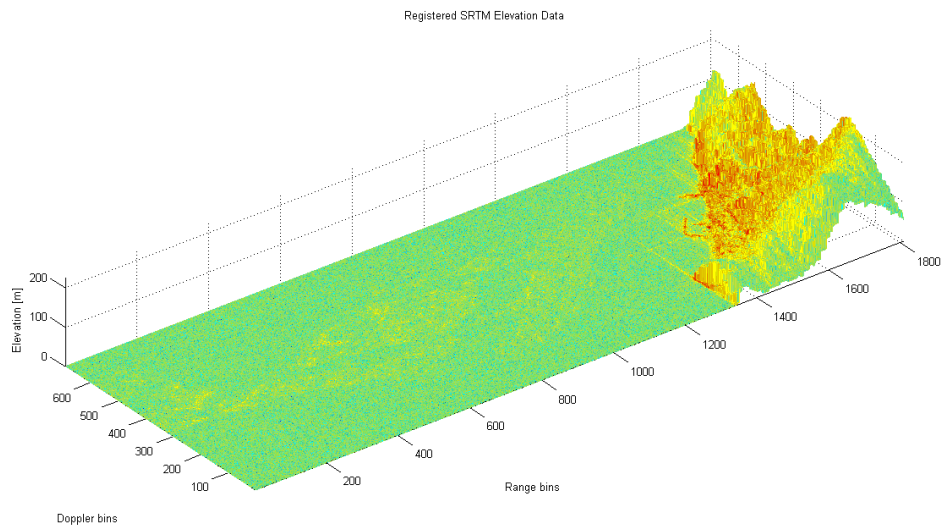
Figure 3.6: A sample DBS map.



Figure 3.7: 3D View of the SRTM data with the DBS map draped over.

### 3.1.4 Optical Imagery

Optical images can be implemented as an a priori knowledge source in an attempt to determine homogeneous regions in the region of interest. Satellite imagery or aerial photography obtained during flight trials can be given as examples for sources of optical imagery. However, in order to use such sources as knowledge databases, the data is required to contain the geographical coordinates so that the georeferencing process can be applied.

### 3.2 Use of A Priori Knowledge in Space Time Adaptive Processing

### 3.2.1 Indirect Use of A Priori Knowledge

The indirect approach makes use of prior information contained in terrain/clutter databases in an effort to perform a segmentation operation on the region of interest, thereby allowing adaptive filters to be tailored to the region at hand. This approach is also known as the Intelligent Training and Filter Selection (ITFS) technique as stated in [6]. In [17], a STAP training method that makes use of secondary data selection based on available digital terrain data. With this approach, the clutter region of interest is geographically registered with the terrain database, and training data can be chosen appropriately based on the type of terrain.

### 3.2.2 Direct Use of A Priori Knowledge

The direct use case corresponds to using the prior knowledge directly in the adaptive filter to help improve the adaptation performance of the clutter notch in distributed non-stationary clutter. This approach is also known as the Bayesian Filtering and Data Prewhitening technique as stated in [6] and involves the colored loading method, which can be summarized as the blending of the a priori clutter covariance matrix and the sample based estimate of the clutter covariance matrix in order to obtain adaptive filter weights which aim to maximally whiten the input data based on the a priori knowledge at hand. The details of the colored loading process is given in Section

3.2.2.2.

### 3.2.2.1  Non-Homogeneity Detection

Heterogeneous clutter which exists in the training data of the space-time processing lead to errors in the estimation of the clutter covariance matrix, thereby reducing the overall clutter suppression and detection performances. To address this issue, several non-homogeneity detection (NHD) techniques are proposed in the literature [22], [23]. The non-homogeneity detection technique is a processing step which is performed prior to the space-time adaptive processing in an attempt to remove the said heterogeneities existent in the training data.

The proposed technique in [22] makes use of the Generalized Inner Product (GIP) statistic to test for possible heterogeneities in the training data. The following processing step is stated to be applied to the training data which consists of $L + L'$ range bins, where $L$ is the number of range bins used for the estimation of the clutter covariance matrix, and $L'$ denotes the number of range bins to be tested.

$$z_k^{(L)} = \mathbf{r_k^H} \hat{R}_{L0,2}^{-1} \mathbf{r_k} \tag{3.1}$$

where

$$\hat{R}_{Lp,q} = \frac{1}{L} \sum_{\substack{k=-(L+q)/2 \\ k \neq p-q/2,\ldots,p,\ldots,p+q/2}}^{(L+q)/2} \mathbf{r_k r_k^H} \tag{3.2}$$

Afterwards, the obtained GIP values are ordered by magnitude and a total of $L$ samples which are located symmetrically around the median value are selected [22]. The technique proposed in [22] is illustrated in Figure 3.8.

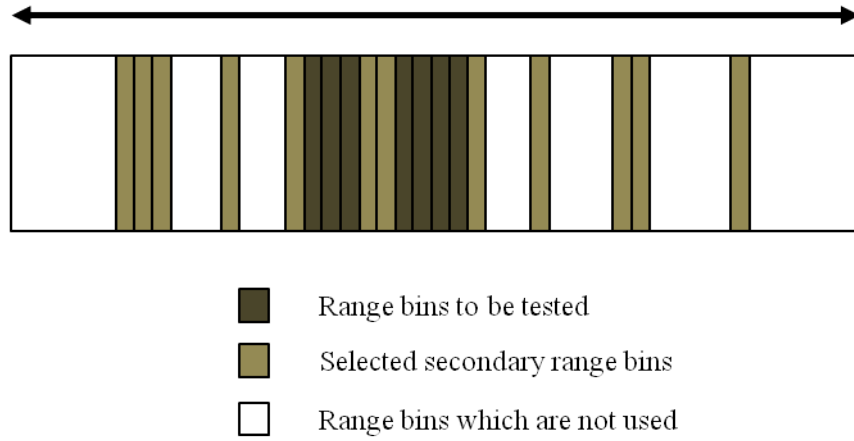$L'$ most homogeneous range bins are selected from a total of $(L + L')$ range bins

Range bins to be tested

Selected secondary range bins

Range bins which are not used

Figure 3.8: NHD range bin selection strategy.

### 3.2.2.2 Colored Loading

Colored loading technique corresponds to the tapering of the estimated clutter covariance matrix with an a priori covariance matrix. This approach assumes that at least a part of the statistical properties of the clutter for a given region of interest is known beforehand, and this knowledge is incorporated during the calculation process of the adaptive filter weights such that the filter weights are orthogonal to the a priori clutter component. The colored loading technique is presented for the full rank and reduced rank adaptations of STAP in the following subsections.

### 3.2.2.3 Full Degree of Freedom Case

Consider an airborne GMTI radar system which uses $M$ pulses in one coherent processing interval and $N$ spatial channels, similar to that given in Section 2.1. In this scenario, the antenna footprint is directed on the ground and the radar platform is in motion. Assuming that the illuminated region of interest on the ground consists of separate clutter patches, the space-time signal model corresponding to the total interference signal is as given in Equation 3.3 [7].

$$\mathbf{x} = \sum_{p=1}^{P_c} \alpha_p \mathbf{v}(\theta_p, f_p) \odot \mathbf{t}_p + \mathbf{n} = \mathbf{x}_c + \mathbf{n} \tag{3.3}$$

where $\mathbf{v} \in C^{MNx1}$ denotes the space-time response vector, $P_c$ denotes the number of clutter scatterers, and $\alpha_p$, $\theta_p$ and $f_p$ denote the complex amplitude, arrival angle and the Doppler shift of the $p^{th}$ clutter patch, respectively. $\mathbf{n} \in C^{MNx1}$ denotes the thermal noise component, ($\odot$) represents the element-wise Hadamard multiplication operation and $\mathbf{t}_p$ is stated to be representing random undesired modulations on the clutter signal and is shown to be comprised of the form given in Equation 3.4.

$$\mathbf{t}_p = 1 + \tilde{\mathbf{t}}_p \tag{3.4}$$

Estimation steps for the covariance matrix of the introduced interference model is given in Equations 3.5 and 3.6 [7].

$$\mathbf{R_{xx}} = E[\mathbf{xx^H}] = \mathbf{R}_c + \sigma^2 \mathbf{I}_{MN} \tag{3.5}$$

where

$$\mathbf{R}_c = E\left[\left\{\sum_{p=1}^{P_c} \alpha_p \mathbf{v}(\theta_p, f_p) \odot (\mathbf{1} + \tilde{\mathbf{t}_p})\right\}\left\{\sum_{p=1}^{P_c} \alpha_p \mathbf{v}(\theta_p, f_p) \odot (\mathbf{1} + \tilde{\mathbf{t}_p})\right\}^H\right]. \tag{3.6}$$

The final form of the covariance matrix, which shows the two known and unknown components, is obtained as shown in Equations 3.7 and 3.8 [7].

$$\mathbf{R}_c = \sum_{p=1}^{P_c} |\alpha_p|^2 \mathbf{v}(\theta_p, f_p) \mathbf{v}^H(\theta_p, f_p) \odot \mathbf{T_p} \in C^{MN \times MN} \quad, \tag{3.7}$$

$$\mathbf{R_c} = \underbrace{\sum_{p=1}^{P_c} |\alpha_p|^2 \mathbf{v}(\theta_p, f_p) \mathbf{v}^H(\theta_p, f_p)}_{known\ component} + \underbrace{\sum_{p=1}^{P_c} |\alpha_p|^2 \mathbf{v}(\theta_p, f_p) \mathbf{v}^H(\theta_p, f_p) \odot \tilde{\mathbf{T}}_p}_{unknown\ component} \tag{3.8}$$

where

$$\tilde{\mathbf{T}}_p = E[\tilde{\mathbf{t}}_p \tilde{\mathbf{t}}_p^H] \ . \tag{3.9}$$

The solution for the full DoF problem is as follows.

$$\min_{w} E[|\mathbf{w}^H \mathbf{x}|^2] \quad s.t. \quad \begin{cases} \mathbf{w}^H \mathbf{v} = 1 \\ \mathbf{w}^H \mathbf{R}_c \mathbf{w} \le \delta_d \\ \mathbf{w}^H \mathbf{w} \le \delta_L \end{cases} \tag{3.10}$$

where

$$\mathbf{w} = \frac{(\mathbf{R}_{\mathbf{xx}} + \beta_d \mathbf{R}_c + \beta_L \mathbf{I})^{-1} \mathbf{v}}{\mathbf{v}^H (\mathbf{R}_{\mathbf{xx}} + \beta_d \mathbf{R}_c + \beta_L \mathbf{I})^{-1} \mathbf{v}} = \frac{(\mathbf{R}_{\mathbf{xx}} + \mathbf{Q})^{-1} \mathbf{v}}{\mathbf{v}^H (\mathbf{R}_{\mathbf{xx}} + \mathbf{Q})^{-1} \mathbf{v}} \tag{3.11}$$

and

$$\mathbf{Q} = \beta_d \mathbf{R}_c + \beta_L \mathbf{I} \ , \tag{3.12}$$

$$\tilde{\mathbf{v}} = \mathbf{Q}^{-1/2} \mathbf{v} \ , \tag{3.13}$$

$$\tilde{\mathbf{x}} = \mathbf{Q}^{-1/2} \mathbf{x} \ , \tag{3.14}$$

$$\tilde{\mathbf{w}} = \frac{(\mathbf{R}_{\mathbf{xx}} + \mathbf{Q})^{-1} \mathbf{v}}{\mathbf{v}^H (\mathbf{R}_{\mathbf{xx}} + \mathbf{Q})^{-1} \mathbf{v}} \ . \tag{3.15}$$

In this manner, the adaptive filter weights for the full degree of freedom case has been obtained. In the following section, this solution will be extended to the reduced rank case which will then bu used in the remainder of this work.

### 3.2.2.4 Reduced Degree of Freedom Case

To obtain the adaptive filter weights for the reduced degree of freedom case, an element space post Doppler rank reduction method is preferred. The solution for the

reduced DoF problem is given in a similar manner to the full DoF case [7].

$$\mathbf{x}_m = \mathbf{H}_m^H \mathbf{x}, \ \mathbf{v}_m = \mathbf{H}_m^H \mathbf{v} \tag{3.16}$$

where $\mathbf{H}_m$ is defined as the reduced DoF transformation matrix which is required for obtaining the element space post Doppler observations [7]. Afterwards, the covariance matrix estimates are given as below.

$$\mathbf{R}_m = \mathbf{H}_m^H \mathbf{R}_{\mathbf{xx}} \mathbf{H}_m \tag{3.17}$$

and

$$\mathbf{R}_{c,m} = \mathbf{H}_m^H \mathbf{R}_{\mathbf{c}} \mathbf{H}_m, \quad \mathbf{R}_{n,m} = \mathbf{H}_m^H \mathbf{R}_{\mathbf{n}} \mathbf{H}_m \tag{3.18}$$

where $\mathbf{R}_{c,m}$ and $\mathbf{R}_{n,m}$ are given as the reduced DoF versions of the a priori clutter and noise covariance matrices [7]. The obtained matrices are then shown to be substituted in the following reduced DoF constraints afterwards.

$$\min_{w} E[|\mathbf{w}_m^H \mathbf{x}_m|^2] \quad s.t. \quad \begin{cases} \mathbf{w}_m^H \mathbf{v}_m = 1 \\ \mathbf{w}_m^H \mathbf{R}_{c,m} \mathbf{w}_m \leq \delta_{d,m} \\ \mathbf{w}_m^H \mathbf{w}_m \leq \delta_{L,m} \end{cases} \tag{3.19}$$

The adaptive filter weights satisfying the reduced DoF constraints are therefore shown to be given as below [7].

$$\mathbf{w}_m = \frac{(\mathbf{R}_m + \beta_{d,m} \mathbf{R}_{c,m} + \beta_{L,m} \mathbf{I}_D)^{-1} \mathbf{v}_m}{\mathbf{v}_m^H (\mathbf{R}_m + \beta_{d,m} \mathbf{R}_{c,m} + \beta_{L,m} \mathbf{I}_D)^{-1} \mathbf{v}_m} = \frac{(\mathbf{R}_m + \mathbf{Q}_m)^{-1} \mathbf{v}_m}{\mathbf{v}_m^H (\mathbf{R}_m + \mathbf{Q}_m)^{-1} \mathbf{v}_m} \tag{3.20}$$

where $\mathbf{Q}_m$ denotes the final loading matrix and is given as

$$\mathbf{Q}_m = \beta_{d,m} \mathbf{R}_{c,m} + \beta_{L,m} \mathbf{I}_D \ . \tag{3.21}$$

43

### 3.2.2.5 Determination of Loading Levels

A more general form of the colored loading process can be stated as

$$\hat{R} = \alpha \hat{R}_0 + \beta \hat{R}_1 \tag{3.22}$$

where $\hat{R}_0$ denotes the a priori clutter covariance matrix, $\hat{R}_1$ denotes the sample based estimate of the clutter covariance matrix, and $\hat{R}$ is the loaded covariance matrix. $\alpha$ and $\beta$ represent the weights for the blending process. Therefore, the selection of the loading levels is an important matter. If one is to choose a large $\alpha$ and a small $\beta$ value, the resulting covariance matrix will mostly be dependent on a priori knowledge, and performance might be negatively affected if the a priori knowledge does not fully represent the statistical properties of the clutter for the given region of interest. Similarly, if a small $\alpha$ value and a large $\beta$ value is chosen, the resulting covariance matrix will mostly depend on the sample based estimate of the clutter covariance matrix. In this case, performance might be negatively affected if the estimated covariance matrix does not fully correspond to the clutter region, such as in the case of target dense environments.

Several approaches are proposed in the literature to address this issue. In [6], it is stated that $\alpha$ can be chosen to maximally whiten the received interference data. In [24], the loading factors are determined in the minimum MSE sense for the convex combination ($\beta = 1 - \alpha$ case) and the general linear combination cases. The loading factor for the convex combination case is given as follows in [24]

$$\alpha = \min\left(1, \hat{\alpha}_0''\right) \tag{3.23}$$

where

$$\hat{\alpha}_0'' = \frac{\hat{\rho}}{\left\|\hat{R}_1 - \hat{R}_0\right\|} \;, \tag{3.24}$$

44

$$\hat{\rho} = \frac{1}{L^2} \sum_{k=1}^{L} \|\mathbf{r_k}\|^4 - \frac{1}{L} \left|\hat{R}_1\right|^2 \quad , \tag{3.25}$$

$$\hat{R}_1 = \frac{1}{L} \sum_{k=1}^{L} \mathbf{r_k} \mathbf{r_k^H} \quad , \tag{3.26}$$

and $\|.\|$ denotes the Frobenius matrix norm.

Similarly, the loading factor for the general linear combination is given as follows in [24].

$$\alpha = \min\left(\hat{\alpha}_0'', \hat{v}\right) \tag{3.27}$$

and

$$\beta = 1 - \frac{\alpha}{\hat{v}} \tag{3.28}$$

where

$$\hat{v} = \frac{tr\left(\hat{R}_0^H \hat{R}_1\right)}{\left\|\hat{R}_0\right\|^2} \tag{3.29}$$

and $tr(.)$ denotes the trace operation.

While these equations provide a means to choose a blending factor for the colored loading process, it is stated in [25] that a closed form expression for the optimal loading factor cannot be determined. Choosing a loading factor manually offers a more controlled analysis environment for the performance evaluation of knowledge aided processing approaches, and is therefore adopted in this manner in this thesis work, while satisfying the convex combination requirement of $\beta = 1 - \alpha$ for Equation 3.22.

# CHAPTER 4

# PROPOSED KA-STAP APPROACH

We propose a novel KA-STAP processing architecture which combines the previously mentioned approaches while suggesting new types of information, which are readily available or obtainable such as SRTM data and DBS maps, as sources of a priori knowledge; and aim to present the results obtained using actual data recorded during flight tests with a radar sensor that makes use of sum and difference beams. The details of the processing steps are explained in the following sections. Finally, performance of the proposed structure will be evaluated and compared to the traditional non-knowledge-aided case. Both real and injected targets are used for performance evaluation purposes for better inspection of the results.

## 4.1 Proposed structure for KA-STAP processing

The proposed processing structure consists of eight main blocks: the knowledge database block, the segmentation block, the colored loading matrix formation block, the GIP non-homogeneity detector block, the loading level determination block, the colored loading block, the multi bin post Doppler STAP block and the constant false alarm rate (CFAR) processing block. The idea behind the processing structure can be summarized as follows: Initially, the a priori knowledge corresponding to the region of interest, which contains the SRTM elevation data and the DBS reflectivity maps, is obtained from the knowledge databases. Afterwards, platform ownship data is used along with the a priori data in order to identify the homogeneous regions in the area. After this, a priori clutter covariance matrices are formed and blended with the instan-
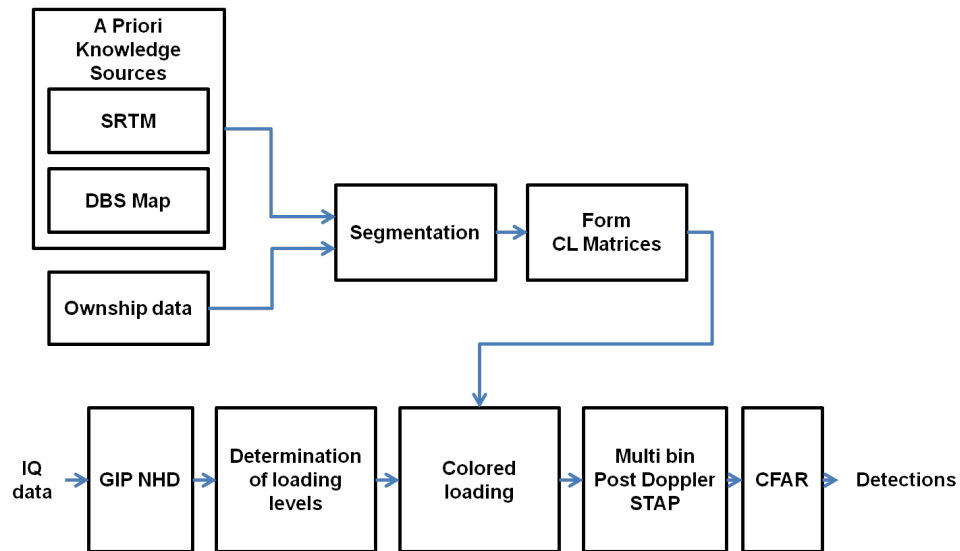
Figure 4.1: The proposed knowledge-aided processing structure.

taneous interference matrices. Finally, the STAP processor is invoked and detections are obtained after thresholding the output. The processing flow is as shown in Figure 4.1.

### 4.1.1 Knowledge Databases

Two separate forms of a priori knowledge are used as knowledge sources in order to complement the Space Time Adaptive Processing technique: SRTM elevation data and DBS maps. Here, SRTM data is used in order to determine the homogeneous clutter regions in complex environments such as sea to land transitions, whereas DBS maps are used in order to obtain a priori knowledge about the radar reflectivity of the region of interest.

### 4.1.2 Platform ownship data

Navigational data obtained via the sensors installed aboard the platform are used in order to obtain the instantaneous position, orientation and velocity measurements. These measurements include the latitude, longitude and altitude values; the roll, pitch and yaw angles and the North, East and Down velocities. The data collection geome-

47

try is described in the following section.

### 4.1.2.1 Data collection geometry

The data collection geometry for a GMTI mode operation is shown in Figure 4.2. The platform flight path is parallel to the swath of interest and the radar antenna is side-looking or squinted. As the platform proceeds, the antenna footprint sweeps the ground, receiving clutter and target echoes from the region of interest. Various operational parameters related to the data collection geometry are self explanatory in Figure 4.2.
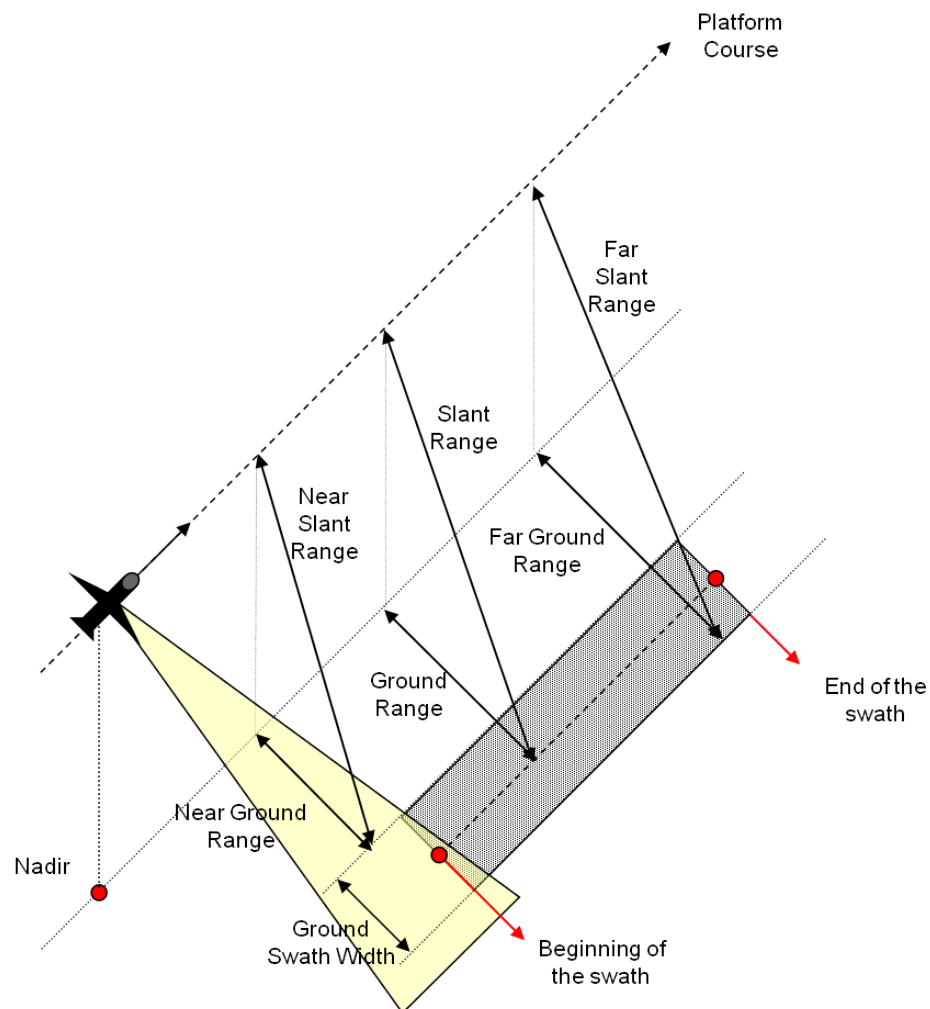


Figure 4.2: The data collection geometry.

### 4.1.3 Segmentation of Homogeneous Regions

In order to determine the homogeneous regions which are required to form the colored loading matrices, a segmentation operation is required. The segmentation operation relies on platform ownship data and SRTM elevation data and the obtained homogeneous regions are then used along with the DBS maps as training data during the formation of colored loading matrices.

#### 4.1.3.1 Use of Ownship Data

Ownship data is used for calculating the geodetic coordinates of the antenna footprint. Afterwards, these coordinates are used along with the SRTM elevation data to obtain terrain height values by using a 2D interpolation operation with the nearest neighbor method. Figure 4.3 depicts the use of sensor ownship data on an SRTM map, where SAR indicates the geographical location of the radar platform and the trapezoid denotes the antenna footprint. Points A and B represent the geographical locations of the beginning and the end of the line which defines the center of the operational swath.
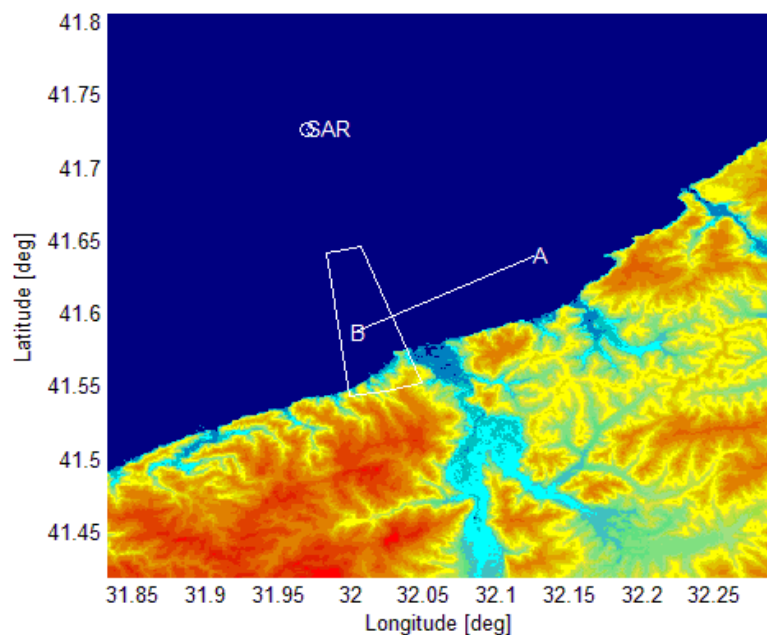
Figure 4.3: Geodetic coordinates of the antenna footprint for a sample data set.

### 4.1.3.2 Use of SRTM Elevation Data

In order to obtain a metric for determining the homogeneous regions in the area of interest, SRTM elevation data is quantized and is georeferenced with the radar footprint. Figure 4.4 depicts the georegistered SRTM elevation data. Figure 4.5 displays the same data after the terrain height is quantized to give a rough estimate of the homogeneous regions. Figure 4.6 displays the iso height contours of the terrain, displaying regions of similar altitude. Figure 4.6 depicts the georegistered SRTM elevation data for a single Doppler bin, and Figure 4.7 displays this same data after the terrain height is quantized.
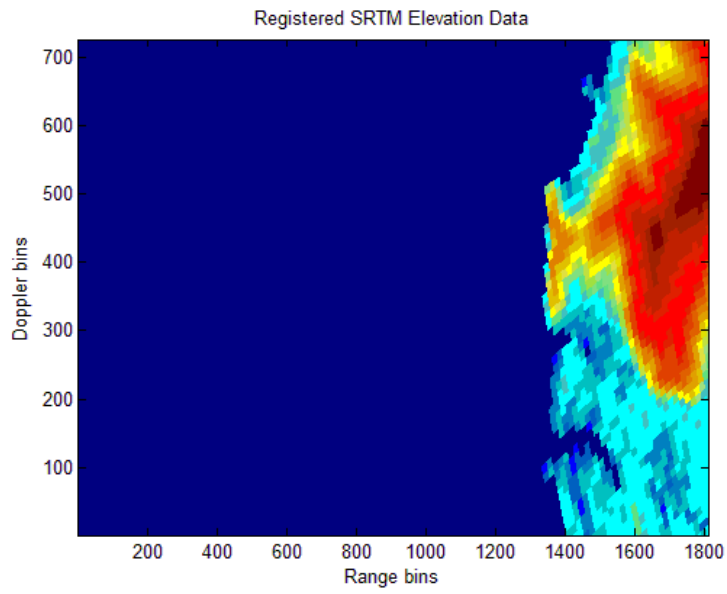
Figure 4.4: Registered SRTM elevation data.
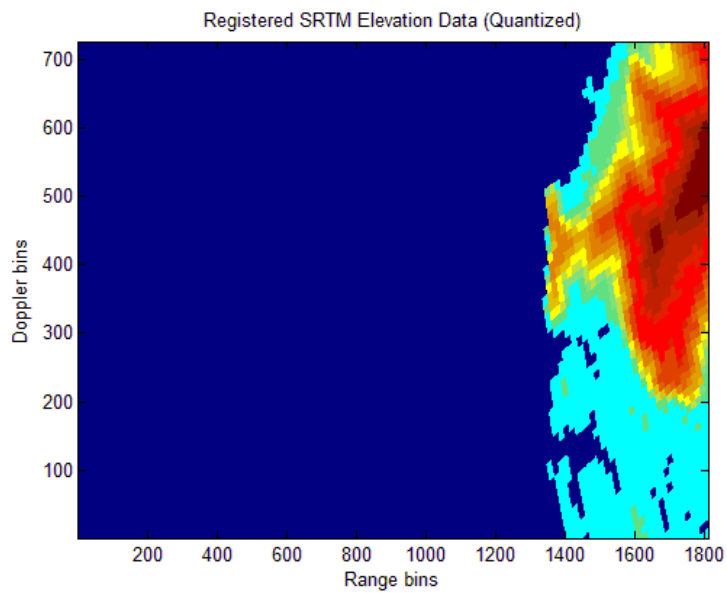


Figure 4.5: Registered SRTM elevation data (Quantized).
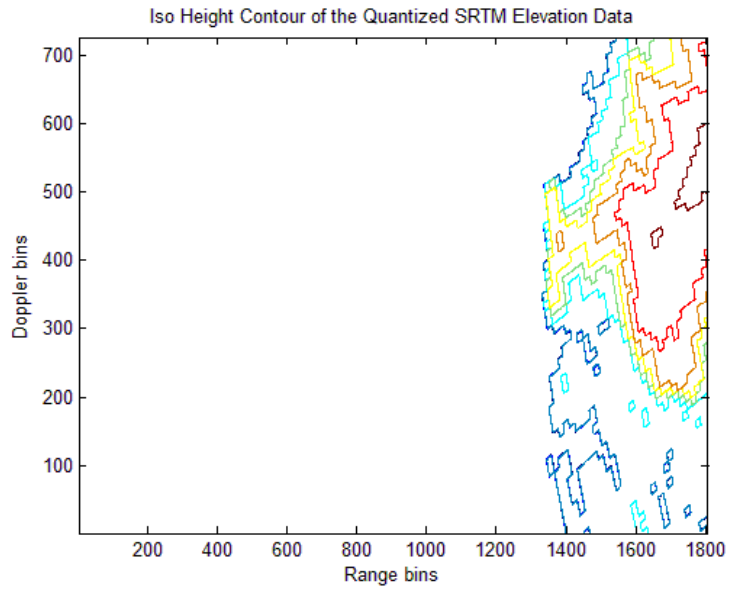
Figure 4.6: The iso height contour of the quantized SRTM elevation data.
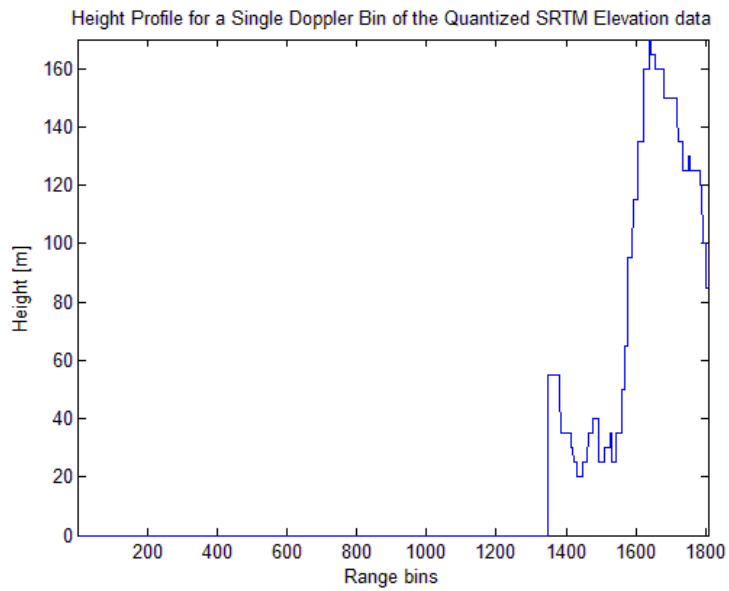


Figure 4.7: The height profile for a single doppler bin of the quantized SRTM elevation data.

### 4.1.3.3 Coordinate Systems

During the georegistration process, the following coordinate systems are used in order to be able to represent the data obtained by different means of acquisition.

- Geodetic Coordinate System

- Earth Centered Earth Fixed (ECEF) Coordinate System

- East - North - Up (ENU) Local Cartesian Coordinate System

Figure 4.8 depicts the coordinate systems and the reference ellipsoid of the Earth [26].
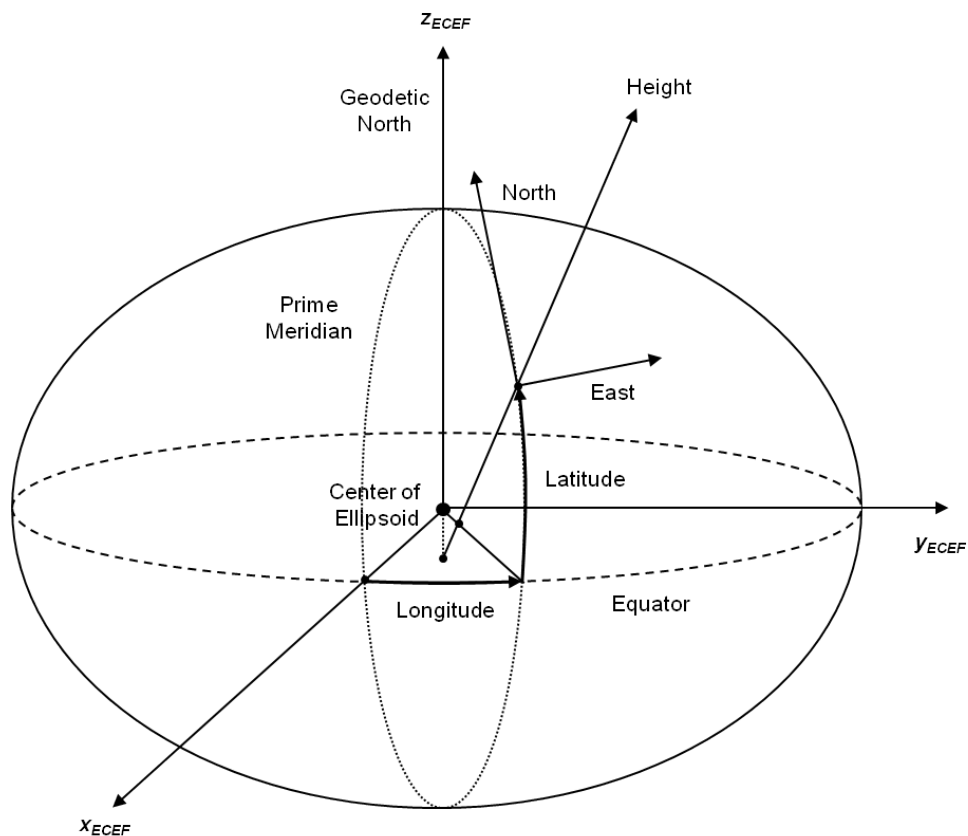


Figure 4.8: The ECEF and the Geodetic coordinate systems.

The geodetic coordinate system consists of parallels and meridians that are equally spaced in angle and is useful for indicating the angular position of a point of interest

with respect to the Prime Meridian and the Equator. The relative angular position with respect to the Prime Meridian is defined as the longitude, whereas the relative angular position with respect to the Equator is defined as the latitude. In this coordinate system, the height of a point is defined as the minimum distance between the point of interest and the point where the surface normal that goes through the point of interest intersects the earth.

The ECEF coordinate system is a Cartesian coordinate system whose origin is defined as the center of ellipsoid. The Z axis goes through the Geodetic North pole of the Earth, while the X axis lies on the Equatorial plane and goes through the Prime Meridian. The Y axis is defined with respect to the right hand rule.

In contrast with the aforementioned coordinate systems, the ENU coordinate system is a local Cartesian coordinate system whose origin resides on the radar sensor. The X axis is defined as the East direction, whereas the Y axis is defined as the North direction. The Z axis defines the height of the sensor with respect to the reference ellipsoid.

#### 4.1.3.4 Coordinate Transformations

In order to obtain the required information about the region of interest, a georegistration operation is performed on the location of the antenna footprint. This is accomplished by initially applying the transformation from the ENU local Cartesian coordinates to ECEF coordinates, and afterwards applying the transformation from ECEF coordinates to geodetic coordinates. The transformations between the coordinate systems are given in Appendix A.

### 4.1.4 Formation of Colored Loading Matrices

Colored loading approach for the reduced rank adaptation of STAP is performed, the details of which are given in Section 3.2.2.4. The colored loading matrices are formed in a way that is similar to the traditional ML estimation of the clutter covariance matrix except for the fact that the training data is obtained from the homogeneous

regions of the DBS map instead of the neighboring cells of the instantaneous radar data.

Since at the time of writing there were no readily available DBS maps of the region of interest, new ones are generated from the received radar data which was recorded in a former pass of the radar platform. The details of the DBS map formation process is given in Appendix B.

### 4.1.5 Non-homogeneity Detection

The GIP statistic based NHD approach of [17] is used, since it can readily be applied to the sample matrix inversion (SMI) applications. The GIP statistic is obtained as in Equation 3.1. For purposes of comparison, sample results for real and simulated data are given for the cases in which NHD is not applied and is applied respectively. It can be seen that with the NHD applied, it is possible to detect previously undetectable targets that are close together in range. Another conclusion that can be deduced from the obtained results is that the overall number of false alarms is reduced in the case where NHD is applied. The details of the target injection process is given in Appendix C.

Figure 4.9 shows the range - Doppler spectrum after the space time processing of a single CPI of the data set 1, which was obtained from the Gölbek region of Ankara, Turkey. A simulated target is also injected in the same Doppler bin as the actual test target in a close by range bin, so that both targets are endoclutter and mask each other in space - time adaptive processing training. Obtained detections are marked with black circles on top of the range - Doppler image. Figure 4.10 shows a zoomed view of the same image. In these cases, non-homogeneity detection is not applied, and as can be seen, the injected target could not be detected using the aforementioned CFAR method. Another thing to note is that the overall number of false alarms is large in this case.

Figure 4.11 and 4.12 present the same data, however after the non-homogeneity detection process is applied. It can be seen that both the injected target and the actual target are now detected since the targets no longer mask each other.
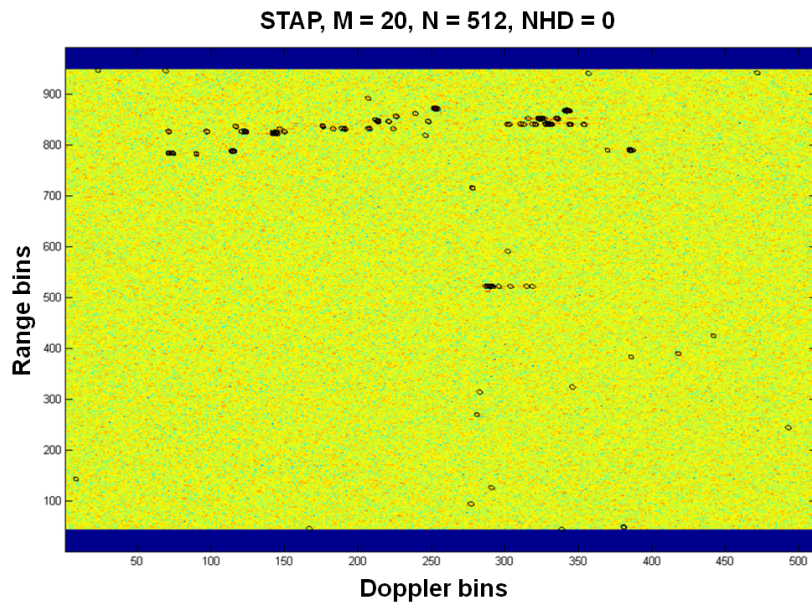
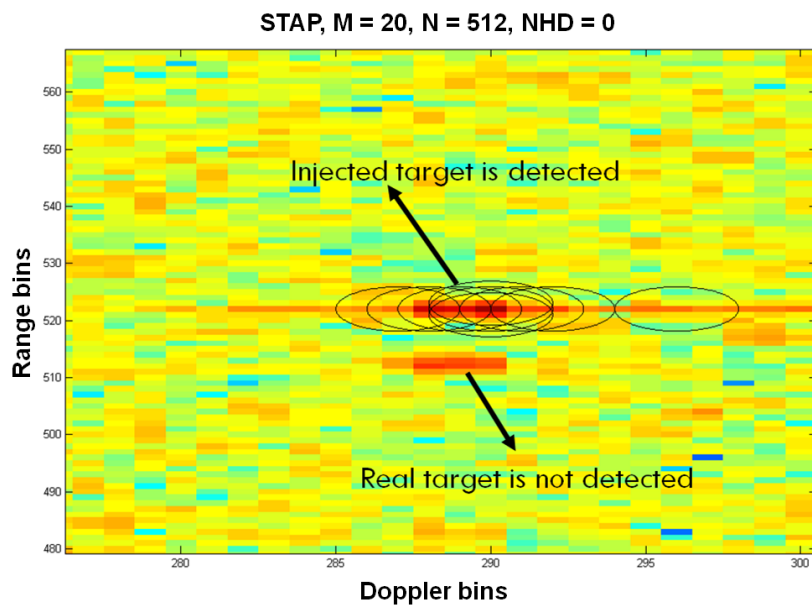Figure 4.9: Range - Doppler spectrum of data set 1 (NHD = 0).



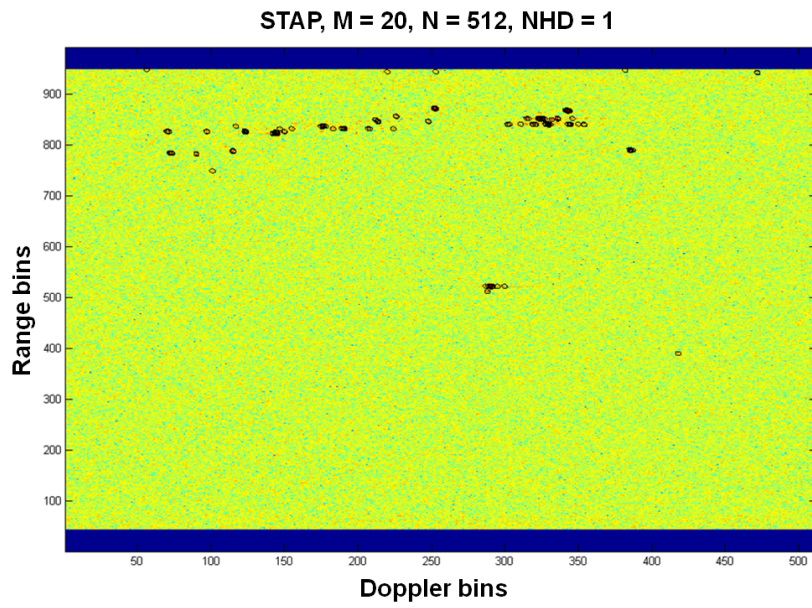Figure 4.10: Zoomed view of the Range - Doppler spectrum of data set 1 (NHD = 0).

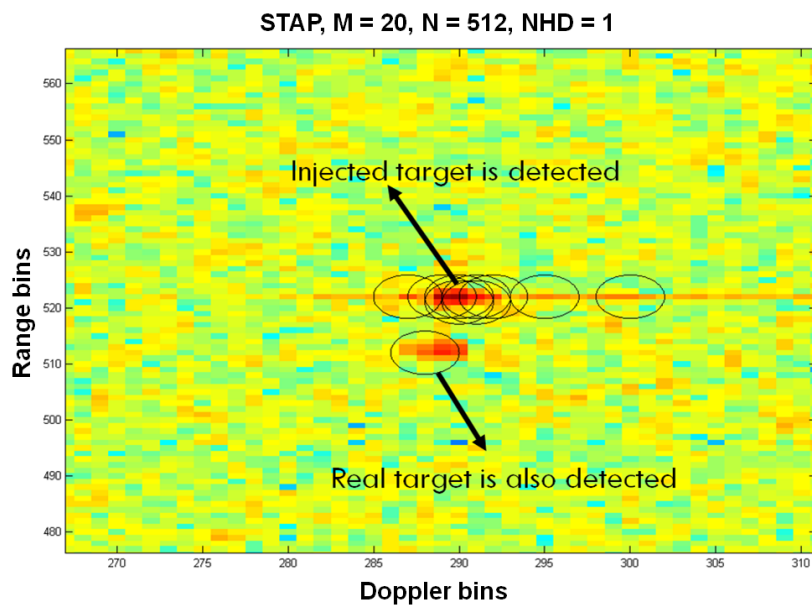Figure 4.11: Range - Doppler spectrum of data set 1 (NHD = 1).



Figure 4.12: Zoomed view of the Range - Doppler spectrum of data set 1 (NHD = 1).

### 4.1.6   Determination of loading levels

For the determination of colored loading level, the convex combination approach of [24] is used. The loading factor is set manually for better inspection of the results, and follows the convex combination rule described in 3.2.2.5.

### 4.1.7   Colored Loading

After obtaining the colored loading matrices and determining the loading levels, the colored loading operation is performed on the sample based ML estimate of the clutter covariance matrix. For purposes of comparison, sample results are given below for the cases in which CL is not applied and is applied respectively. It can be seen that with the CL applied, it is possible to detect previously undetected targets. Another conclusion that can be deduced from the obtained results is that the overall number of false alarms is reduced in the case where CL is applied.

Figure 4.13 depicts the range - Doppler spectrum of a single CPI of the data set 1 after space - time processing is applied. In this case, the colored loading process is not applied, and as can be seen several false alarms are present. Figure 4.14 depicts the same data, however after the colored loading process is applied. Several new detections corresponding to the Ankara - Konya highway are now available, which can be seen in the farther range. In addition, the overall number of false alarms is shown to be reduced in this case.
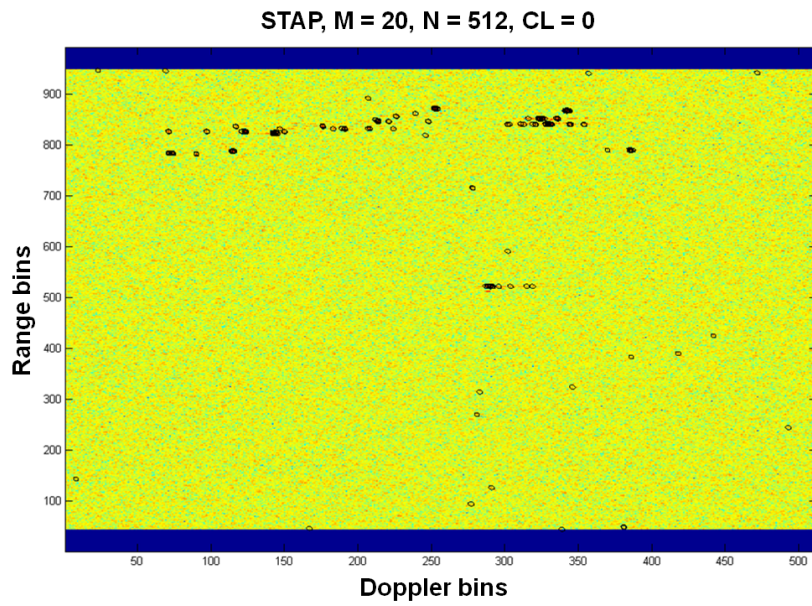
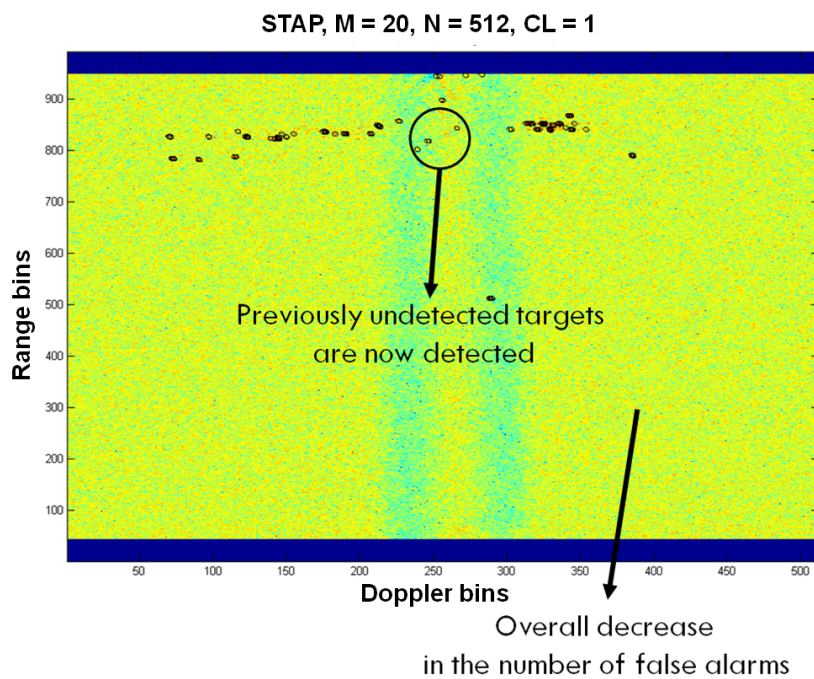Figure 4.13: Range - Doppler spectrum of data set 1 (CL = 0).



Figure 4.14: Range - Doppler spectrum of data set 1 (CL = 1).

59

### 4.1.8 Multi Bin Post Doppler STAP

Multi bin post Doppler space time adaptive processing approach is performed in the following manner: Initially, doppler processing is performed for each receiving channel. A total of two receiver channels and two Doppler bins are used, resulting in a covariance matrix of size four by four. To accomplish this, a windowed Fast Fourier Transform (FFT) process is applied in the first place. Figure 4.15 shows this operation, where initially a Hamming window of size $M$ is applied to the received data of size $MxK$ along the slow time axis.

After the windowed FFT operation, the interference covariance matrices required for the calculation of the adaptive filter weights are estimated using secondary range bins. This is achieved by averaging over the neighboring range bins for each cell under test in each Doppler bin. This process makes use of two Doppler bins at any time, which are the current Doppler bin under test and an adjacent neighbor of it. At the end of this process, filter weights are obtained with respect to the target signal model of interest. Figure 4.16 shows this operation, where $R$ denotes the estimated clutter covariance matrix, $b$ denotes the target signal model, and $w$ denotes the adaptive filter weights. $( )^{-1}$ denotes the matrix inversion operation.
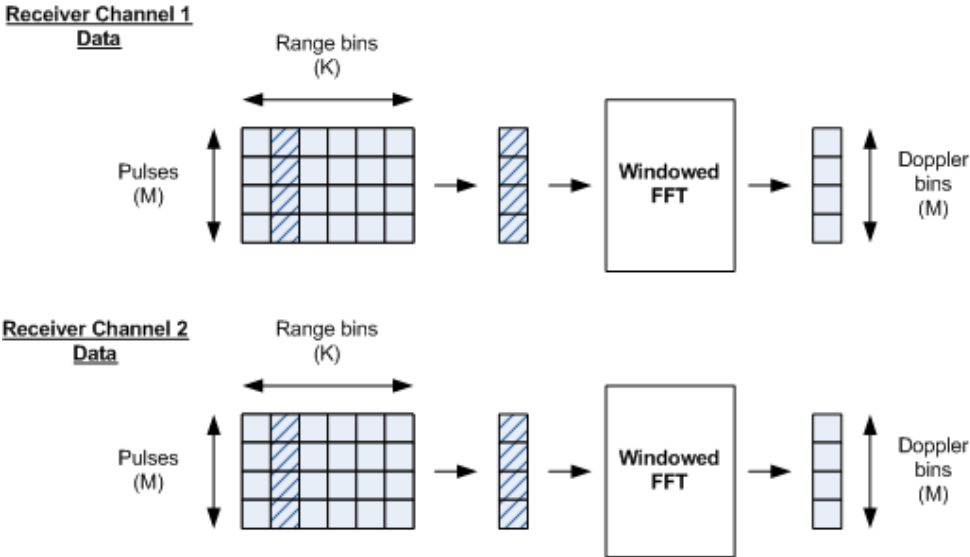


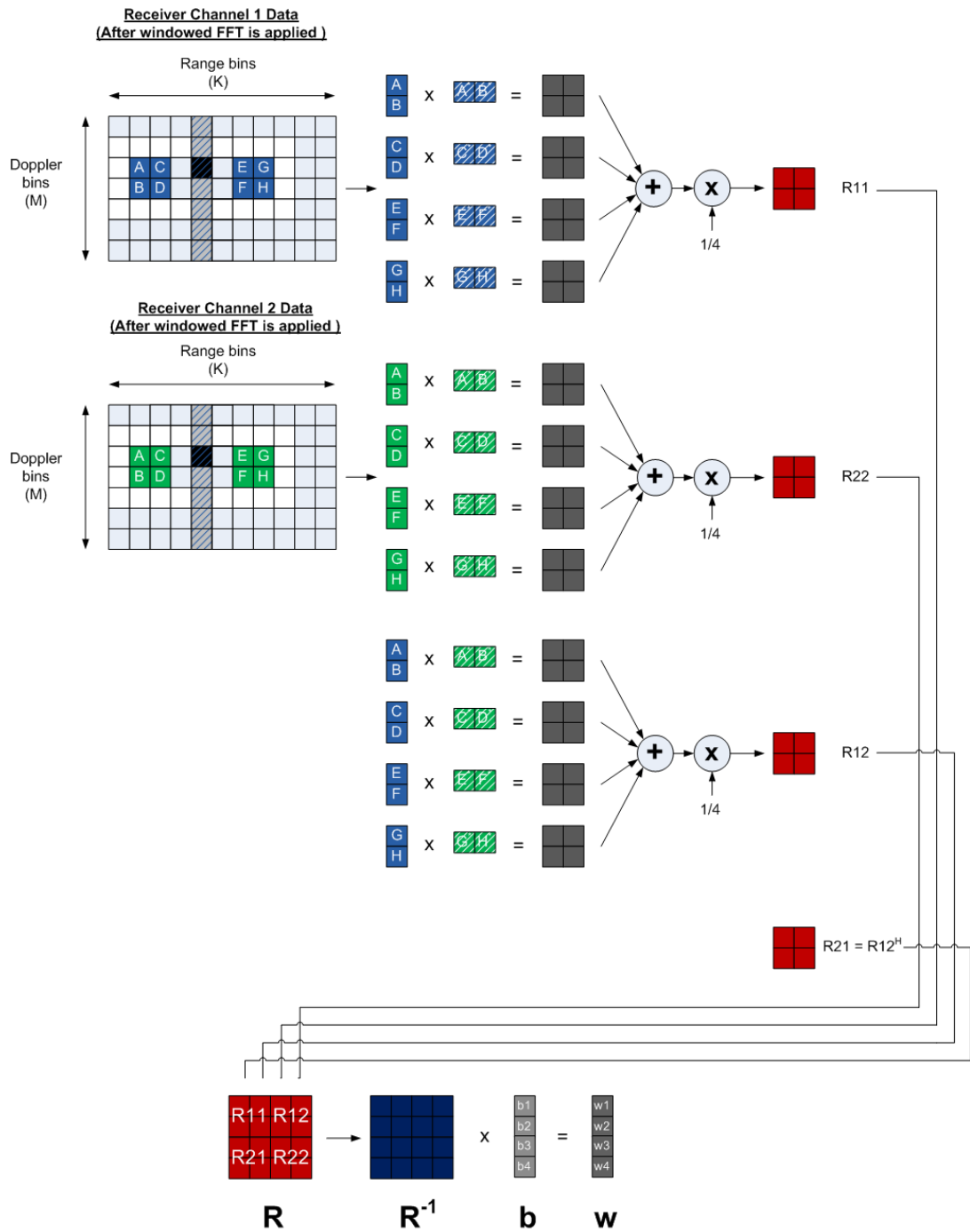Figure 4.15: The windowed FFT process.

60

Figure 4.16: Computation of the adaptive filter coefficients.

After the adaptive filter weights are obtained, the received radar data is filtered. This operation produces a single output for every range - Doppler cell, which becomes the input of the constant false alarm rate (CFAR) detector. Figure 4.17 depicts the
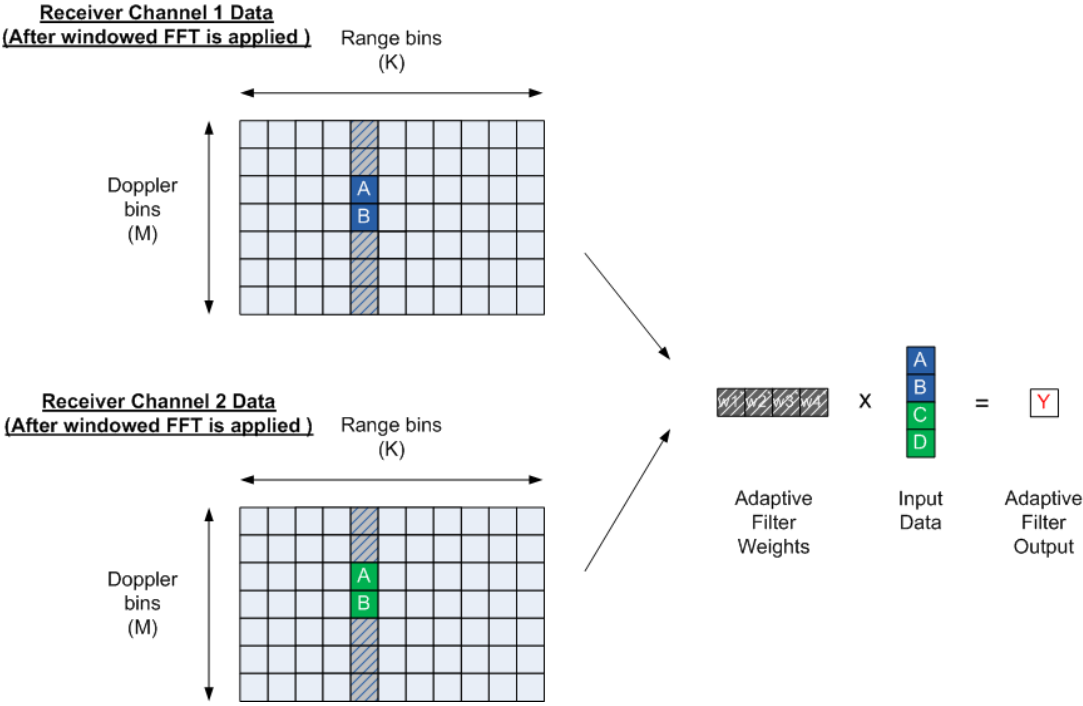
61

adaptive filtering operation.



Figure 4.17: The process of filtering the data using the adaptive filter weights.

### 4.1.9 CFAR

For making the detection decisions, the cell averaging CFAR (CA-CFAR) method is used. The CFAR processing is performed along the range bins for each Doppler bin in the data matrix. The CFAR operation is shown in Figure 4.18, where $L$ denotes the one sided length of the CFAR window, $g$ denotes the number of guard cell used during the CFAR process and $(*)$ denotes the one dimensional convolution operation.
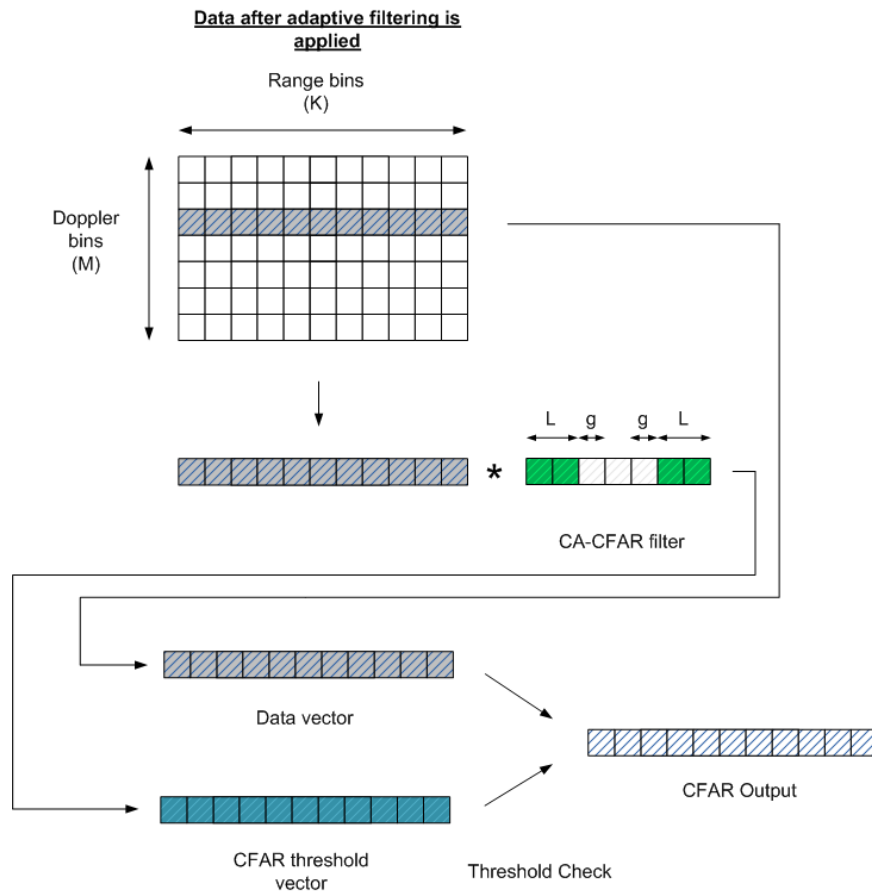
Figure 4.18: The cell averaging CFAR process.

## 4.2 Results obtained with the proposed KA-STAP processing structure

Results are organized in the following manner: Initially, the results corresponding to the traditional adaptive approach is presented. Secondly, the results obtained when only the non homogeneity detection process is applied are given. Finally, the results obtained when both the colored loading and the non homogeneity detection processes are applied are presented for different levels of loading factors.

Figure 4.19 shows the complete range - Doppler spectrum of a single CPI of the input data. Similar to the case presented in Section 4.1.5, a total of two simulated targets are also created and injected at the range - Doppler bins shown in Figure 4.20 for better analysis of the obtained results. The target signals are constructed so that they have the same amplitude, and are injected in the same Doppler bin and in close proximity in range; so that both targets mask each other in the training data. Figure 4.21 shows the range - Doppler spectrum of the data after the target injection process is applied. The details of the target injection process is given in Appendix C.
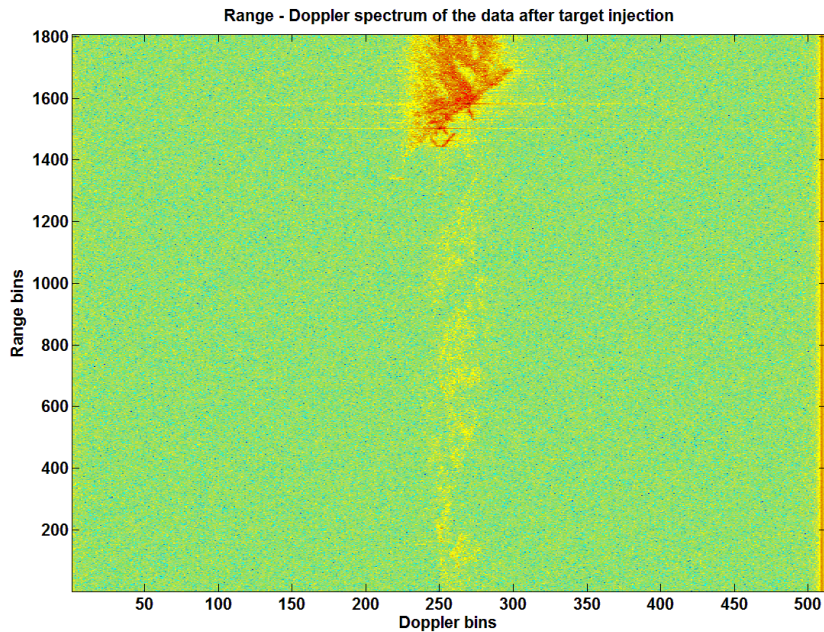


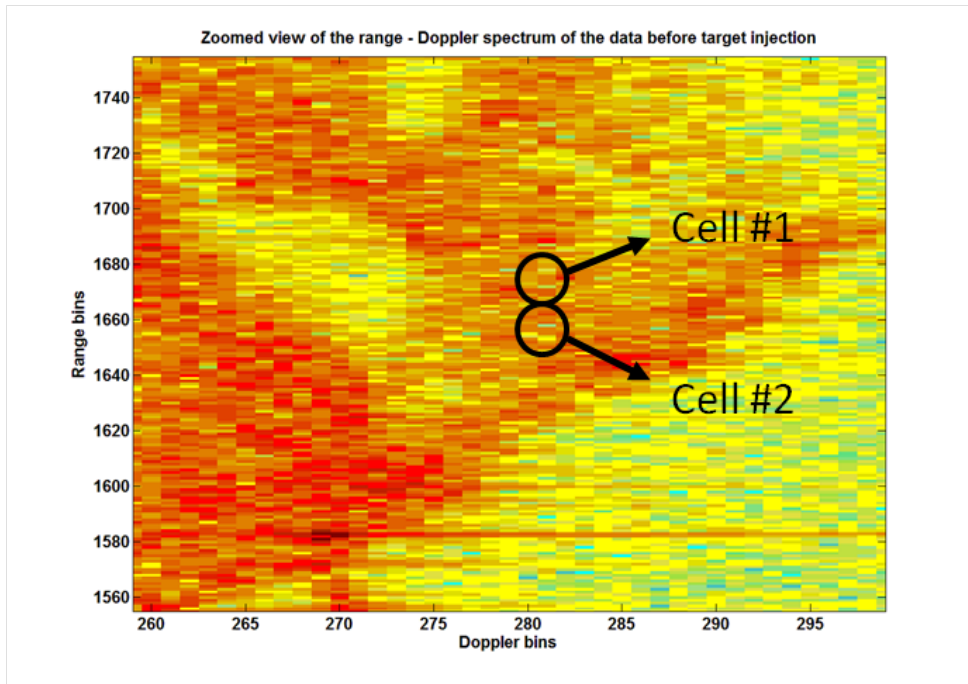Figure 4.19: Complete Range - Doppler spectrum of a single CPI of the input data.

Figure 4.20: Zoomed view on the Range - Doppler spectrum of the data before the target injection process.
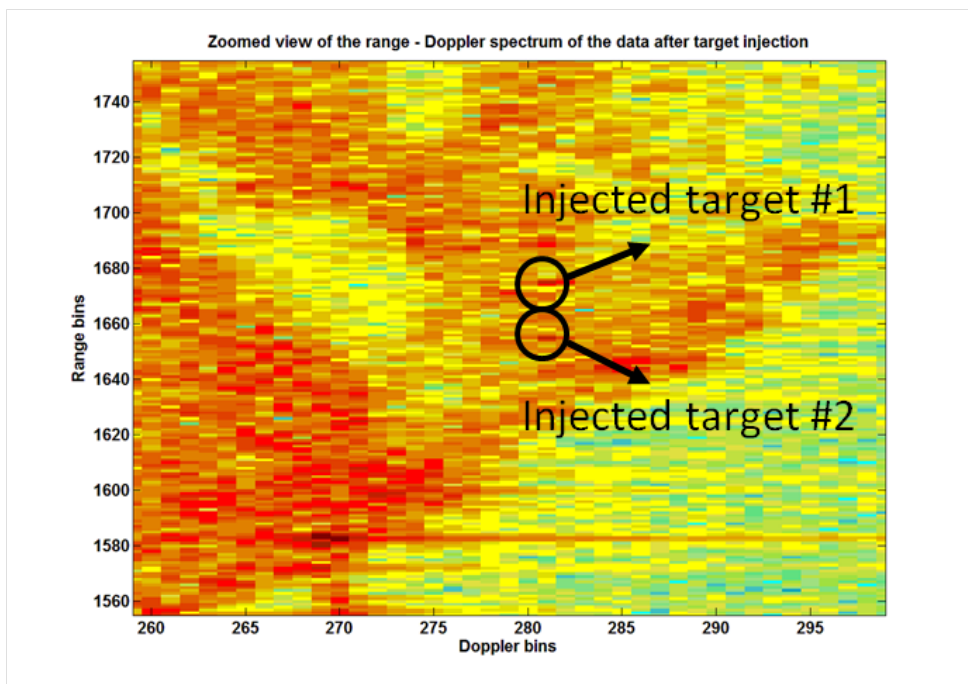


Figure 4.21: Zoomed view on the Range - Doppler spectrum of the data after the target injection process.

### 4.2.1 Results obtained with the traditional adaptive approach

Figure 4.22 depicts the range - Doppler spectrum of a single CPI of the sum channel data obtained from the Black Sea coastline near Zonguldak, Turkey. A better view of the region is presented in Section 3.1.3.2 in Figure 3.6. In this case, neither the NHD, nor the CL processes are applied; thus this case corresponds to the traditional adaptive processing approach. Obtained detections are marked on top of the image with black circles as before. It can be said that the overall number of false alarms is large, and several false alarms caused by the lighthouse at the end of the pier in the middle are present. Also, in this case only one of the injected targets are detected since these targets mask each other in range and NHD processing is not applied. In addition, several detections which will be present in the results where NHD is applied are missing in this case. Figure 4.23 depicts the range - Doppler spectrum of the STAP processor output of the same data for purposes of demonstration, where the clutter notch is visible.
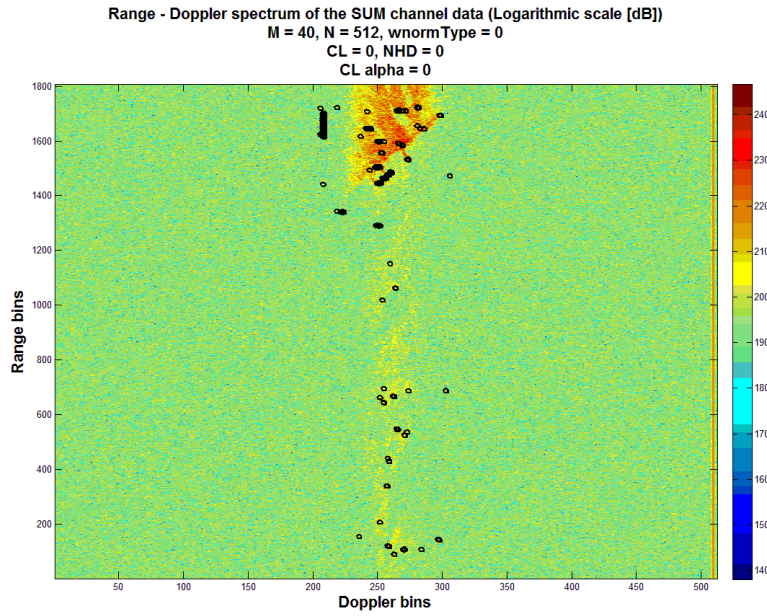
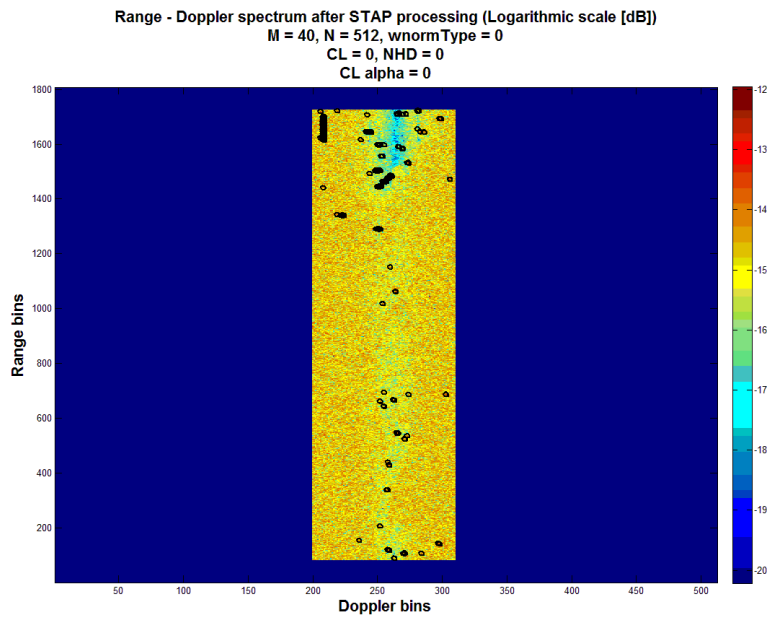Figure 4.22: Range - Doppler spectrum of the SUM channel data (NHD = 0, CL = 0).



Figure 4.23: Range - Doppler spectrum after STAP processing is applied (NHD = 0, CL = 0).

### 4.2.2 Results obtained when only the Non Homogeneity Detection process is applied

In this section, the results presented belong to the case in which only the NHD process is applied. Figure 4.24 and 4.25 depict the range - Doppler spectra of the same data, only after NHD processing is applied. Similar to the results presented in Section 4.1.5, overall decrease in the number of false alarms is visible. It should be noted that since the NHD process is applied in this case, the injected targets no longer mask each other in range and both of them are detected. In addition, near the pier which is on the left hand side of the image are several new detections which were not present in the previous case.
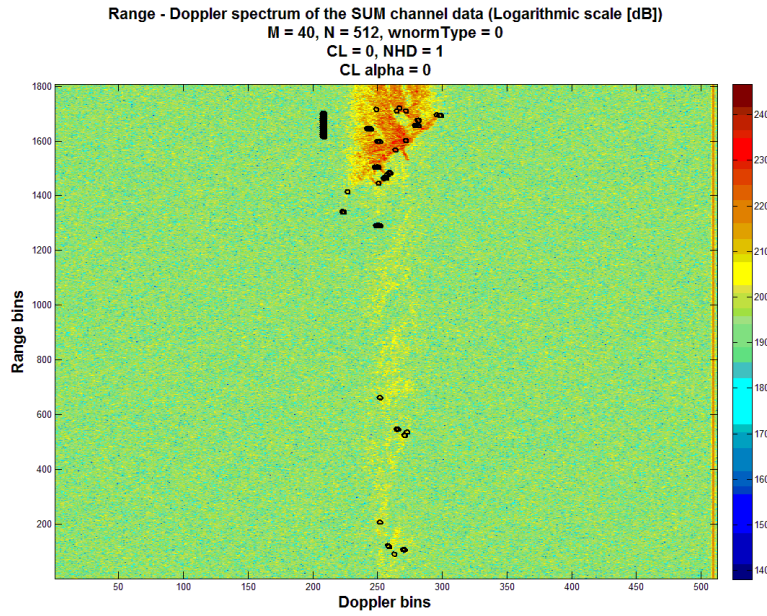
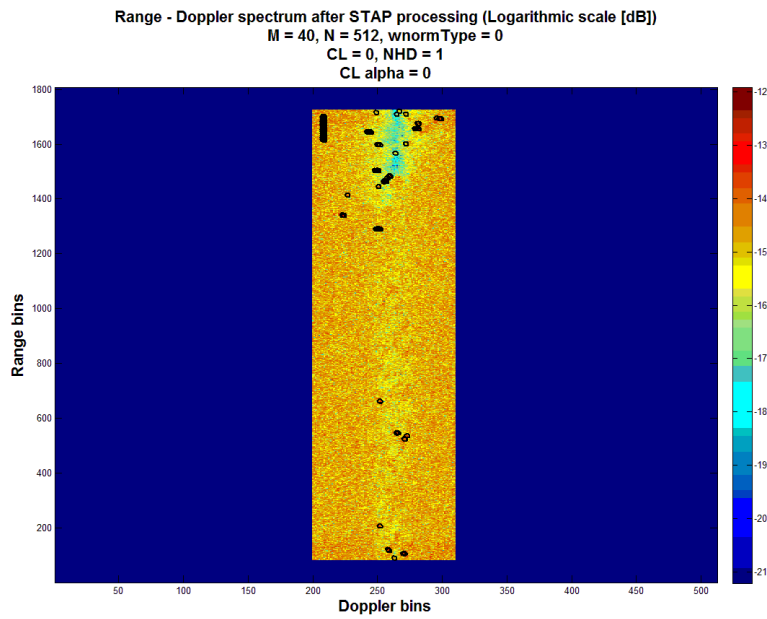Figure 4.24: Range - Doppler spectrum of the SUM channel data (NHD = 1, CL = 0).



Figure 4.25: Range - Doppler spectrum after STAP processing is applied (NHD = 1, CL = 0).

### 4.2.3 Results obtained when only the Colored Loading process is applied

In this section, the results presented belong to the case in which only the CL process is applied. In the following sections, several different values are chosen for the a priori knowledge blending factor, also known as the colored loading level, and the obtained results are presented.

#### 4.2.3.1 Colored loading factor is set to 0.05

In this case, the a priori knowledge blending factor is set to 0.05. Figure 4.26 depicts the sum channel range - Doppler spectrum of a single CPI of the data, with the CL processing applied. Since the loading factor is close to zero, the results herein do not differ greatly from the traditional adaptive case. Figure 4.27 depicts the range - Doppler spectrum of the STAP processor output of the same data for purposes of demonstration, where the clutter notch is visible. One thing to note here is that, false alarms caused by the lighthouse are also present in this case, since the NHD is not applied.
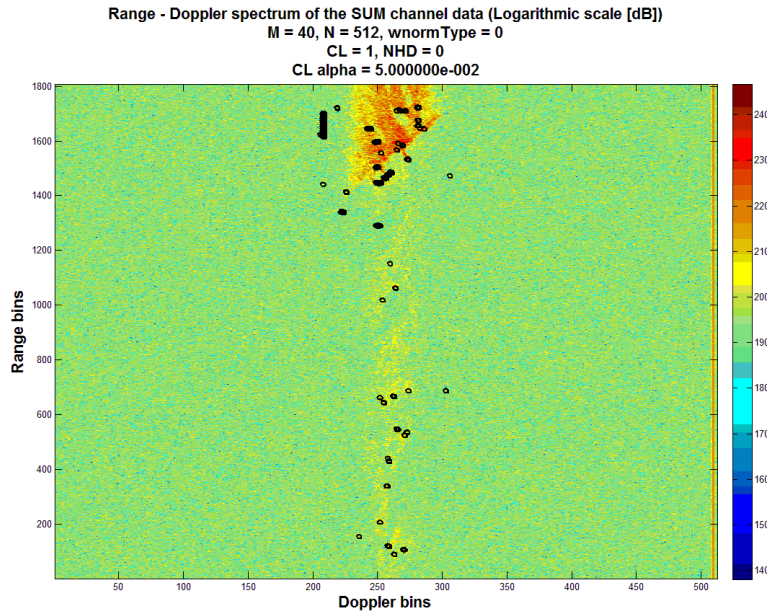
Figure 4.26: Range - Doppler spectrum of the SUM channel data (NHD = 0, CL = 1, CL alpha = 0.05).
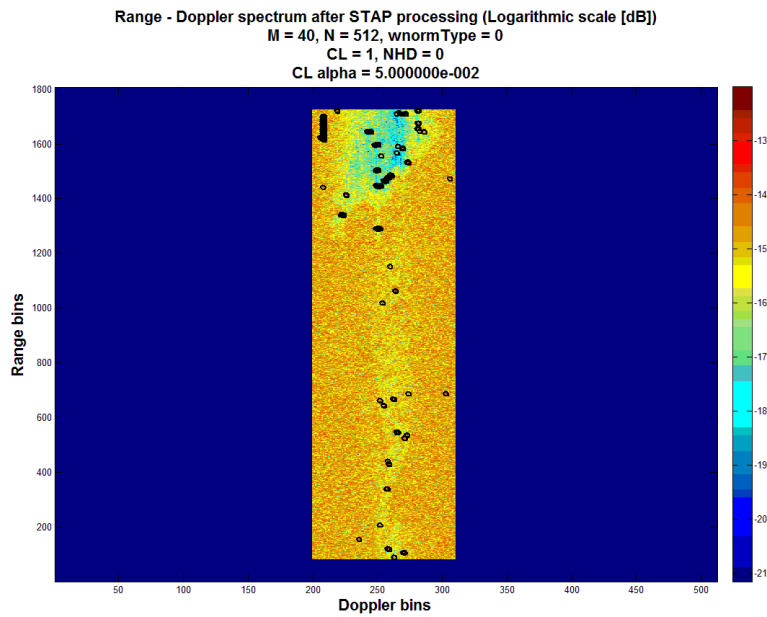


Figure 4.27: Range - Doppler spectrum after STAP processing is applied (NHD = 0, CL = 1, CL alpha = 0.05).

### 4.2.3.2 Colored loading factor is set to 0.10

In this case, the a priori knowledge blending factor is set to 0.10. Figure 4.28 depicts the sum channel range - Doppler spectrum of a single CPI of the data, with the CL processing applied. In this case, while some reduction in the number of false alarms is visible in both of the images, no real advantage is gained in terms of recovering previously missed detections. Figure 4.29 depicts the range - Doppler spectrum of the STAP processor output of the same data for purposes of demonstration, where the clutter notch is visible. False alarms caused by the clutter discretes are also present in this case, since the NHD is not applied.
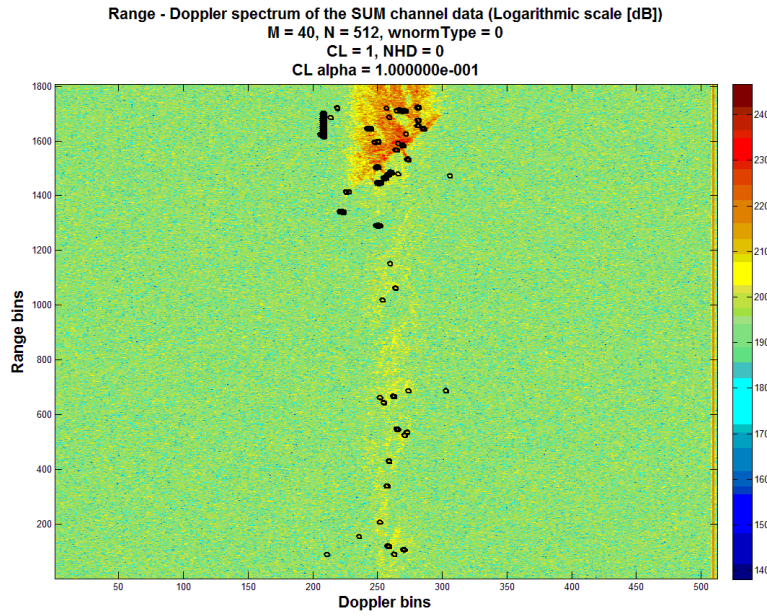
Figure 4.28: Range - Doppler spectrum of the SUM channel data (NHD = 0, CL = 1, CL alpha = 0.1).
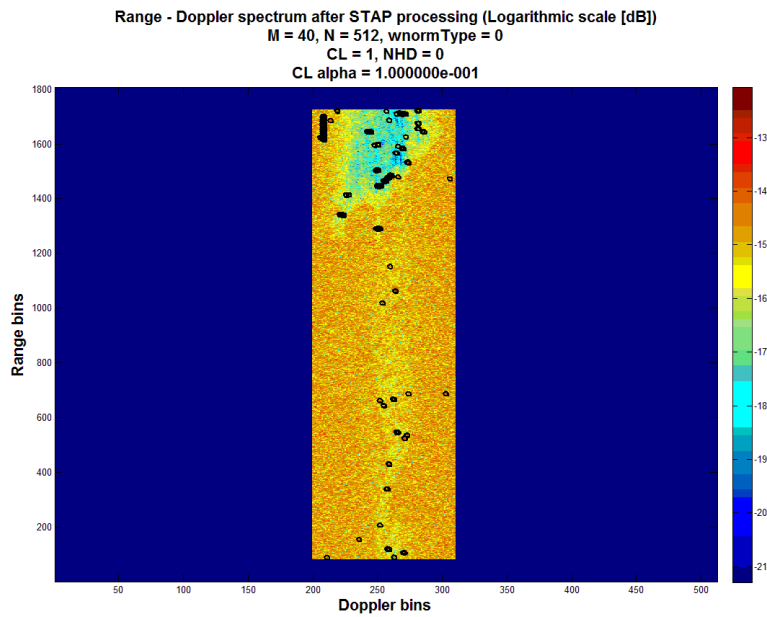


Figure 4.29: Range - Doppler spectrum after STAP processing is applied (NHD = 0, CL = 1, CL alpha = 0.1).

### 4.2.3.3  Colored loading factor is set to 0.25

In this case, the a priori knowledge blending factor is set to 0.25. Figure 4.30 depicts the sum channel range - Doppler spectrum of a single CPI of the data, with the CL processing applied. In this case, some reduction in the number of false alarms is visible in both of the images, and also some new detections are obtained along the shoreline, which can be related to actual targets. Figure 4.31 depicts the range - Doppler spectrum of the STAP processor output of the same data for purposes of demonstration, where the clutter notch is visible. False alarms caused by the clutter discretes are also present in this case, since the NHD is not applied.
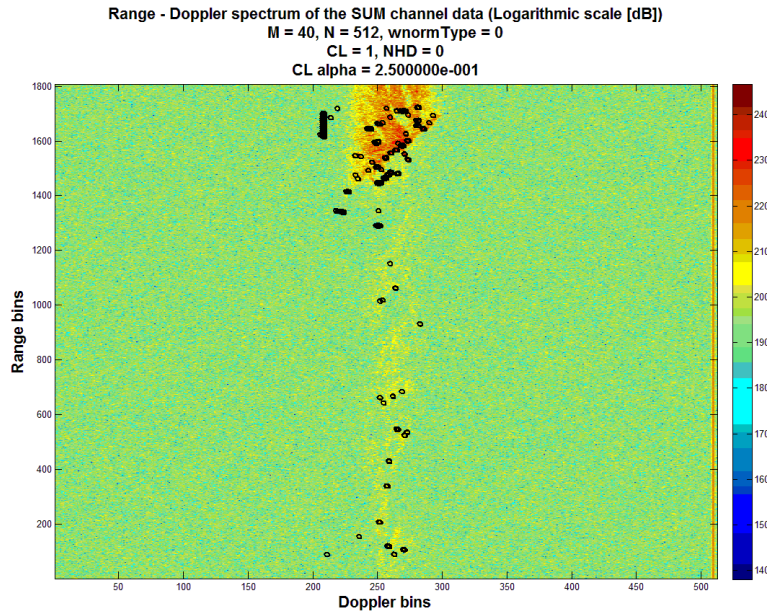
Figure 4.30: Range - Doppler spectrum of the SUM channel data (NHD = 0, CL = 1, CL alpha = 0.25).
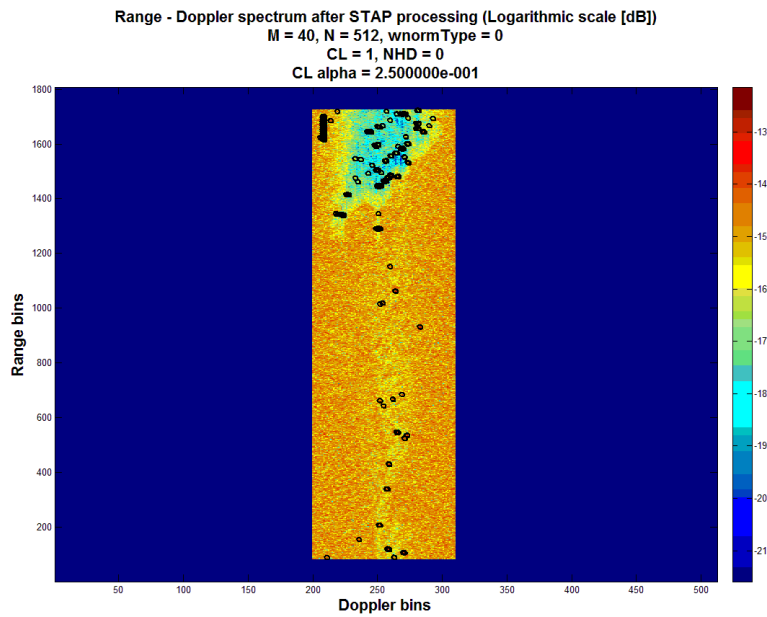


Figure 4.31: Range - Doppler spectrum after STAP processing is applied (NHD = 0, CL = 1, CL alpha = 0.25).

### 4.2.3.4   Colored loading factor is set to 0.50

In this case, the a priori knowledge blending factor is set to 0.50. Figure 4.32 depicts the sum channel range - Doppler spectrum of a single CPI of the data, with the CL processing applied. It should be noted that in this case, the a priori knowledge and the instantaneous knowledge are of equal weight in the blending process. Minor reduction in the number of false alarms is visible in both of the images, and also a large number of new detections are obtained both along the shoreline and inland, which could be because of the mismatch between the a priori data and the instantaneous data. Figure 4.33 depicts the range - Doppler spectrum of the STAP processor output of the same data for purposes of demonstration, where the clutter notch is visible. False alarms caused by the clutter discretes are also present in this case, since the NHD is not applied.
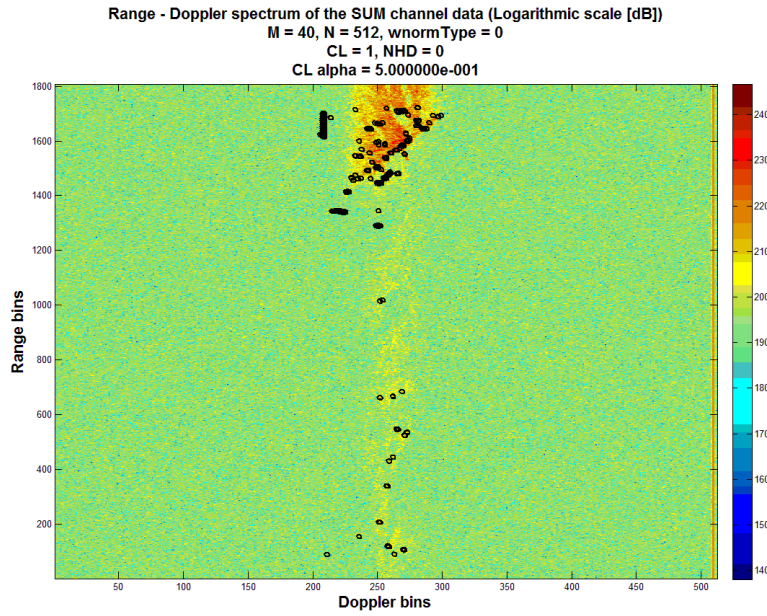
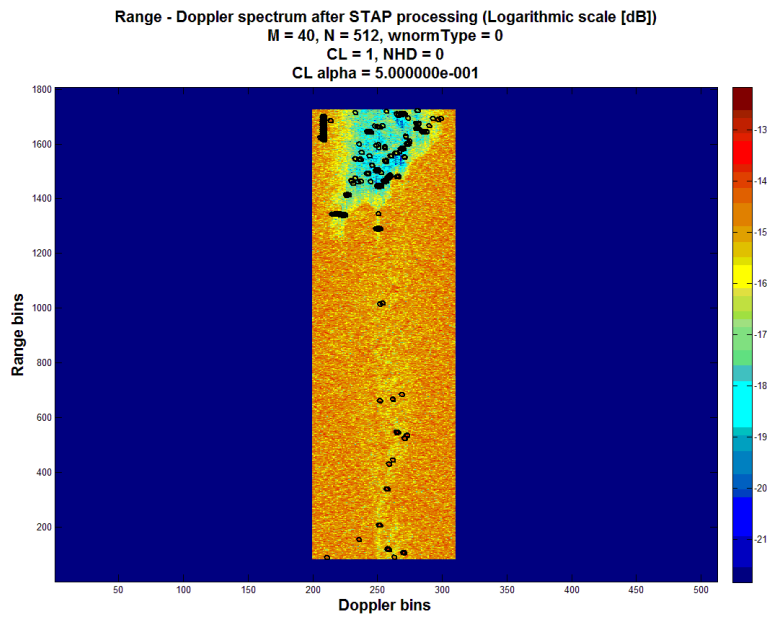Figure 4.32: Range - Doppler spectrum of the SUM channel data (NHD = 0, CL = 1, CL alpha = 0.5).



Figure 4.33: Range - Doppler spectrum after STAP processing is applied (NHD = 0, CL = 1, CL alpha = 0.5).

### 4.2.3.5  Colored loading factor is set to 0.75

In this case, the a priori knowledge blending factor is set to 0.75. Figure 4.34 depicts the sum channel range - Doppler spectrum of a single CPI of the data, with the CL processing applied. A big reduction in the number of false alarms is visible in both of the images, and also some new detections are obtained both along the shoreline and inland. Since in this case, the a priori knowledge has more weight than the instantaneous data in the blending process, the results obtained are more prone to errors, as the employed information might have lost its validity due to possible changes in the environment. Figure 4.35 depicts the range - Doppler spectrum of the STAP processor output of the same data for purposes of demonstration, where the clutter notch is visible. False alarms caused by the clutter discretes are also present in this case, since the NHD is not applied.
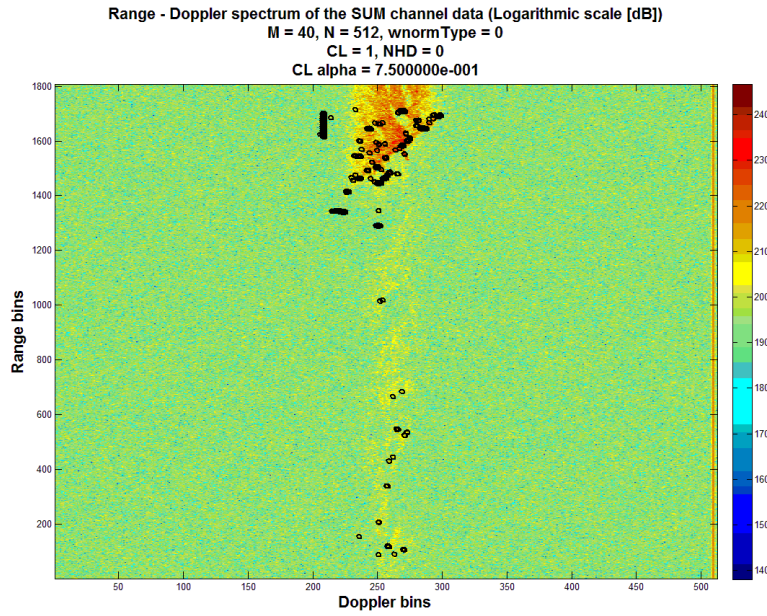
Figure 4.34: Range - Doppler spectrum of the SUM channel data (NHD = 0, CL = 1, CL alpha = 0.75).
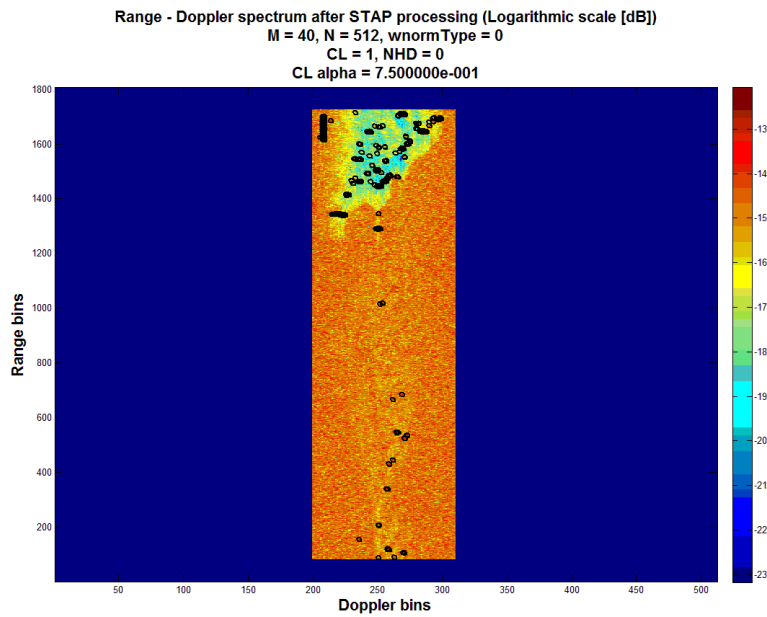


Figure 4.35: Range - Doppler spectrum after STAP processing is applied (NHD = 0, CL = 1, CL alpha = 0.75).

### 4.2.3.6 Colored loading factor is set to 1

This case, in which the a priori knowledge blending factor is set to 1.0, is given for demonstration purposes only; since this case corresponds to the situation in which only the information obtained from a priori knowledge sources is employed, and instantaneous radar data is disregarded. Figure 4.36 depicts the sum channel range - Doppler spectrum of a single CPI of the data, with the CL processing applied. The range - Doppler spectra is erroneous and is littered with many detections which may or may not be actual targets. Figure 4.37 depicts the range - Doppler spectrum of the STAP processor output of the same data for purposes of demonstration, where the clutter notch is visible. Although the NHD process was not applied in this case, false alarms caused by the lighthouse are not present; however the overall output is unusable.
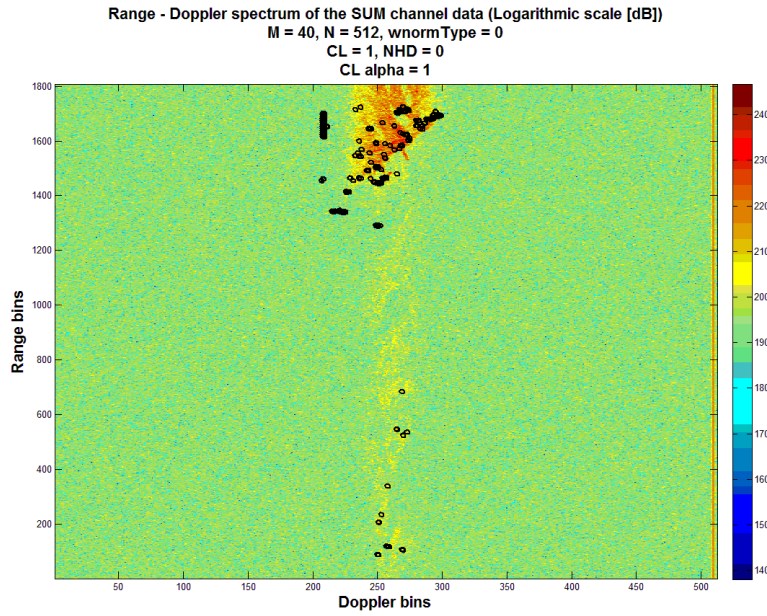
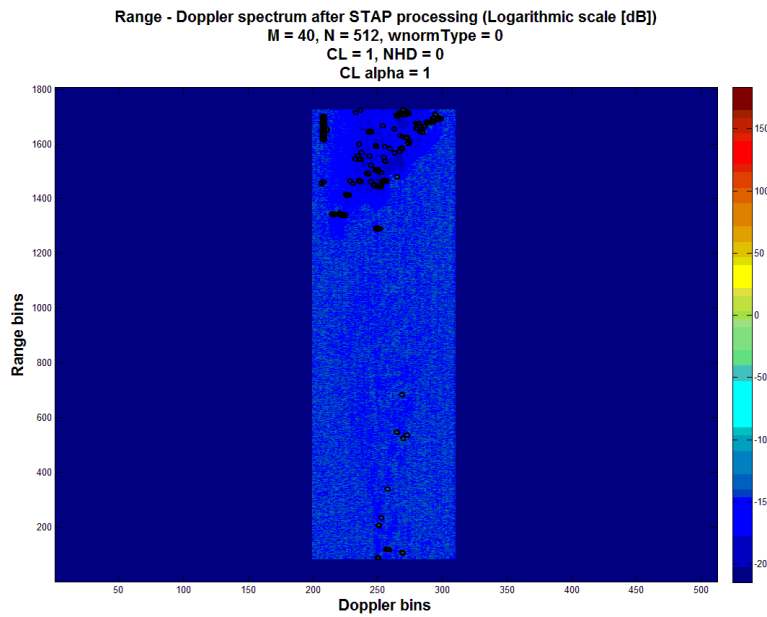Figure 4.36: Range - Doppler spectrum of the SUM channel data (NHD = 0, CL = 1, CL alpha = 1).



Figure 4.37: Range - Doppler spectrum after STAP processing is applied (NHD = 0, CL = 1, CL alpha = 1).

### 4.2.4 Results obtained when both the Colored Loading and the Non Homogeneity Detection process is applied

In this section, the results presented belong to the case in which both the NHD and the CL processes are applied. In the following sections, several different values are chosen for the a priori knowledge blending factor, and the obtained results are presented.

#### 4.2.4.1 Colored loading factor is set to 0.05

In this case, the a priori knowledge blending factor is set to 0.05. Figure 4.38 depicts the sum channel range - Doppler spectrum of a single CPI of the data, with the NHD and the CL processing applied. Since the loading factor is close to zero, the results herein do not differ greatly from the case in which only the NHD processing was applied. Figure 4.39 depicts the range - Doppler spectrum of the STAP processor output of the same data for purposes of demonstration, where the clutter notch is visible. Contary to the previous cases however, false alarms caused by the lighthouse are not present in this case, since the NHD is applied. And also the target which is located near the pier on the left hand side of the image is now detected.
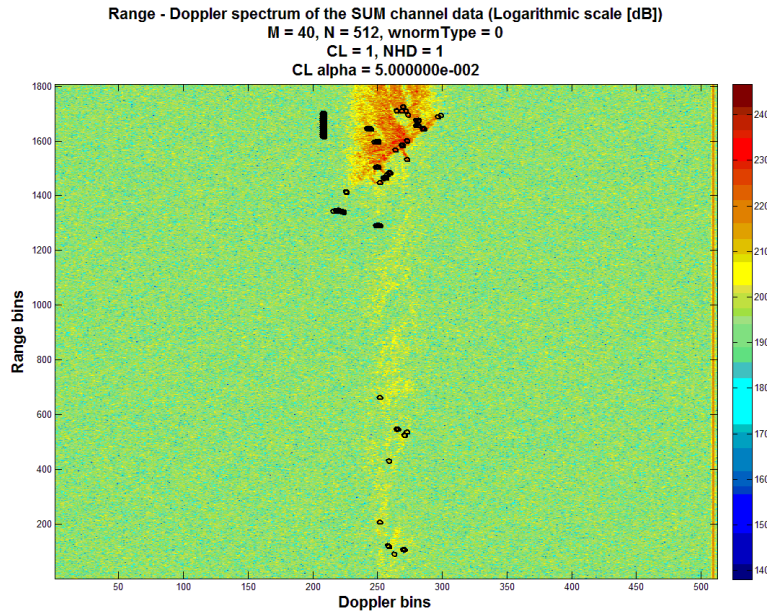
Figure 4.38: Range - Doppler spectrum of the SUM channel data (NHD = 1, CL = 1, CL alpha = 0.05).
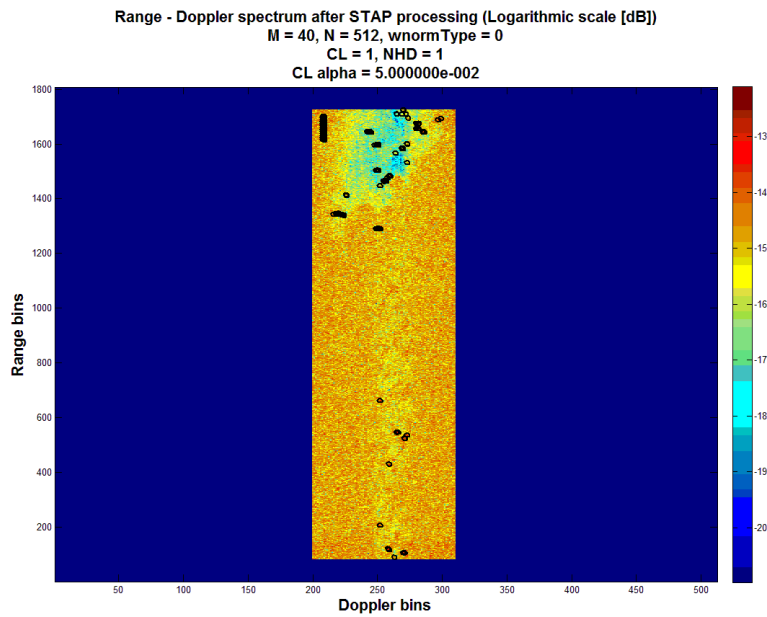


Figure 4.39: Range - Doppler spectrum after STAP processing is applied (NHD = 1, CL = 1, CL alpha = 0.05).

### 4.2.4.2    Colored loading factor is set to 0.10

In this case, the a priori knowledge blending factor is set to 0.10. Figure 4.40 depicts the sum channel range - Doppler spectrum of a single CPI of the data, with the NHD and the CL processing applied. The obtained results are very similar to the results in the previous case where the CL factor was set to 0.05 and NHD processing was applied. Figure 4.41 depicts the range - Doppler spectrum of the STAP processor output of the same data for purposes of demonstration, where the clutter notch is visible. False alarms caused by the lighthouse are not present in this case, since the NHD is applied. The target which is located near the pier on the left hand side of the image is also detected.

Figure 4.40: Range - Doppler spectrum of the SUM channel data (NHD = 1, CL = 1, CL alpha = 0.1).



Figure 4.41: Range - Doppler spectrum after STAP processing is applied (NHD = 1, CL = 1, CL alpha = 0.1).

### 4.2.4.3 Colored loading factor is set to 0.25

In this case, the a priori knowledge blending factor is set to 0.25. Figure 4.42 depicts the sum channel range - Doppler spectrum of a single CPI of the data, with the NHD and the CL processing applied. Some improvement is visible in terms of the overall number of false alarms. Also, several additional targets are now detected along the shoreline. Figure 4.43 depicts the range - Doppler spectrum of the STAP processor output of the same data for purposes of demonstration, where the clutter notch is visible. False alarms caused by the lighthouse are not present in this case, since the NHD is applied. The target which is located near the pier on the left hand side of the image is also detected.
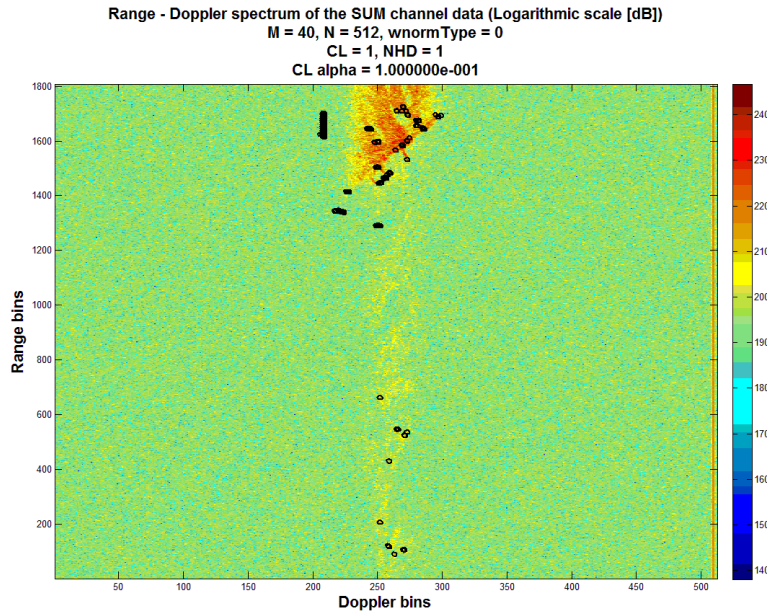
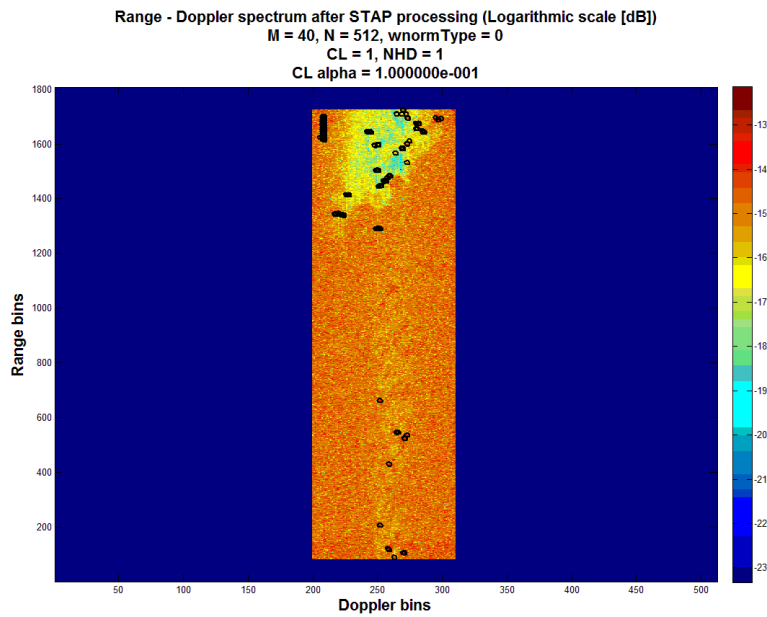Figure 4.42: Range - Doppler spectrum of the SUM channel data (NHD = 1, CL = 1, CL alpha = 0.25).



Figure 4.43: Range - Doppler spectrum after STAP processing is applied (NHD = 1, CL = 1, CL alpha = 0.25).

### 4.2.4.4 Colored loading factor is set to 0.50

In this case, the a priori knowledge blending factor is set to 0.50. Figure 4.44 depicts the sum channel range - Doppler spectrum of a single CPI of the data, with the NHD and the CL processing applied. Several additional targets are detected along the shoreline. Figure 4.45 depicts the range - Doppler spectrum of the STAP processor output of the same data for purposes of demonstration, where the clutter notch is visible. False alarms caused by the lighthouse are not present in this case, since the NHD is applied. The target which is located near the pier on the left hand side of the image is also detected.
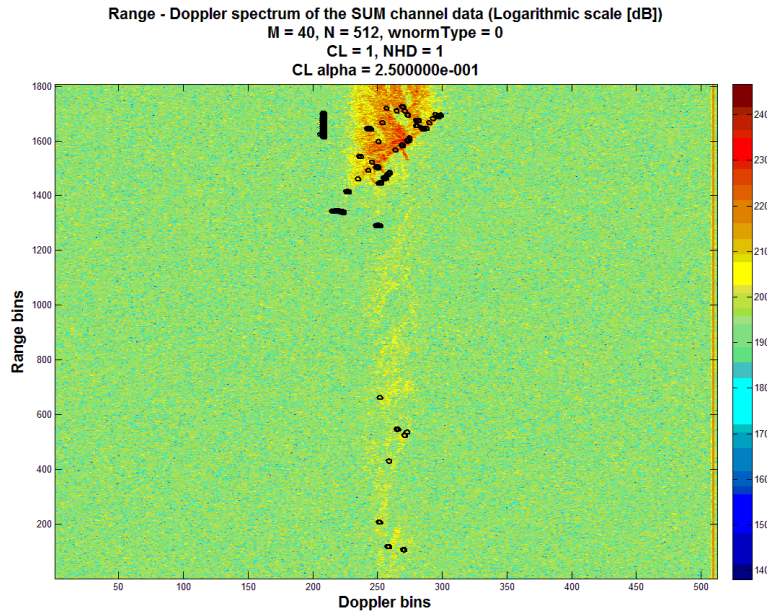
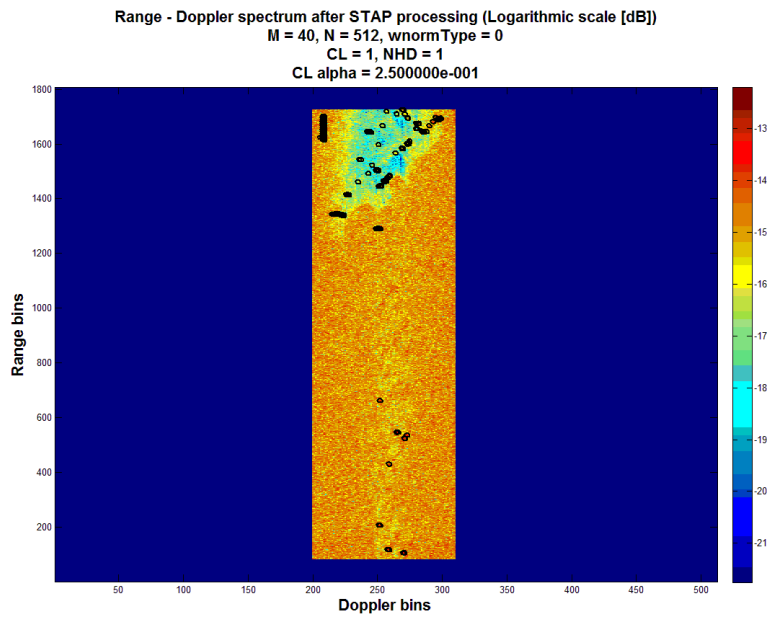Figure 4.44: Range - Doppler spectrum of the SUM channel data (NHD = 1, CL = 1, CL alpha = 0.5).



Figure 4.45: Range - Doppler spectrum after STAP processing is applied (NHD = 1, CL = 1, CL alpha = 0.5).

### 4.2.4.5 Colored loading factor is set to 0.75

In this case, the a priori knowledge blending factor is set to 0.75. Figure 4.46 depicts the sum channel range - Doppler spectrum of a single CPI of the data, with the NHD and the CL processing applied. Several additional targets are detected along the shoreline and inland. Figure 4.47 depicts the range - Doppler spectrum of the STAP processor output of the same data for purposes of demonstration, where the clutter notch is visible. False alarms caused by the lighthouse are not present in this case, since the NHD is applied. The target which is located near the pier on the left hand side of the image is also detected.
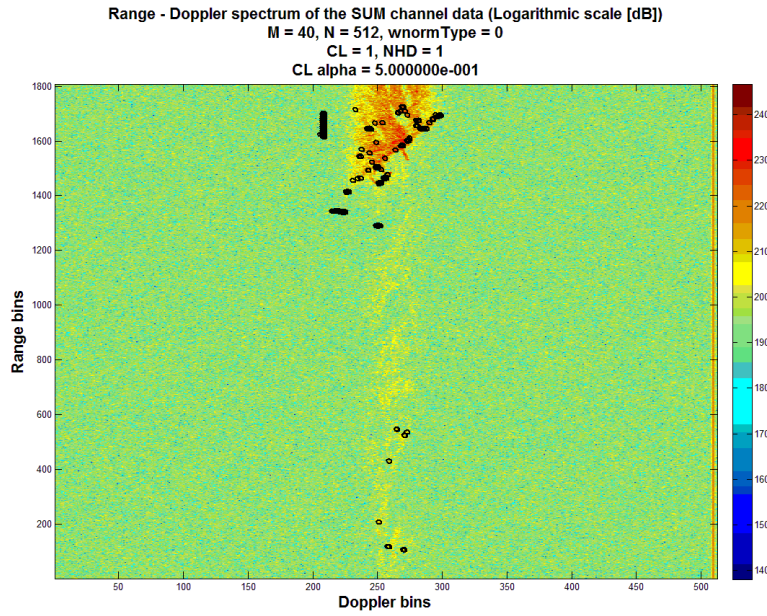
Figure 4.46: Range - Doppler spectrum of the SUM channel data (NHD = 1, CL = 1, CL alpha = 0.75).
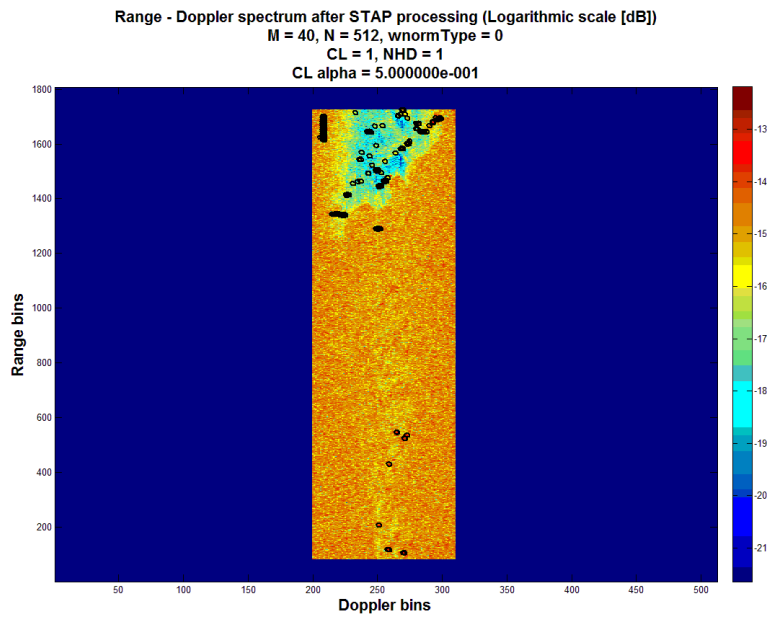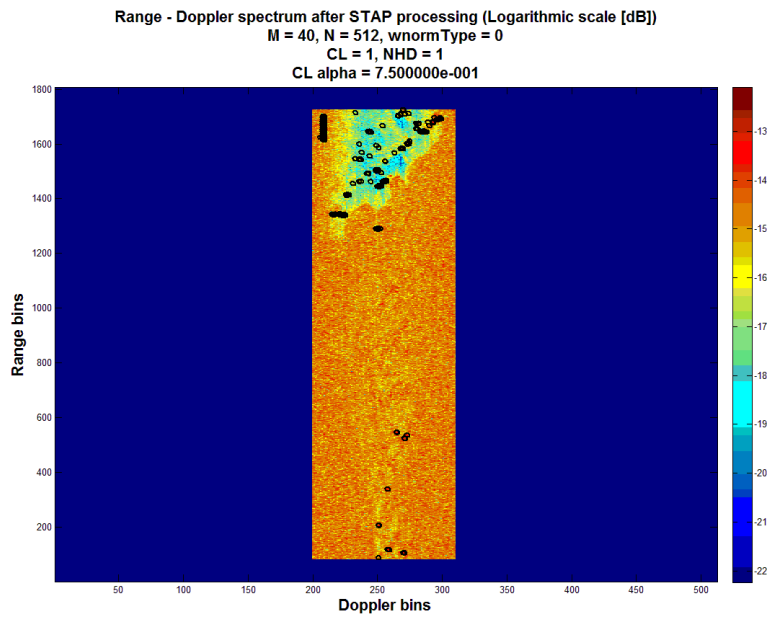


Figure 4.47: Range - Doppler spectrum after STAP processing is applied (NHD = 1, CL = 1, CL alpha = 0.75).

### 4.2.4.6   Colored loading factor is set to 1.00

In this case, the a priori knowledge blending factor is once again set to 1.0 for demonstration purposes. Figure 4.48 depicts the sum channel range - Doppler spectrum of a single CPI of the data, with the NHD and the CL processing applied. The output is once again far from usable. Figure 4.49 depicts the range - Doppler spectrum of the STAP processor output of the same data for purposes of demonstration, where the clutter notch is visible.
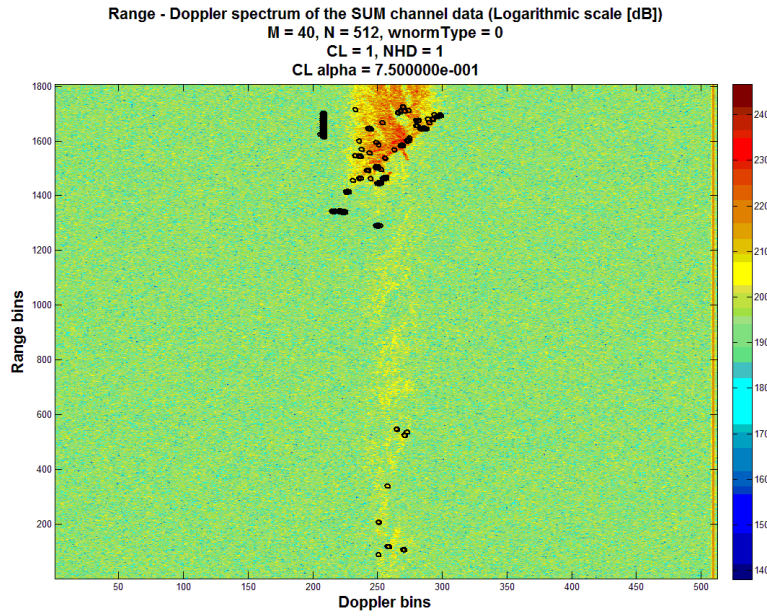
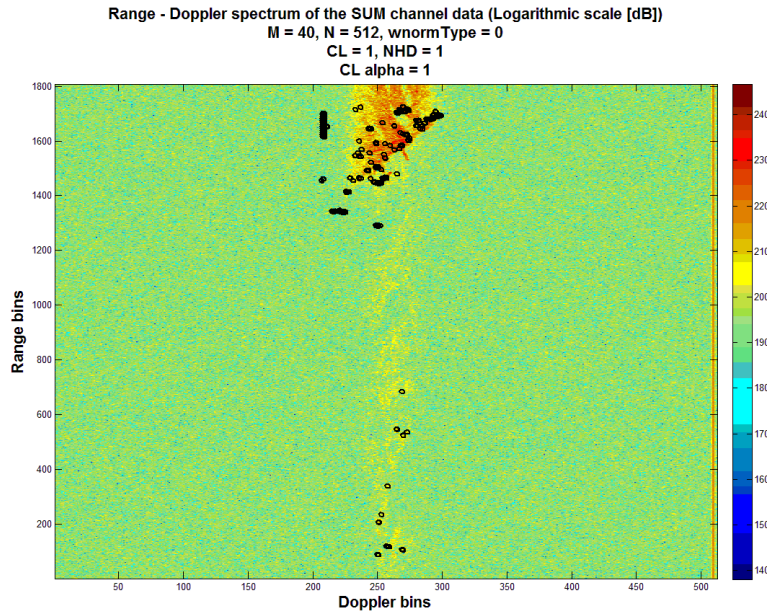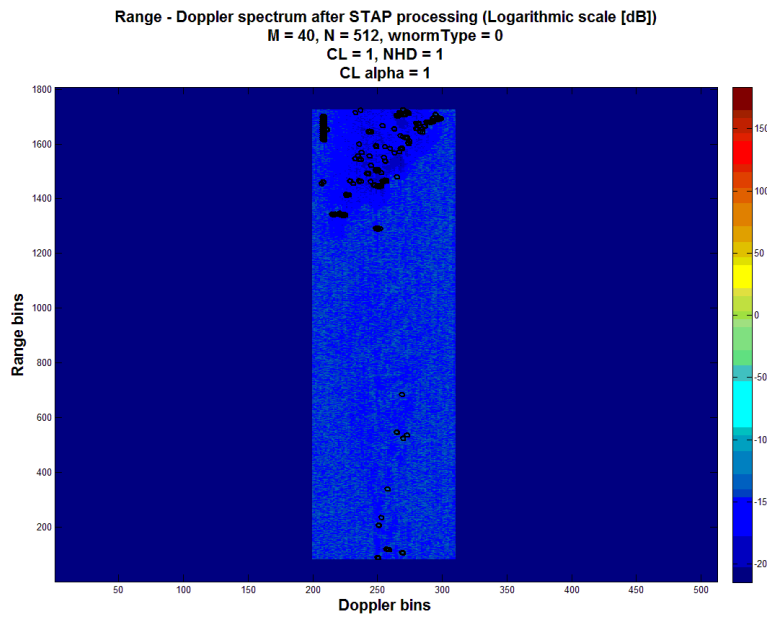Figure 4.48: Range - Doppler spectrum of the SUM channel data (NHD = 1, CL = 1, CL alpha = 1).



Figure 4.49: Range - Doppler spectrum after STAP processing is applied (NHD = 1, CL = 1, CL alpha = 1).

# CHAPTER 5

# CONCLUSIONS

## 5.1    Thesis Summary

Real world test scenarios include heterogeneous clutter and target rich environments, which degrade STAP performance. In an attempt to address this issue, a novel knowledge aided processing approach which makes use of additional processing steps along with space-time processing is proposed in this thesis work. The proposed processing architecture is based on the element space post Doppler implementation of the reduced rank space time adaptive processing methods, and performs further knowledge aided steps which combine techniques such as the colored loading process and the non homogeneity detection process while using both a priori and instantaneous information, and suggesting new types of information which are readily available or obtainable such as SRTM data and DBS maps, as sources of a priori knowledge.

The processing structure can be summarized as follows: Initially, the a priori knowledge corresponding to the region of interest, which contains the SRTM elevation data and the DBS reflectivity maps, is obtained from the knowledge databases. Afterwards, platform ownship data is used along with the a priori data in order to identify the homogeneous regions in the area. After this, a priori clutter covariance matrices are formed and blended with the instantaneous interference matrices. Finally, the STAP processor is invoked and detections are obtained after thresholding the output.

The proposed method is implemented in MATLAB and applied to real flight data that contains heterogeneous clutter. Both real and injected targets are used for performance evaluation purposes for better inspection of the results. Obtained results

indicate that:

- Detection of previously undetected targets is possible,

- Targets which are close together in range are detected more easily compared to the SMI case,

- Use of smaller sample support for training data is possible,

- Better false alarm performance can be obtained compared to the SMI case.

In conclusion, results indicate that by proper selection of the blending factor and by applying the non homogeneity detection process, knowledge aided signal processing can be beneficial in improving detection performance in space - time adaptive processing schemes.

## 5.2 Future Work

Several topics that can be further researched to reach a more complete understanding on the matter can be listed as follows:

1. Investigation of numerical techniques so as to reduce the number of operations required to implement the proposed method,

2. Further evaluation of the proposed technique after more data sets become available for purposes of optimization in different types of terrain,

3. Use of additional knowledge sources to be used in KA-STAP, such as weather conditions, road networks, etc.

# REFERENCES

[1] R. S. Adve, M. C. Wicks, T. B. Hale, and P. Antonik, "Ground moving target indication using knowledge based space time adaptive processing,"

[2] P. W. Moo, "GMTI performance of Sigma – Delta STAP for a forward-looking radar," 2001.

[3] R. D. Brown, R. A. Schneible, M. C. Wicks, H. Wang, and Y. Zhang, "STAP for clutter suppression with sum and difference beams," *IEEE Transactions on Aerospace and Electronic Systems*, vol. 36, no. 2, 2000.

[4] W. L. Melvin and G. A. Showman, "An approach to knowledge-aided covariance estimation," *IEEE Transactions on Aerospace and Electronic Systems*, vol. 42, no. 3, 2006.

[5] I. S. Reed, J. D. Mallet, and L. E. Brennan, "Rapid convergence rate in adaptive arrays," *IEEE Transactions on Aerospace and Electronic Systems*, vol. AES-10, no. 6, 1974.

[6] J. R. Guerci and E. J. Baranoski, "Knowledge-aided adaptive radar at DARPA," *IEEE Signal Processing Magazine*, 2006.

[7] J. S. Bergin, C. M. Teixeira, P. M. Techau, and J. R. Guerci, "Improved clutter mitigation performance using knowledge-aided space time adaptive processing," *IEEE Transactions on Aerospace and Electronic Systems*, vol. 42, no. 3, 2006.

[8] J. Bergin, G. Chaney, and P. Techau, "Development and implementation of a knowledge aided stap algorithm," tech. rep., Information Systems Laboratories, Inc., 2005.

[9] D. Wu, D. Zhu, and Z. Zhu, "Knowledge-aided multichannel SAR/GMTI processing: Algorithm and experimental results," *EURASIP Journal on Advances in Signal Processing*, 2010.

[10] J. R. Guerci, "Theory and application of covariance matrix tapers for robust adaptive beamforming," *IEEE Transactions on Signal Processing*, vol. 47, no. 4, 1999.

[11] C. Baktır, "Simulation-based comparison of some GMTI techniques," Master's thesis, Middle East Technical University, 2009.

[12] G. Yıldırım, "Antenna patterns for slowly moving targets in two channel GMTI processing," Master's thesis, Middle East Technical University, 2010.

[13] Ö. Eryiğit, "Interference suppression by using space-time adaptive processing for airborne radar," Master's thesis, Middle East Technical University, 2008.

[14] J. R. Guerci, *Space-Time Adaptive Processing for Radar.* Artech House, 2003.

[15] J. Ward, "Space-time adaptive processing for airborne radar," *IEEE*, 1998.

[16] R. C. DiPetro, "Extended factored space-time processing for airborne radar systems," *IEEE*, 1992.

[17] C. T. Capraro, D. D. Weiner, and M. C. Wicks, "Improved STAP performance using knowledge-aided secondary data selection," *IEEE*, 2004.

[18] N. A. Goodman and P. R. Gurram, "STAP training through knowledge-aided predictive modeling," *IEEE*, 2004.

[19] "Performance specification for digital terrain elevation data," tech. rep., National Imagery and Mapping Agency, 1996.

[20] N. J. P. Laboratory, "Shuttle Radar Topography Mission home page." Retrieved on September 2012, from http://www2.jpl.nasa.gov/srtm/.

[21] M. A. Richards, "Interferometric 3D spotlight SAR." Technical presentation presented on during the training course titled Fundamentals of Radar Signal Processing, 2008.

[22] M. C. Wicks, W. L. Melvin, and P. Chen, "An efficient architecture for nonhomogeneity detection in space-time adaptive processing airborne early warning radar," in *Radar 97*, United States Air Force Rome Laboratory, Signal Processing Branch, USA, 1997.

[23] E. Aboutanios and B. Mulgrew, "Heterogeneity detection for hybrid stap algorithm," *IEEE*, 2008.

[24] P. Stoica, J. Li, X. Zhu, and J. R. Guerci, "On using a priori knowledge in space-time adaptive processing," *IEEE*, 2008.

[25] J. S. Bergin, D. R. Kirk, G. Chaney, and S. McNeil, "Evaluation of knowledge-aided STAP using experimental data," *IEEE*, 2007.

[26] C. T. Capraro, G. T. Capraro, I. Bradaric, D. D. Weiner, M. C. Wicks, and W. J. Baldygo, "Implementing digital terrain data in knowledge-aided space-time adaptive processing," *IEEE*, 2006.

[27] M. Kuzuoğlu, "Radar registration." Technical presentation presented on December 14th, 2009 for Aselsan, Inc., 2009.

[28] M. A. Richards, "SAR data, doppler beam sharpening, and the range - doppler algorithm." Technical presentation presented on during the training course titled Fundamentals of Radar Signal Processing, 2008.

# Appendix A

# CONVERSION BETWEEN THE GEODETIC, ECEF AND ENU COORDINATE SYSTEMS

This appendix presents the equations required for converting between the geodetic coordinate system (latitude, longitude and altitude), the ECEF coordinate system ($X$, $Y$ and $Z$) and the ENU local Cartesian coordinate system ($x$, $y$, $z$) as given in [26] and [27].

## A.1 Conversion from the Geodetic Coordinate System to the ECEF Coordinate System

The process of converting from the geodetic coordinate system to the ECEF coordinate system is given in Equation A.1 [26], [27].

$$
\begin{aligned}
X &= (N + h)\cos(d_{lat})\cos(d_{lon}) \\
Y &= (N + h)\cos(d_{lat})\sin(d_{lon}) \\
Z &= [(1 - e^2)N + h]\sin(d_{lat})
\end{aligned}
\tag{A.1}
$$

where

$$
N = \frac{a}{\sqrt{1 - e^2 \sin^2(d_{lat})}}
\tag{A.2}
$$

and $a$ denotes the semi-major axis of the WGS-84 reference ellipsoid, $h$ denotes height and $d_{lat}$ and $d_{lon}$ denote the latitude and the longitude respectively. $e$ is the eccentricity of the WGS-84 ellipsoid and equals to 0.0818 [27].

## A.2 Conversion from the ECEF Coordinate System to the ENU Coordinate System

The ENU local Cartesian coordinates $(x, y, z)$ for a point with the ECEF coordinates $(X, Y, Z)$ is obtained by Equation A.3 [27].

$$\begin{bmatrix} x \\ y \\ z \end{bmatrix} = L \left( \begin{bmatrix} X \\ Y \\ Z \end{bmatrix} - \begin{bmatrix} X_0 \\ Y_0 \\ Z_0 \end{bmatrix} \right) \tag{A.3}$$

where $(X_0, Y_0, Z_0)$ denotes the ECEF coordinates of the reference point for the ENU local Cartesian system. $L$ denotes the transformation matrix required for converting from the ECEF coordinates to the ENU local Cartesian coordinates and is given by Equation A.4.

$$L = \begin{bmatrix} -\sin(d_{lon}) & \cos(d_{lon}) & 0 \\ -\sin(d_{lat})\cos(d_{lon}) & -\sin(d_{lat})\sin(d_{lon}) & \cos(d_{lat}) \\ \cos(d_{lat})\cos(d_{lon}) & \cos(d_{lat})\sin(d_{lon}) & \sin(d_{lat}) \end{bmatrix} \tag{A.4}$$

and $d_{lat}$ and $d_{lon}$ denote the latitude and longitude of the reference point for the ENU local Cartesian system respectively.

## A.3 Conversion from the ENU Coordinate System to the ECEF Coordinate System

The ECEF coordinates of a point with the ENU local Cartesian coordinates $(x, y, z)$ with respect to the ENU coordinate system reference point is obtained by Equation A.5.

$$\begin{bmatrix} X \\ Y \\ Z \end{bmatrix} = \begin{bmatrix} X_0 \\ Y_0 \\ Z_0 \end{bmatrix} + L^T \begin{bmatrix} x \\ y \\ z \end{bmatrix} \tag{A.5}$$

where $(X_0, Y_0, Z_0)$ denotes the ECEF coordinates of the reference point for the ENU local Cartesian system. $L$ denotes the transformation matrix required for converting from the ECEF coordinates to the ENU local Cartesian coordinates and is given by Equation A.4. $(^T)$ is the matrix transpose operation.

## A.4 Conversion from the ECEF Coordinate System to the Geodetic Coordinate System

The process of converting from the ECEF coordinate system to the geodetic coordinate system is a recursive process and requires a number of iterations in order to converge to an accurate result. The process is given by Equation A.6 [27]. Initial conditions are given as $h = 0$, $N = a$ and $p = \sqrt{X^2 + Y^2}$.

$$
\begin{aligned}
\sin(d_{lat}) &= \frac{Z}{N(1-e^2)+h} \\
d_{lat} &= tan^{-1}\left(\frac{Z+e^2 N \sin(d_{lat})}{p}\right) \\
N &= \frac{a}{\sqrt{1-e^2 \sin^2(d_{lat})}} \\
h &= \frac{p}{\cos(d_{lat})} - N
\end{aligned}
\tag{A.6}
$$

and

$$
d_{lon} = \arctan(Y, X) \tag{A.7}
$$

where $(X, Y, Z)$ denotes the ECEF coordinates and $d_{lat}$, $d_{lon}$ and $h$ denote the latitude, longitude and height of the point of interest. $a$ denotes the semi-major axis of the WGS-84 reference ellipsoid and $e$ is the eccentricity of the WGS-84 ellipsoid.

# Appendix B

# DOPPLER BEAM SHARPENING MAP FORMATION PROCESS

This appendix presents the equations required for forming a Doppler Beam Sharpening image from previously acquired GMTI radar data, following the processing approaches presented in [28]. In the GMTI mode operation, slow time samples (pulses) are collected coherently in short intervals of time, which are known as bursts or coherent processing intervals, which are on the order of several milliseconds. Compared with the observation times required for SAR and DBS imagery, this observation time is relatively low and does not allow the coherent integration of slow time samples for long durations. To compensate for this effect, a phase correction needs to be applied to the received data before Doppler processing, which removes the phase jumps that occur during different bursts.

The following sections describe the burst to burst phase correction process which is applied before Doppler processing and summarizes the geometric transformations required for converting the range - Doppler image to Cartesian coordinates.

## B.1   Burst to Burst Phase Correction and Doppler Processing

The raw data of a GMTI mode operation before any processing is applied is as seen in Figure B.1. The displayed data contains more than one burst of pulses and therefore includes the aforementioned phase jumps. Figure B.2 shows the range - Doppler spectrum before any phase correction is applied. As it can be seen, the image is blurred in azimuth due to the extraneous phase jumps, which in turn create undesired

signal components in Doppler. Another issue of note here is that in this example, the received data is aliased in Doppler due to the fact that the Doppler centroid frequency of the mainlobe clutter is greater than half of the pulse repetition frequency. This effect was caused by the high radial velocity components at the edges of the antenna beam because of the squinted look direction of the antenna.
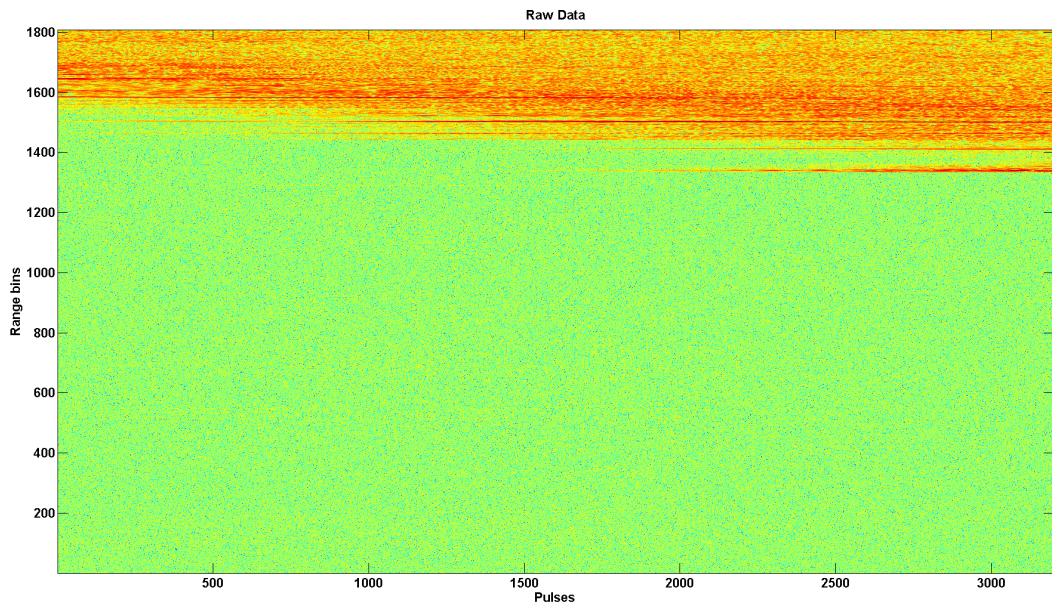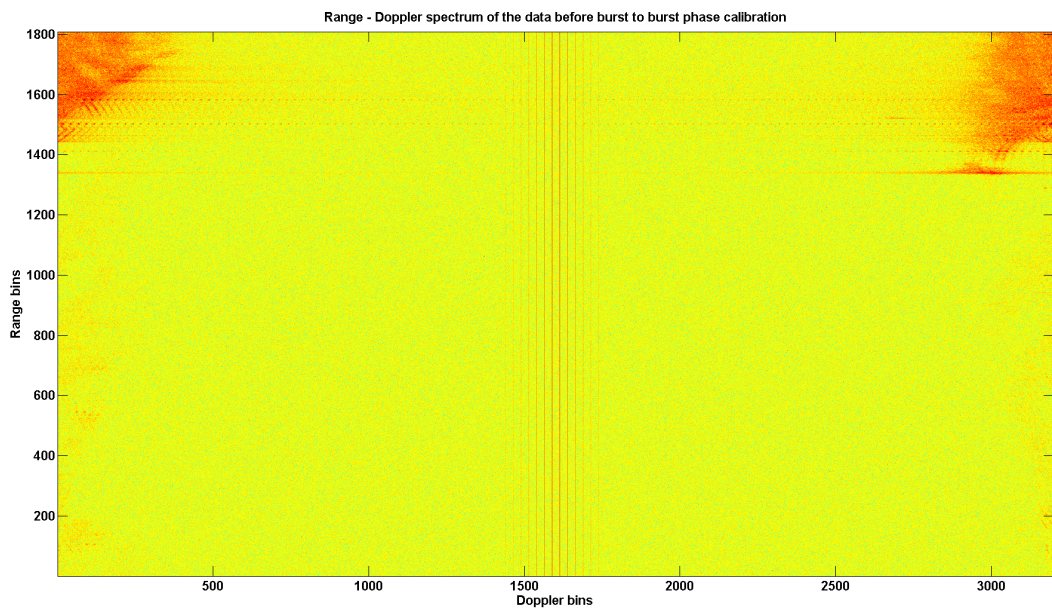
Figure B.1: Raw GMTI data



Figure B.2: Range - Doppler spectrum of the data before phase correction

Let $\mathbf{r_{k,n}} \in C^{M' \times 1}$ denote the space time observations received from $M'$ pulses and a single receiver element for a single range bin $k$. Let $M$ denote the number of pulses in a single burst. The phase corrected space time observations $\mathbf{r_{k,n,pc1}}$ can be obtained as

$$\mathbf{r_{k,n,pc1}} = \mathbf{r_{k,n}} \odot \mathbf{h_{k,n,pc1}} \tag{B.1}$$

where $\odot$ represents the Hadamard element-wise multiplication operation and $\mathbf{h_{k,n,pc1}} \in C^{M' \times 1}$ denotes the phase correction multiplier which can be stated as

$$\mathbf{h_{k,n,pc1}} = \begin{bmatrix} \left. \begin{pmatrix} 1 \\ \vdots \\ 1 \end{pmatrix} \right\} & \begin{matrix} 1 \\ \vdots \\ M \end{matrix} \\ \left. \begin{pmatrix} exp(-j\pi 1 \Delta\Phi) \\ \vdots \\ exp(-j\pi 1 \Delta\Phi) \end{pmatrix} \right\} & \begin{matrix} 1 \\ \vdots \\ M \end{matrix} \\ \vdots \\ \left. \begin{pmatrix} exp(-j\pi \left(\frac{M'}{M} - 1\right)\Delta\Phi) \\ \vdots \\ exp(-j\pi \left(\frac{M'}{M} - 1\right)\Delta\Phi) \end{pmatrix} \right\} & \begin{matrix} 1 \\ \vdots \\ M \end{matrix} \end{bmatrix} \tag{B.2}$$

where $\Delta\Phi$ represents the constant phase shift term which is caused by the time interval between following bursts.

After the burst to burst phase correction process, the range - Doppler spectrum of the data is as seen in Figure B.3. Since the extraneous phase terms are compensated for, the blurring effect which was present before in the azimuth axis is removed.
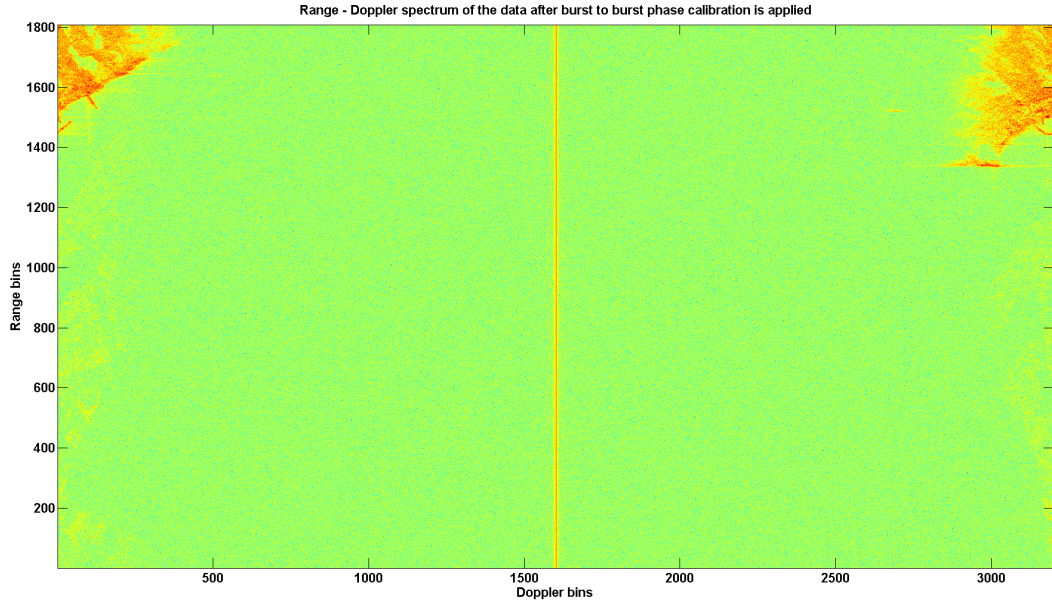
Figure B.3: Range - Doppler spectrum of the data after burst to burst phase correction

Afterwards, the Doppler centroid frequency of the mainlobe clutter is centered at 0 Hz to form an unwrapped image of the range - Doppler spectrum by means of an extra phase multiplication process. This is accomplished as following:

$$\mathbf{r_{k,n,pc2}} = \mathbf{r_{k,n,pc1}} \odot \mathbf{h_{k,n,pc2}} \tag{B.3}$$

where $\mathbf{r_{k,n,pc1}}$ is the phase corrected space time observations obtained in Equation B.1, and $\mathbf{h_{k,n,pc2}} \in C^{M' x 1}$ denotes the Doppler centroid correction multiplier which can be stated as

$$\mathbf{h_{k,n,pc2}} = \begin{bmatrix} 1 \\ exp(-j2\pi f_{dc}/f_{PRF}1) \\ \vdots \\ exp(-j2\pi f_{dc}/f_{PRF}M') \end{bmatrix} \tag{B.4}$$

where $f_{dc}$ denotes the Doppler centroid frequency of the mainlobe clutter and $f_{PRF}$ denotes the pulse repetition frequency of the radar sensor.

Figure B.4 depicts the final form of the range - Doppler spectrum, which is obtained

after the burst to burst phase correction and the Doppler centroid correction processes are applied.
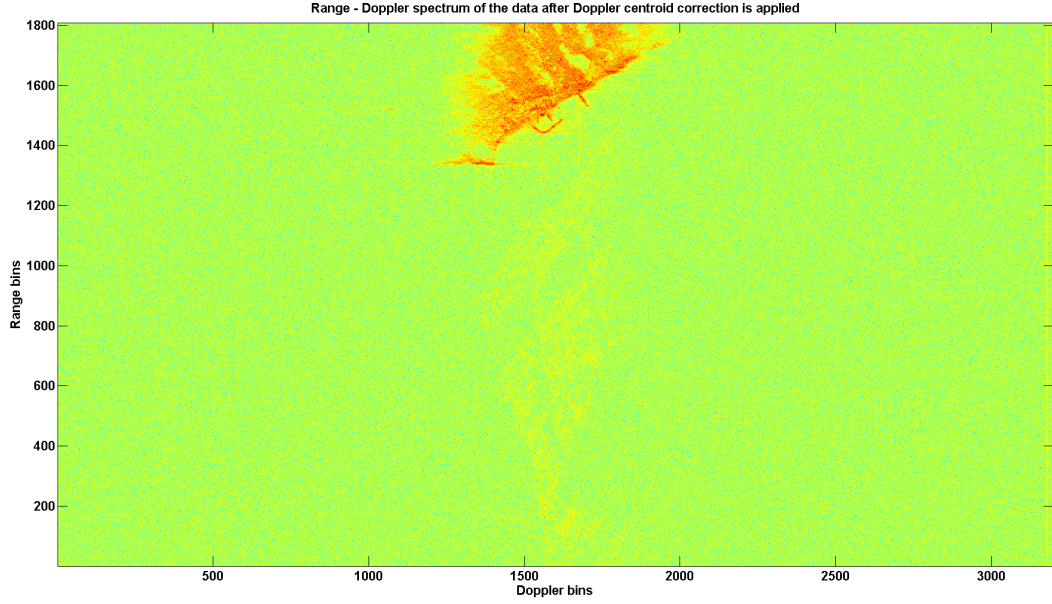


Figure B.4: Range - Doppler spectrum of the data after burst to burst phase correction and Doppler centroid correction

## B.2  Geometric Transformations

After the range - Doppler image is formed, the following geometric transformations are applied in order to obtain a map in Cartesian coordinates. Initially, the azimuth angle corresponding to the Doppler bin of interest in the range - Doppler spectrum of the radar data is calculated in the following manner.

$$\theta = \arcsin\left(\frac{f_{Doppler}\lambda}{2v_P}\right) \tag{B.5}$$

where $\theta$ denotes the azimuth angle of interest, which is equal to $0\,\mathrm{deg}$ for a target that is directly located at the boresight for a side-looking antenna, $f_{Doppler}$ represents the Doppler frequency of the aforementioned Doppler bin, $\lambda$ denotes the wavelength of the radar sensor and $v_P$ denotes the platform velocity.

Secondly, the ground range corresponding to each of the range bin is calculated.

106

$$R_{ground,k} = \sqrt{R^2_{slant,k} - h^2_{agl}} \qquad\qquad (B.6)$$

where $h_{agl}$ denotes the sensor altitude with respect to the ground level and $R_{slant,k}$ denotes the slant range corresponding to the range bin $k$. $R_{slant,k}$ is calculated as follows.

$$R_{slant,k} = R_{min} + (k - 1)\Delta R_{bin} \qquad\qquad (B.7)$$

where $R_{min}$ denotes the minimum sampled range and $\Delta R_{bin}$ denotes the range bin size in meters.

# Appendix C

# TARGET INJECTION PROCESS

This appendix presents the operations performed in order to create a simulated target of desired range, Doppler and amplitude parameters to be injected within the radar data. The necessary steps involve initially creating the target signal model according to the desired target range and velocity parameters, and afterwards injecting the obtained target signal within the actual radar data according to the desired range and amplitude values. The processing steps are described in the following sections.

## C.1    Creating the Target Signal Model

For a radar sensor which employs linear frequency modulation (LFM) in its transmit waveform, the transmitted signal for a single pulse is of the following form.

$$s_{tx}(t) = exp(j\pi k_r t^2) \tag{C.1}$$

where $s_{tx}(t)$ denotes the transmitted signal and $t$ denotes the fast time. $k_r$ denotes the LFM chirp rate and is given as

$$k_r = \frac{B_{tx}}{\tau} \tag{C.2}$$

where $B_{tx}$ is the transmit signal bandwidth and $\tau$ is the transmitted pulse length.

Let $s_{target}$ denote the target returns from an ideal point target in the region of interest. The associated target signal model therefore becomes a replica of the transmitted

radar signal which is delayed in time and shifted in Doppler frequency due to the range and the velocity of the target. For the aforementioned transmit signal waveform, the target signal model therefore becomes of the following form.

$$s_{target}(t, u) = exp(j\pi k_r(t - \frac{2v_r u T_{PRI}}{c})^2) exp(\frac{-j2\pi 2v_r u T_{PRI}}{\lambda}) \qquad \text{(C.3)}$$

where $t$ denotes the fast time, $u$ denotes the slow time sample indices and $k_r$ denotes the LFM chirp rate as given in C.2. $v_r$ is the target radial velocity, $T_{PRI}$ is the pulse repetition interval (PRI), $c$ is the speed of light and $\lambda$ is the radar wavelength.

## C.2 Injection of the Target Signal

After the target signal model is constructed according to the desired target range and velocity parameters, the obtained data vectors must be added to the actual radar data cube. To accomplish this, the target signal is initially scaled in amplitude according to the desired target signal power and the associated receiver gains corresponding to each of the receiver elements.

Let $s_{target,n}$ denote the target signal component which is received from the $n^{th}$ receiver element. The scaled versions of the target returns are obtained as follows.

$$s_{target,n}(t, u) = \sqrt{P_{target}} Z_n s_{target}(t, u) \qquad \text{(C.4)}$$

where $P_{target}$ denotes the desired target signal power, $Z_n$ denotes the complex receiver gain associated with the $n^{th}$ receiver element and $s_{target}(t, u)$ is the target signal model obtained in Equation C.3.

After this step, the data samples are summed with the corresponding data cube at the range bin of interest, thereby yielding a radar data cube which contains the desired target signal. The target returns will be visible in the range - Doppler spectrum of the radar data after matched filtering and Doppler processing is applied, similar to the actual targets which are present in the data itself.

Figure C.1 depicts the injected target signal after range compression, showing the change of target's range over time. Figure C.2 and C.3 show the range - Doppler spectrum of the radar data, before and after the target injection process respectively.
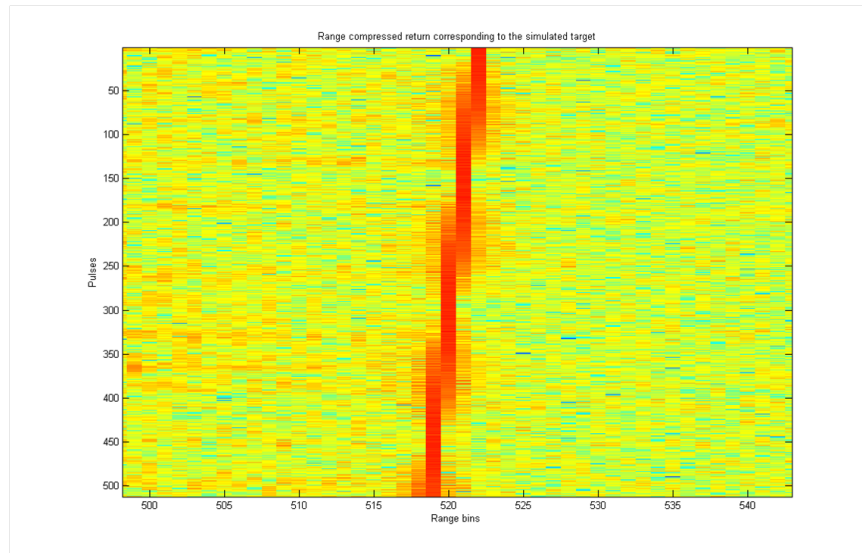


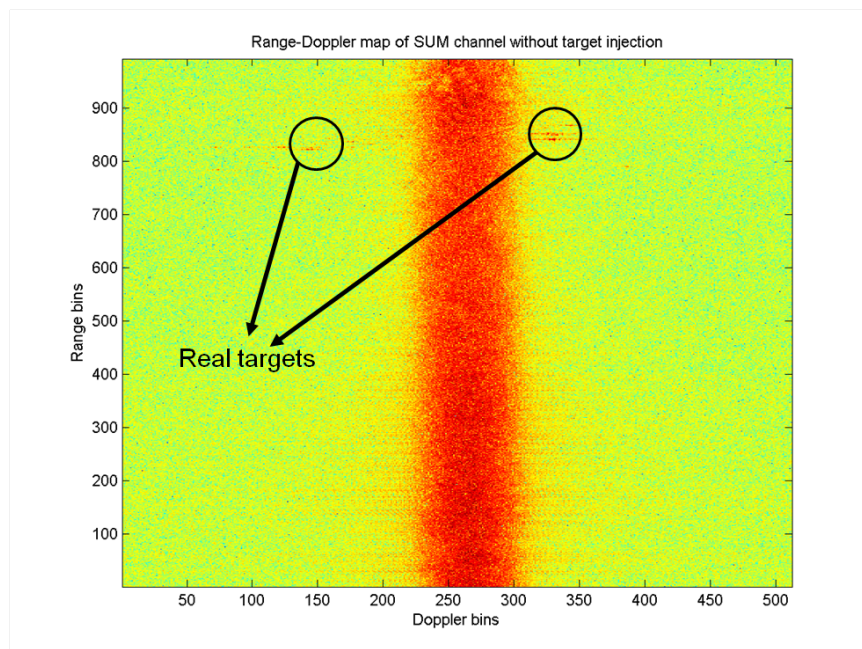Figure C.1: Injected target signal after range compression



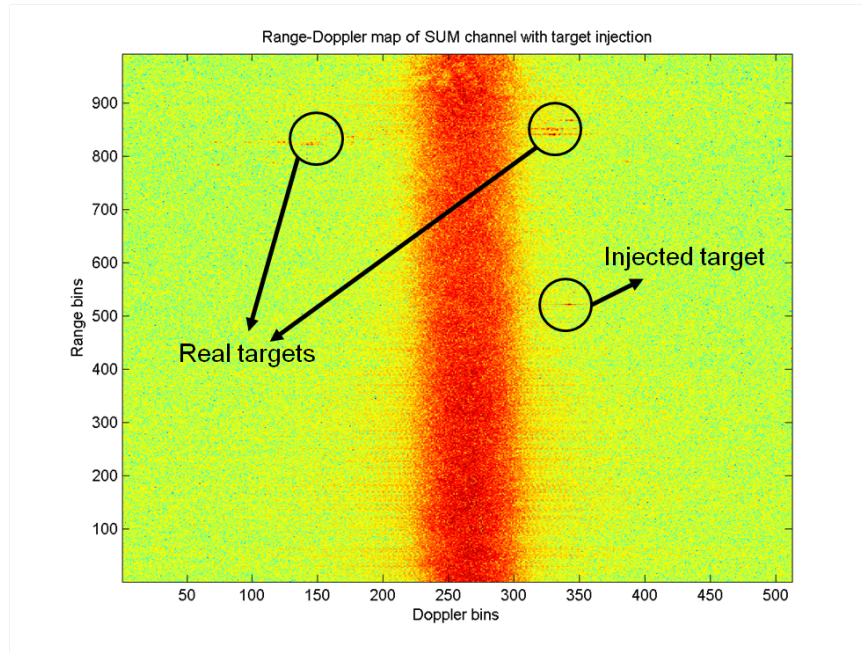Figure C.2: Range - Doppler spectrum of the radar data before target injection

Figure C.3: Range - Doppler spectrum of the radar data after target injection